ADAPTIVE CONTROL FOR THE POSITION OF MAGNETIC PARTICLES USING MAGNETIC TRAPS

by

Jason G. Pickel

B.S. in Mechanical Engineering

University of Pittsburgh 2007

Submitted to the Graduate Faculty of

the Swanson School of Engineering in partial fulfillment

of the requirements for the degree of

Master of Science

University of Pittsburgh

2009

UNIVERSITY OF PITTSBURGH

SWANSON SCHOOL OF ENGINEERING

This thesis was presented

by

Jason G. Pickel

It was defended on

October 22, 2009

and approved by

Daniel G. Cole, Ph.D, Assistant Professor

Zhi-Hong Mao, Ph.D, Assistant Professor

William W. Clark, Ph.D, Professor

Thesis Advisor: Daniel G. Cole, Ph.D, Assistant Professor

ADAPTIVE CONTROL FOR THE POSITION OF MAGNETIC PARTICLES USING MAGNETIC TRAPS

Jason G. Pickel, M.S.

University of Pittsburgh, 2009

Magnetic traps are an important instrument for analyzing the behavior of systems and biological processes. They manipulate magnetic particles by applying a force under the influence of magnetic fields. Controlling the position of the magnetic particle for single molecule studies is difficult due to the complexity of the instrument because its dynamics can change per experiment. This results in users spending an immense amount of time designing compensators to meet experimental requirements, yielding insufficient time spent concentrating on the experiment.

One method to alleviate users of designing compensators is to incorporate adaptive control methods into the design of magnetic traps. Adaptive control is able to adjust the parameters of the compensator to ensure the performance of the instrument meets specific requirements. The magnetic particle constantly moves from the Brownian disturbances acting upon it. These disturbances can be minimized by using an adaptive Q-parametrized compensator structure with LMS to minimize a frequency weighted version of the displacement of the magnetic particle for low frequencies.

An adaptive Q-parametrized compensator structure was incorporated into the design of the magnetic trap, resulting in the position of the magnetic particle being stabilized, the effects of the Brownian disturbances being reduced, and the dynamics of the instrument changing into account. The displacement of the magnetic particle due to the Brownian disturbances was suppressed more as the number of FIR weights increased than using the nominal adaptive compensator.

TABLE OF CONTENTS

LIST OF TABLES

LIST OF FIGURES

1.0 INTRODUCTION

The development of single molecule manipulation has allowed biophysicists to gain valuable knowledge of biological processes and molecular functions in real time. By manipulating biomolecules, biophysicists have gained insight into the governing inter-conversion of mechanical and chemical energy in biological processes including: protein folding, DNA elasticity, and the behavior of molecular motors [22, 5].

There are several micromanipulation techniques available to analyze the behavior of biological specimens: optical tweezers, atomic force microscopy, permanent magnet magnetic traps, and electromagnet magnetic traps, that was used for this thesis. There are several advantages electromagnetic magnetic traps offer over the other methods. Permanent magnets offers scientists a tool that is simple, portable, and requires no external power source however their main drawback is the controllability of the magnetic particles [15, 6]. Optical tweezers are able to manipulate microscopic objects using a laser as long as the refractive index is different from the surrounding medium. However optical tweezers could have difficulty analyzing the components of the cell because the cell contains many myriad objects similar to the dielectric particle [17]. This results in the refractive indices of the dielectric particle and the components of the cell being similar, meaning the optical tweezer may no longer be able to selectively operate within the cell. In addition, the laser used to control the dielectric particle can cause localized heating damage to the biological material [15]. Electromagnet magnetic traps have advantages in that the magnetic particle is easily controllable by controlling the current in a electromagnet, that the biological specimen has very low magnetic susceptibility resulting in the magnetic particle being controlled independently within the specimen, and finally that the magnetic particle is controlled by external magnetic fields which eliminates the possibility of localized photodamage [22, 6].

1.1 BACKGROUND

Magnetic tweezers are an important tool used in studying the viscoelastic properties of the cell. The viscoelasticity of the cell is vital for many cellular processes including the transportation of vesicles and the regulation of the cell shape [3]. Analysis of the viscoelastic properties allow insight into how drugs and diseases affect the cell structure while also gaining knowledge of the internal cytoskeleton of the cell. Ziemann studied the frequency dependence of viscoelastic moduli of entangled F-actin networks using magnetic traps to account for the local thermal fluctuations and local inhomogeneities from non equilibrium effects [39]. The results highlight how magnetic traps can be used to study cell locomotion and cellular shape changes. Bausch used a magnetic trap to quantify the viscoelastic property of fibroblasts on the cell envelope. After attaching the fibroblasts to a solid substrate, the three-phasic creep response curves of the cell were analyzed [3]. In addition, Bausch used magnetic tweezers to analyze the viscoelastic moduli of macrophages and the local active forces inside cytoplasm [2].

Magnetic traps are also used in DNA supercoiling analysis, in that the DNA twists to become a double-helical structure. DNA supercoiling has applications in transcription, which is the forming of RNA from the DNA template, the condensation of DNA to prepare for cell division, the separation of homologous chromosomes during the anaphase of mitosis, and the separation of sister chromatids during meiosis [7] [31]. Strick examined the elasticity of linear DNA molecules by attaching magnetic particles to the free ends of DNA and measured the magnetic force applied to the DNA molecules [31]. As a result, Strick analyzed the coiling and uncoiling of DNA by studying the transverse Brownian fluctuations of the DNA using the equipartition theorem [31].

Magnetic traps have been used at the macroscopic level for magnetic drug targeting applications to target certain cells within the body. Possible applications include targeting tumor cells of cancer patients and treating localized diseases like restenosis in coronary arteries [29]. Chemotherapy is a very toxic treatment as it does not differentiate between tumorgenic and healthy cells in the patient. In magnetic drug targeting, magnetic nanoparticles are attached to prescriptions and injected into the patient as a ferro-fluid. The ferro-fluid

is then directed towards the desired location using external magnetic fields [35]. The first applications used static magnetic fields outside the body to move the nanoparticles to the desired locations. However this method targets cells within 5cm of the patient's skin which is not sufficient when the goal is to target cells deep within the body. Shapiro is in the preliminary stages of controlling magnetic nanoparticles deep within the body by using feedback control techniques to manipulate the magnetic fields at the drug targeting location [29]. Once the magnetic nanoparticles are injected into the patient, they move toward the highest field gradient through blood vessels, located at the drug targeting location [35]. The blood vessel will then absorb the nanoparticle, which will move to the targeted cells through the control of the magnetic fields [29].

1.2 MOTIVATION

The open-loop displacement of the magnetic particle is inherently unstable due to Earnshaw's theorem [22]. The particle moves in the direction of the electromagnet that generates the highest field gradient, until the particle contacts the electromagnet. However implementing magnetic traps to examine the behavior or the mechanical properties of biological specimen requires the precise control for the displacement of the magnetic particle. Feedback control techniques must be incorporated into the design of magnetic traps to stabilize the position of the particle by controlling the current in the electromagnets.

The dynamics of the magnetic trap change for each experiment for several reasons. The location of the magnetic particle in solution produces a viscous drag on the particle, however the particle experiences less viscous drag near the bulk of the solution than near the microscope slide or the coverslip. The magnetic properties for the individual particles fluctuate because manufacturers provide the average magnetic properties for a sample of particles [30]. The average magnetic properties are characterized due to the manufacturing processes of the magnetic particles being complex [30]. This results in the magnetic properties of

individual magnetic particles varying from the bulk magnetic properties [30]. In addition to the dynamics changing, Brownian disturbances causes the particle to constantly drift in the solution.

Feedback control techniques must also be incorporated into the design of magnetic traps to compensate for the changes in experimental conditions and to minimize the effects of the Brownian disturbances. However biophysicists are currently spending an enormous amount of time designing compensators to satisfy their experimental conditions which results in minimal time allotted to investigate their experiments. The effort spent on designing compensators highlights the lack of knowledge biophysicists have in control theory.

Automated methods for compensator design can alleviate user's time spent designing controllers. Adaptive control techniques provide one method for automated compensator design by automatically adjusting the control law to change the parameters of the compensator. This ensures the performance of the system meets specified criteria while compensating for the changing dynamics of the micromanipulator. By incorporating adaptive control techniques into the design of magnetic traps, users will be able to concentrate more time and energy into their experiments.

This research demonstrates how adaptive control techniques can be incorporated into the design of magnetic traps to accommodate different experimental conditions while minimizing the effects of the Brownian disturbances. The adaptive controller has a Q-parametrization structure while the parameters are updated using filtered-x least mean squares (FX-LMS) techniques.

1.3 LITERATURE REVIEW

The following section discusses the historical aspects of the critical parts for this work. The background of adaptive control, coprime factorization, and least mean squares will be given.

1.3.1 Adaptive Control

In the 1950's, the design of autopilots for aircraft was critical because an aircraft had to operate at different air speeds and altitudes. Single constant gain compensators were attempted to design the autopilots, however due to the large variations in the conditions, a single constant gain compensator could only obtain good performance at one operating condition [28, 18]. The design of autopilots to operate at the various operating conditions required a more advanced compensation method. The compensation method invented was adaptive control, that changed the parameters of the compensator to the changes in the plant.

The first adaptive control method implemented to design autopilots for aircraft was gain scheduling which occurred in the 1950's and 1960's. Gain scheduling used single constant gain compensators for each operating condition of the plant. This was accomplished by finding auxiliary variables of the system that correlated well to the dynamics of the plant [28]. The advantage of this method is the parameters of the compensator can change quickly as functions of the auxiliary variables. There were several disadvantages to this method: it is an open-loop adaptation resulting in no learning of the system and there had to be a constant gain compensator for every operating condition.

After the gain scheduling method was created, H.P. Whitaker proposed another adaptive control method called model reference adaptive control (MRAC), that adjusted the parameters of the compensator by comparing the output of the feedback system to the output of a reference system that satisfied the design criteria [28, 18]. The parameters of the compensator were adjusted until the difference between the outputs or the error was zero. The first applications updated the compensator parameters until the error was zero using gradient update methods. However, the unknown plant parameters were contained within the gradient updates causing the gradient to be unavailable. The MIT rule was invented to obtain estimates of the unknown plant parameters at certain times. Unfortunately, the closed-loop stability of the compensated system was difficult to prove with the MIT rule because it only worked if the adaptation gain and the magnitude of the reference input were small [28]. Closed-loop stability of the feedback system was determined by P.C. Parks in

1966 through the use of Lyapunov theory. Lyapunov theory determines the update laws for the compensator parameters, causing the error to decrease thus proving the feedback compensated system is stable.

There is another MRAC scheme called the series high-gain scheme. In this scheme, the reference signal is fed into the reference model transfer function, whose output is then fed into a unity feedback system with the feedforward gain being the product of a single constant gain and the plant. The objective is to make the single constant gain very large to yield the resultant transfer function of the feedback loop to be one, resulting in the output of the plant matching the output of the reference model. The disadvantage occurs when the single constant gain becomes very large, resulting in the system saturating, which mask oscillations within the system allowing the value of the single constant gain to go beyond a critical value causing instability [28].

In 1958, R.E. Kalman invented self tuning compensators that update the parameters of the compensator using the certainty equivalence principle. The plant parameters are estimated using a recursive algorithm while the parameters of the compensator are obtained as if the estimated plant parameters are the actual plant parameters.

1.3.2 Coprime Factorization

Fractional representation models to analysis feedback control problems are critical in defining the set of compensators that causes the feedback system to be stable. Dante Youla in 1976 was able to characterize an optimal controller that guaranteed asymptotical stability for a feedback system when the plant is stable, unstable or minimum phase [37]. Youla accomplished this by minimizing a least-square Wiener-Hopf equation. C.A. Desoer in 1980 was able to characterize the set of stabilizing compensators using left and right coprime factorization within a subring instead of a ring of polynomials, while M. Vidyasagar in 1982 concentrated on characterizing the set of stabilizing compensators to multiple input multiple output systems [10, 9, 33]. Characterizing the set of of stabilizing compensators using coprime factorization with a state-space approach was finally implemented in 1982 by

P. Khargonekar and E.Sontag while C.N. Nett derived computational algorithms to obtain the set of stabilizing compensators using coprime factorization with a state-space approach in 1984 [10].

1.3.3 Least Mean Squares

The interest of interpreting observations and making predictions have been around since the Babylonians, who used Fourier series to make their predictions [19]. Galileo Galilei in 1632 began making estimates by minimizing various error functions. The use of least squares has been around since the last 1700's where Gauss was the first person to use this method, however the method was not documented until Legendre in 1805 [19].

Least squares estimation was used to solve stochastic processes by A.N. Kolmogorov in 1939, who derived a comprehensive method of prediction problems for discrete-time stationary processes [19]. M.G. Krien used least squared estimation in 1945 to work on orthogonal polynomials and extended those results to continuous-time using bilinear transformations [19]. N. Wiener in 1942 was the first to provide solutions of stochastic processes using least squares estimation although his work was not published until 1949. [19, 20]. Wiener was interested in deriving a formula to predict the optimal predictor from applications in anti-aircraft fire-control problems, which he used a variational argument to solve [19]. This resulted in Wiener solving the Wiener-Hopf integral equation, which first arose in astrophysics in 1894 [19]. The accomplished of Wiener allowed others to continue his work and make additional contributions to linear filter theory. H.W. Bode and C.E. Shannon in 1950 showed how arbitrary random signals can be represented as an output of a linear system that is excited by white noise [20]. M.C. Yovits and J.L. Jackson derived an expression for the mean square error for an uncorrelated signal and noise, that can be used to determine if the optimal filter is useful for the particular application.

2.0 THEORY

This chapter discusses the theory of the four primary aspects of this project: the modeling of the dynamics of the magnetic particle, the actuation of the magnetic particle, the sensing mechanism to measure the displacement of the magnetic particle, and the control theory needed to stabilize and manipulate the position of the magnetic particle.

2.1 MAGNETIC PARTICLE DYNAMICS

The magnetic trap system is shown in figure 1. The equation of motion (EOM) describing the position of the magnetic particle is:

$$m\ddot{x} + \gamma\dot{x} = F_m + F_e + \tilde{F}_B, \tag{2.1}$$

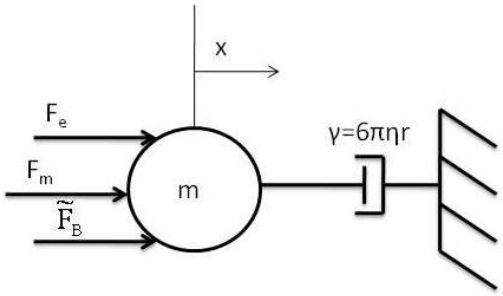

Figure 1: Schematic of the forces applied to a magnetic particle suspended in a fluid medium

where x is the displacement of the magnetic particle, m is the mass of the magnetic particle, and γ is the Stokes drag acting on the magnetic particle due to the surrounding fluid. The external forces applied to the magnetic particle are: the fluctuating Brownian force, $\tilde{F_B}$, the exogenous force, F_e, that may include molecular forces and van der Waals forces, and the magnetic force, F_m, that can be controlled by the electromagnetic current as discussed later.

As the particle moves through the solution due to the magnetic force, there is an additional force acting on the magnetic particle in the opposite direction, a viscous Stokes drag given by

$$\vec{F_s} = -6\pi\eta r\vec{x} = -\gamma\vec{x}, \tag{2.2}$$

where η is the viscosity of the surrounding fluid, r is the radius of the magnetic particle, and $\vec{x}$ is the velocity of the magnetic particle [17] [16]. Stokes drag simplifies the Navier-Stokes equations by neglecting the inertial effects but only holds for low Reynold's numbers [16]. The viscous drag is modeled as a viscous damper, the damping coefficient is $\gamma = 6\pi\eta r$ because the velocity of the particle is on the order of microns per second, yielding the Reynold's number of the magnetic particle being on the order of 10^{-5} [15]. The equation for Stokes drag is valid when the particle is in the bulk of the solution to minimize wall effects associated near the microscope slide or the coverslip [15, 17]. These wall effects can be accounted for by using the Oseen boundary condition term in equation 2.2 [1, 16].

$$\vec{F_s} = -6\pi\eta r\vec{x}[1 + \frac{3}{8}N_{Re} + \frac{9}{40}N_{Re}^2 \ln N_{Re} + O(N_{Re}^2)] \tag{2.3}$$

The transfer function for the magnetic trap, $G_m(s)$, relating the position of the magnetic particle, x, to the applied magnetic force, F_m, is a second order type one system.

$$G_m(s) = \frac{x}{F_m} = \frac{1}{s(ms + \gamma)} \tag{2.4}$$

2.1.1 Brownian Disturbances

The magnetic particle experiences a fluctuating force, $\tilde{F}_B$, in the absence of magnetic forces due to the surrounding water molecules colliding into it. The EOM describing the velocity of the magnetic particle, $\dot{x}$:

$$m\frac{d(\dot{x})}{dt} = -\gamma\dot{x} + \tilde{F}_B, \tag{2.5}$$

where $\gamma = 6\pi\eta r$ is the viscous drag coefficient due to Stokes drag. The water molecules collide into the magnetic particle from all directions yielding the mean displacement of the magnetic particle being zero, $\langle x \rangle = 0$. The magnitude of the fluctuating force is important when designing compensators to eliminate the random motion of the magnetic particle and is characterized by the mean squared displacement of the magnetic particle, $\langle x^2 \rangle$. The mean squared displacement of the magnetic particle is found by multiplying equation 2.5 by the position of the magnetic particle, x, and taking the expected value of both sides.

$$m\left\langle \frac{d(\dot{x})x}{dt} \right\rangle = m\frac{d(\langle x\dot{x}\rangle)}{dt} - m\left\langle \dot{x^2} \right\rangle = -\gamma\left\langle \dot{x}x \right\rangle + \left\langle \tilde{F}_B x \right\rangle \tag{2.6}$$

The fluctuating force is independent of the position of the magnetic particle, resulting in the expected value for the product of the fluctuating force and position of the magnetic particle, $\left\langle \tilde{F}_B x \right\rangle$, being zero. The product for the mass of the particle and its mean squared velocity, $m\left\langle \dot{x^2} \right\rangle$, equals the thermal energy of the system, $k_b T$, due to the equipartition theorem where k_b is Boltzmann's constant and T is the absolute temperature of the water solution in kelvin. The simplification of equation 2.6 yields a first order differential equation in $\langle x\dot{x} \rangle$ with an initial condition that states: the position of the magnetic particle is zero when time is zero.

$$\frac{1}{2}m\left\langle \dot{x^2} \right\rangle = \frac{1}{2}k_b T, \qquad \left\langle \dot{x^2} \right\rangle = \frac{k_b T}{m} \tag{2.7}$$

$$\frac{d\left\langle x\dot{x} \right\rangle}{dt} = \frac{k_b T}{m} - \frac{\gamma}{m}\left\langle x\dot{x} \right\rangle, \qquad x(t=0) = 0 \tag{2.8}$$

Solving for $\langle x\dot{x} \rangle$ produces a first order differential equation for the mean squared displacement of the magnetic particle, $d\left\langle \dot{x^2} \right\rangle/(dt)$. The solution of $\langle x^2 \rangle$ allows the control engineer to

analyze the effects of the random motion of the magnetic particle due to the fluctuating force.

$$\langle x\dot{x}\rangle = \frac{1}{2}\frac{d\langle x^2\rangle}{dx} = \frac{k_bT}{\gamma}(1-\exp\frac{-t}{\tau}), \qquad \tau = \frac{m}{\gamma} \tag{2.9}$$

$$\left\langle x^2\right\rangle = \frac{2k_bT}{\gamma}(t-\tau(1-\exp\frac{-t}{\tau})) \tag{2.10}$$

The mean squared displacement of the magnetic particle is found to be proportional to time when the magnetic particle is in the water solution for a longer time duration than the characteristic time $t \gg \tau$. This results in the random motion of the magnetic particle due to the fluctuating force being unstable.

$$\left\langle x^2\right\rangle = \frac{2k_bT}{\gamma}t \tag{2.11}$$

The fluctuating disturbances acting on the magnetic particle has two effects: its the resistive force acting on the magnetic particle as it moves through the solution due to Stokes drag and the driving force that causes the particle to constantly move. These effects are from the same source resulting in the viscosity of the water solution being related to the magnitude of the fluctuating force. As the particle moves through the solution due to the fluctuating force, the particle experiences a resistive viscous force due to the water molecules it collides into. These effects are related by analyzing the system using energy methods. Kinetic energy is added to the system as a result of the water molecules colliding into the magnetic particle, however the kinetic energy of the system is decreased as the magnetic particle moves through the solution due to the viscous effects. The expression relating the change in the kinetic energy of the system from the interaction between the magnetic particle and the water molecules is obtained by the following: multiplying equation 2.5 by the velocity of the magnetic particle, integrating with respect to time and taking the expected value.

$$\frac{1}{2}m\left\langle \dot{x^2}\right\rangle |_{t_1}^{t_2} = \int_{t_1}^{t_2}(\left\langle \tilde{F}_B\dot{x}\right\rangle - \gamma\left\langle \dot{x^2}\right\rangle)dt \tag{2.12}$$

The kinetic energy in the system is constant due to the equipartition theorem yielding $\left\langle \tilde{F}_B\dot{x}\right\rangle$ being equal to $\gamma\left\langle \dot{x^2}\right\rangle$ in equation 2.12.

$$\left\langle \tilde{F}_B\dot{x}\right\rangle = \gamma\left\langle \dot{x^2}\right\rangle = \frac{\gamma k_bT}{m} \tag{2.13}$$

$\left\langle \tilde{F}_B \dot{x} \right\rangle$ can be further simplified by solving for the velocity of the particle in equation 2.5, multiplying by the fluctuating force and then taking the expected value:

$$\left\langle \tilde{F}_B \dot{x} \right\rangle = \exp\left(\frac{-t}{\tau}\right) \left\langle \tilde{F}_B v_o \right\rangle + \frac{1}{m} \int_0^t \exp\left(\frac{-(t-s)}{\tau}\right) \left\langle \tilde{F}_B \tilde{F}_B(s) \right\rangle ds, \tag{2.14}$$

where v_o is the initial velocity of the magnetic particle. As the time that the magnetic particle is in the solution becomes much greater than the characteristic time, the following assumption is usually made: the fluctuating forces, $\tilde{F}_B(t)$ and $\tilde{F}_B(s)$, are only correlated over infinitesimally time scales.

$$\left\langle \tilde{F}_B \tilde{F}_B(s) \right\rangle = \sigma^2 \delta(t-s), \qquad \sigma^2 = 2\gamma k_b T \tag{2.15}$$

The position of the magnetic particle is open-loop stable because its mean squared displacement is proportional to time due to the fluctuating force acting upon it. The position of the magnetic particle from the Brownian disturbance cannot be confined to a stable equilibrium point using time-independent magnetic fields due to Earnshaw's theorem [22].

Theorem 1 Earnshaw's theorem: *Time-independent magnetic fields cannot confine a magnetic particle to a stable equilibrium point.*

2.2 MAGNETIC FORCES ACTING ON THE PARTICLE

Magnetic traps are a crucial micromanipulator biophysicists use to manipulate biological specimen. The behavior of the biological specimen is examined by applying magnetic forces to micron sized magnetic particles attached to the specimen [8, 22].

The magnetic force, $\vec{F}_m$, acting on the magnetic particle depends upon the particle's magnetic dipole moment, $\vec{m}$, and the applied magnetic field, $\vec{B}$. The particle's magnetic dipole moment is the product of the magnetization of the particle, $\vec{M}$, and the volume of the particle, V.

$$\vec{F}_m = \vec{m} \cdot \nabla \vec{B} \tag{2.16}$$

$$\vec{m} = \vec{M} V \tag{2.17}$$

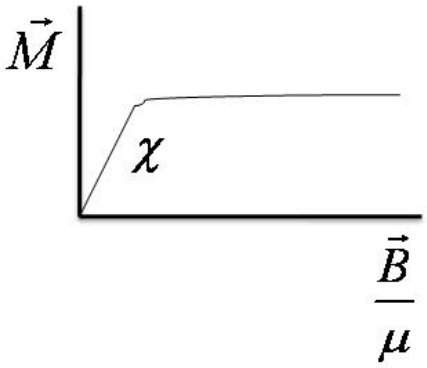

Figure 2: Plot showing how the magnetization of the particle depends upon the applied magnetic field

The magnetization of the particle is proportional to the applied magnetic field by the following: χ/μ_o, where χ is the susceptibility of the particle and μ_o, $400\pi(10^{-9})$ H/m, is the permeability of free space.

$$\vec{M} = \frac{\chi}{\mu_o}\vec{B} \tag{2.18}$$

The susceptibility of the particle describes the ability of the particle's magnetic dipole moments to align in the direction parallel to the applied magnetic field, $\vec{B}$ [14, 26]. The magnetic dipole moments will align in the direction parallel to the applied magnetic field as the magnitude of the field increases. The magnetic dipole moments will continue to align until the particle is magnetically saturated, which implies increasing the magnitude of the magnetic field no longer has an effect on the magnetization of the particle as shown in figure 2 [17]. The manipulation of the particle requires a change in the magnitude of the magnetic field producing a corresponding change in the magnetization of the particle. This results in the linear region of figure 2 being of interest.

The magnetic dipole moment of the particle can be expressed as a function of the applied magnetic field by substituting equation 2.18 into equation 2.17. This results in the magnetic force being a function of the magnetic field, $\vec{B}$, and the field gradient, $\nabla\vec{B}$.

$$\vec{m} = \frac{V\chi}{\mu_o}\vec{B} \tag{2.19}$$

$$\vec{F}_m = \frac{V\chi}{\mu_o}\vec{B}\cdot\nabla\vec{B} \tag{2.20}$$

The following assumption is made to simplify the analysis: the magnetic field only has a x component, $B_y = B_z = 0$, reducing the magnetic force in equation 2.20 to

$$F_m = \frac{V\chi}{\mu_o}B_x\frac{\partial B_x}{\partial x}. \tag{2.21}$$

The magnetic field, B_x, acting on the magnetic particle due to the electromagnets can be modeled as a tightly wound solenoid:

$$B_x = \frac{\mu_o N a^2}{2(x^2+a^2)^{\frac{3}{2}}}I \tag{2.22}$$

where a is the radius of the coils, N is the number of turns, x is the distance between the particle and the electromagnet along the electromagnet's axis, and I is the current in the electromagnet [38]. The magnetic field is proportional to the current in the electromagnet, $B_x = \beta I$, where β depends upon the radius of the coils, number of coils, and the distance between the particle and electromagnet along the electromagnet's axis [38]. Since the magnetic field depends upon the distance between the particle and the electromagnet, and a multiple electromagnet setup is used, the following assumption is made to simplify the analysis: the particle is located at the center of the electromagnet setup causing the proportionality constant, β, to be equal for all electromagnets.

The field gradient, $\partial B_x/\partial x$, is found by taking the derivative of the magnetic field in equation 2.22 with respect to x.

$$\frac{\partial B_x}{\partial x} = -\frac{\frac{3}{2}\mu_o N x a^2}{(x^2+a^2)^{\frac{5}{2}}}I \tag{2.23}$$

The relationship between the magnetic force, F_m, and the current in the electromagnet, I, is nonlinear by substituting the magnetic field and the field gradient, equation 2.22 and equation 2.23 respectively, into equation 2.21. This nonlinear relationship does not permit the use of linear control theory.

$$F_m = \frac{-3}{4}\frac{V\chi\mu_o x(Na^2)^2}{(x^2+a^2)^4}I^2 \tag{2.24}$$

Linear control theory is used by using the following variables to create a linear relationship between the magnetic force and the current in the electromagnet: define the nominal current in the electromagnets, $\overline{I}$, and the change in the current between the electromagnets, ΔI. These variables are arranged for $\overline{I}$ is constant while ΔI changes, yielding a linear relationship between the magnetic force and the change in the current of the electromagnet, where I_1 and I_2 are the currents in the respective electromagnets.

$$\overline{I} = \frac{I_1 + I_2}{2}, \qquad \Delta I = \frac{I_2 - I_1}{2} \tag{2.25}$$

The transfer function relating the magnetic force to the change of the current in the electromagnets is found by redefining the magnetic field and the field gradient in terms of $\overline{I}$ and ΔI as discussed below.

The magnetic fields produced by the electromagnet setup are approximated to decrease with distance exponentially as shown in figure 3. The decay rates for the magnetic fields are λ_1 and λ_2 for electromagnet 1 and electromagnet 2 respectively. The following assumption is made to simplify the analysis: the decay rate for the electromagnets are the same, $\lambda = \lambda_1 = \lambda_2$.

$$B_1(x) = B_1 e^{-\lambda x}, \qquad B_2(x) = B_2 e^{\lambda(x-L)}. \tag{2.26}$$

The total magnetic field, B_x, at the center of the electromagnet configuration is found by the following analysis:

- The total magnetic field between the electromagnets, $B_x(x)$, is found by superimposing the individual magnetic fields produced by the separate electromagnets in equation 2.26.
- Simplifying the exponents of the individual magnetic fields using first order Taylor series expansion

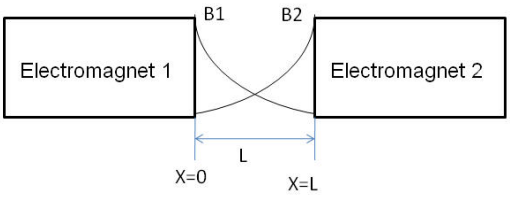

Figure 3: Magnetic fields from each electromagnet for one dimensional analysis where L is the distance between electromagnets, and B_1 and B_2 are the magnitude of the respective electromagnets

- Evaluating $B_x(x)$ at $x = L/2$, the location of the magnetic particle.

The Taylor series approximation for the exponents of the individual magnetic fields are: $e^{-\lambda x} = 1 - \lambda x$ and $e^{\lambda(x-L)} = 1 + \lambda(x - L)$ for $B_1(x)$ and $B_2(x)$ respectively. These first order approximations are valid if the characteristic length that the magnetic field decays, $L_c = 1/\lambda$, is longer than the distance the magnetic particle moves, x, or $||\lambda x|| \ll 1$. The total magnetic field is found by substituting these first order approximations into equation 2.26 and superimposing the individual magnetic fields.

$$B_x(x) = B_1(1 - \lambda x) + B_2(1 + \lambda x - \lambda L) \tag{2.27}$$

The following assumption is made to further simplify the calculations for the total magnetic field acting on the magnetic particle: the electromagnet's decay characteristic length is equated to the length between the electromagnets, $L_c = L = 1/\lambda$. The total magnetic field, B_x, acting on the magnetic particle is found by evaluating equation 2.27 at $x = L/2$.

$$B_x = \frac{B_1 + B_2}{2} = \beta\frac{I_1 + I_2}{2} = \beta\overline{I} \tag{2.28}$$

The total field gradient, $\partial B_x/\partial x$, acting on the particle is found by taking the derivative of the total magnetic field with respect to x and applying the following assumption already given, $L_c = L = 1/\lambda$.

$$\frac{\partial B_x}{\partial x} = \frac{B_2 - B_1}{L} = \frac{2\beta}{L}\frac{I_2 - I_1}{2} = \frac{2\beta}{L}\Delta I \tag{2.29}$$

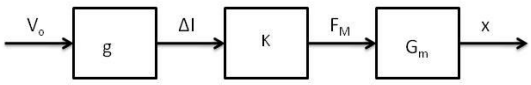

Figure 4: Block diagram for the plant

The linear relationship relating the applied magnetic force, F_m, to the change in the current of the electromagnets, ΔI, is found by substituting equation 2.28 and equation 2.29 for the magnetic field and field gradient respectively into equation 2.21.

$$F_m = \kappa \Delta I, \qquad \kappa = \frac{2\bar{I}V\chi\beta^2}{\mu_o L} \tag{2.30}$$

2.2.1 Resulting Dynamics of the Actuator and Plant

The total system is composed of 3 subsystems shown in figure 4, which are: g is the transconductance amplifier, κ is the gain of the magnet, and G_m is the transfer function relating the displacement of the magnetic particle to the applied magnetic force. The transfer function for the system, $G(s)$, yields a linear relationship between the input voltage of the amplifier, V_o and the position of the magnetic particle, x.

$$G(s) = g\kappa G_m(s) = \frac{x}{V_o} = \frac{g\kappa}{s(ms+\gamma)} \tag{2.31}$$

2.3 SENSOR

Sensors are a vital aspect of feedback controls by measuring the states of the system quantitatively. These measurements are compared to the desired values to determine if the system is performing correctly.

2.3.1 Sensing Principle

Feedback control for the magnetic particle requires the use of a position sensor and laser for the comparison of its actual position with its desired position. The laser enters the optical axis of the microscope using a dichroic mirror and strikes the particle, resulting in the scattered light off the magnetic particle being reflected in both the forward and backward directions. The scattered light contains the information about the displacement of the magnetic particle in both directions [12, 34]. The advantage of measuring the backward scattered light is the measurements can be performed on non-transparent particles, like magnetic particles.

The position sensor to measure the displacement of the magnetic particle is a quadrant photodiode, QPD. The QPD must be placed at the back focal plane of the microscope objective to measure the angular spectrum of the reflected light to obtain accurate measurements. However the sensing laser passes through the back focal plane of the microscope, resulting in an optical system being created to translate the angular spectrum of the reflected light for measurements. The optical system is shown in figure 5, where the beam splitting cube, BSC, redirects the reflected light for the QPD to measure its intensity.

The displacement of the magnetic particle is measured by examining the intensity distribution of the reflected light at the QPD. When the particle is at the center of the laser, the intensity distribution of the reflected light will be symmetric, however if the particle is off center, the resulting intensity distribution will not be symmetric. This results in the displacement of the particle not causing a change in the displacement of the reflecting light striking the QPD, but a change in the location of the maximum of the intensity distribution as shown in figure 6 [21].

2.3.2 QPD

The QPD quantitatively measures the displacement of the particle by converting the photons of the reflected light into current for four diodes simultaneously. When the laser is striking the center of the QPD, the difference between the sum of the two top diodes and the bottom two diodes is zero while the sum of the two right diodes and the two left diodes is zero.

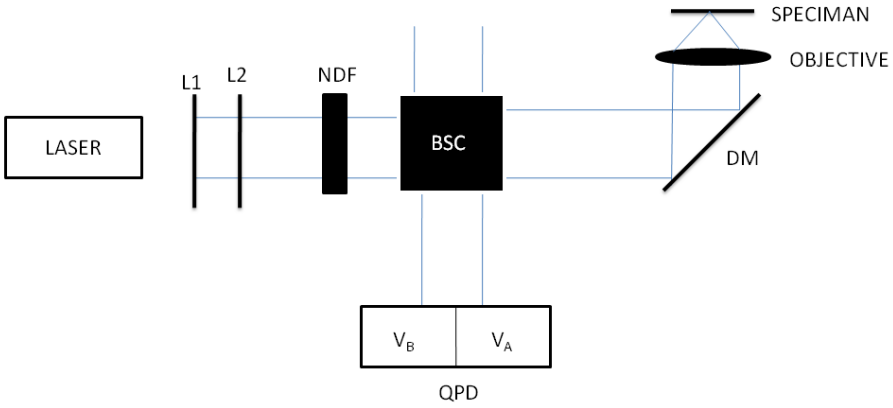

Figure 5: Schematic of the optical system to translate the angular intensity of the reflected light: The laser is expanded then enters the optical path of the microscope by a dichroic mirror. The backward scattered light is redirected by a beam splitting cube to be measured by the QPD. The neutral density filter, NDF, reduces the amount of light power that passes through for all frequencies.

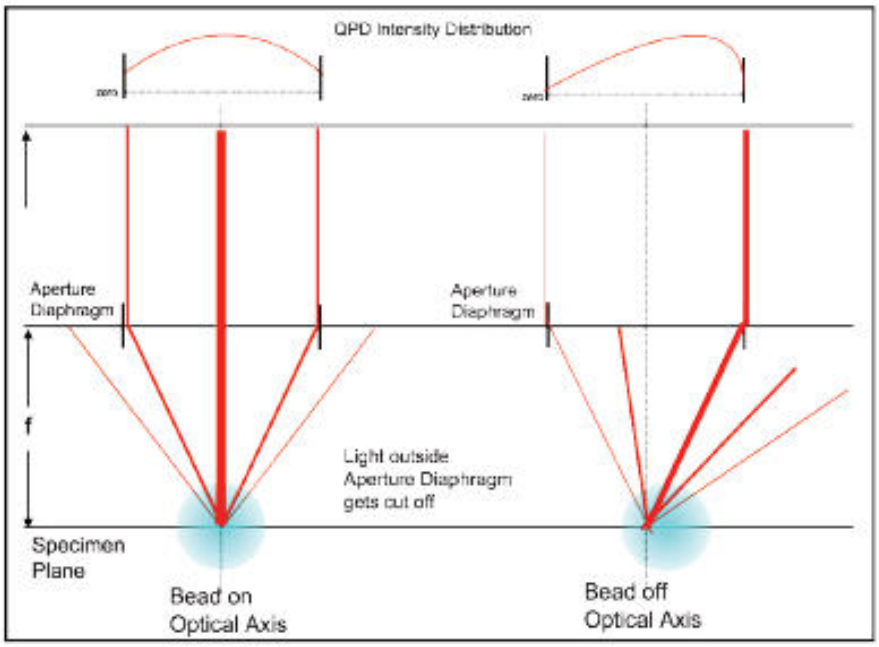

Figure 6: Illustrates that a displacement in the particle does not translate the backward scattered light striking the QPD. The displacement of the particle translates in the movement of the maximum light intensity striking the QPD resulting in displacement measurements.

The actual position of the particle is determined using the difference signals of the QPD. The x difference signal measures the position of the particle in the x direction by subtracting the current from the two right diodes from the two left diodes, while the y difference signal measures the y position of the particle by subtracting the current from the two top diodes from the two bottom diodes as shown in figure 7 [21]. These QPD difference signals are compared with the desired signals to determine if the magnetic particle is located at the desired position. The response of the QPD difference signals as the particle moves from the negative direction to the position direction on a particular axis is shown in figure 8 [21]. The displacement measurements of the particle requires a proportional change in the output voltage of the sensor to movements of the particle. This requires the measurements being performed in the linear region of figure 8.

2.4 CONTROLLER PARAMETRIZATION

This section discusses methods to parametrize all controllers using Q-parametrization techniques by characterizing the entire set of stabilizing controllers that makes the feedback system as shown in figure 9 internally stable. Controller parametrization is useful to adaptive control theory because it enables the designer to characterize the entire set of stabilizing controllers, $\mathcal{K}$. Even though the entire set of controllers stabilizes the feedback system, not all controllers will have good nominal performance or robust stability.

The theory for internal stability will be discussed first to further understand what the entire set of controllers is accomplishing. Next, the design for the set of controllers using both transfer function and state-space techniques are discussed. State-space techniques are discussed because the controller parametrization will be performed using state-space methods and provides useful numerical tools for building controllers. The theory of least mean squares, LMS, is discussed because this will be used to update the parameters of the adaptive compensator.

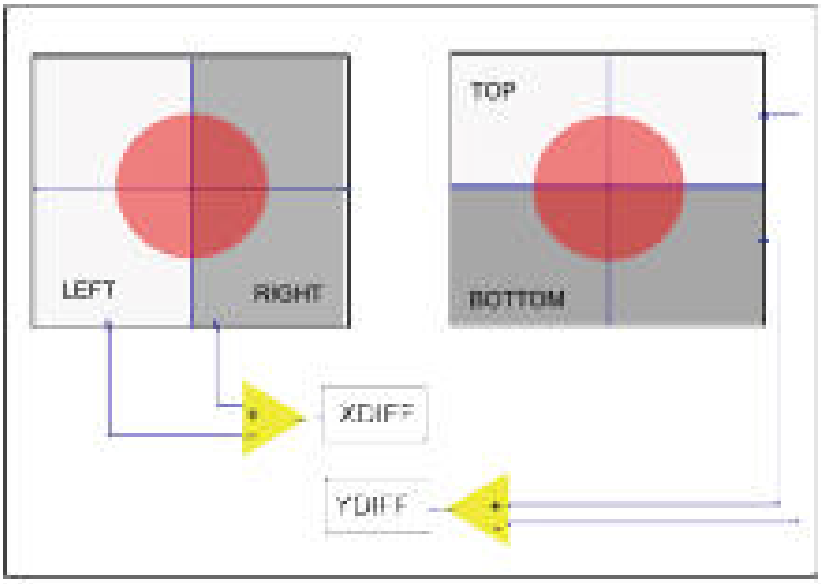

Figure 7: The difference channels of the QPD are the two important signals used to determine the position of the bead.

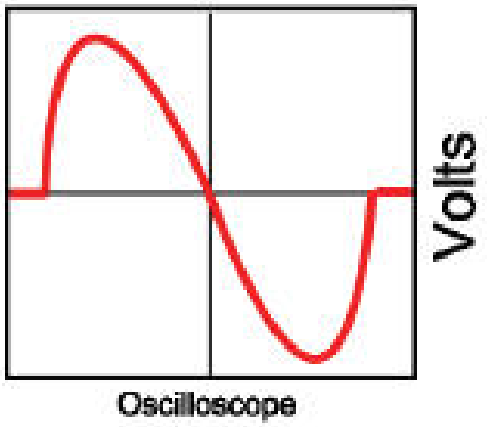

Figure 8: The response of the difference channel of the QPD while the bead is moving in the positive direction of the axis.

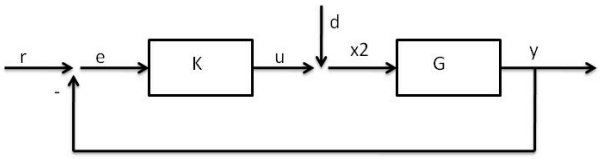

Figure 9: Traditional feedback control loop. r is the desired reference signal, y is the output signal of the controlled system, K is the controller, G is the plant, d is the feedforward disturbance, u is the control signal, e is the error between the desired signal and output signal and x_2 is the input into the plant. [10]

2.4.1 Internal Stability of Feedback Systems

All linear feedback control systems have the following components: a sensor, F, that measures the output y, a plant, G, and a controller, K, that changes the dynamics of the system to meet specified requirements as shown in figure 10 [10]. The input signal for each component is composed of two signals: an external signal and an internal signal. The input signal for the components are composed of the following signals [10]:

- The input of the compensator, x_1, is composed of: r the reference signal and v the output of the sensor
- The input of the plant, x_2, is composed of: d the feedforward disturbance and u the control signal
- The input of the sensor, x_3, is composed of: n the measurement noise and y the output of the system

Internal stability is critical because an internal signal within the feedback system can be unstable while the closed-loop transfer function is stable, causing adverse effects on the system [10]. The system is internally stable if and only if all transfer functions from the external signals: r, d, and n to the input signals of the components: x_1, x_2, and x_3 are stable. The system is internally stable when the external inputs are bounded in magnitude resulting in the input signals of the components being bounded in magnitude [10]. The

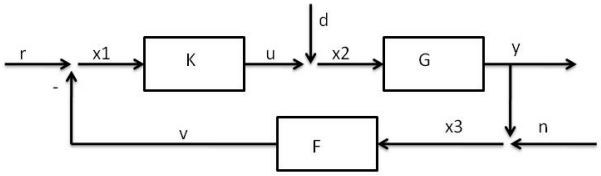

Figure 10: Traditional feedback control loop. r is the desired reference signal, y is the output signal of the controlled system, K is the controller, G is the plant, F is the sensor, d is the feedforward disturbance, n is measurement noise, u is the control signal, v is the sensor output, and $x1$, $x2$, and $x3$ are the input signals for the system components [10].

external signals of the feedback system can be expressed as a function of the input signals of the components in matrix form in the following way:

$$\begin{bmatrix} 1 & 0 & F \\ -K & 1 & 0 \\ 0 & -G & 1 \end{bmatrix} \begin{pmatrix} x_1 \\ x_2 \\ x_3 \end{pmatrix} = \begin{pmatrix} r \\ d \\ n \end{pmatrix}. \tag{2.32}$$

The closed-loop transfer functions relating the input signals of the components to the external signals were found by solving for the input signals of the components: x_1, x_2, and x_3 in equation 2.32. The feedback system is internally stable if the following conditions hold for equation 2.33 [10].

$$\begin{pmatrix} x_1 \\ x_2 \\ x_3 \end{pmatrix} = \frac{1}{1+GKF} \begin{bmatrix} 1 & -GF & -F \\ K & 1 & -KF \\ GK & G & 1 \end{bmatrix} \begin{pmatrix} r \\ d \\ n \end{pmatrix} \tag{2.33}$$

1. The roots of $1+GKF$ are in the unit disk because the compensator is designed digitally.
2. There are no pole-zero cancellations in the loop gain of the system, GKF, outside or on the unit disk.
3. The plant, G, is strictly proper while both the compensator, K, and the sensor, F, are proper to ensure $1+GKF$ is not strictly proper.

2.4.2 Controller Parametrization Using Transfer Function Techniques

This section discusses the conditions to find the entire set of controllers, $\mathcal{K}$, that internally stabilizes the feedback system without considering the stability of the plant. First, the expression for the plant using coprime rational functions is discussed followed by the criterion the coprime rational functions must satisfy for the compensator to achieve internal stability. Finally, the method for internally stabilizing the feedback system using Q-parametrized methods is discussed.

2.4.2.1 Coprime Factorization of the Plant The plant, G, is written as a ratio of coprime rational functions: $N, M \in \mathcal{S}$ where $\mathcal{S}$ implies all stable, proper, and real-rational functions [10]. Coprime implies no common roots in the numerator and denominator. The plant can only be written as a ratio of coprime rational functions if there exists two additional rational functions: $X, Y \in \mathcal{S}$ that satisfies the Bezout identity [10].

$$G = \frac{N}{M} : N, M \in \mathcal{S} \tag{2.34}$$

$$NX + MY = 1 \tag{2.35}$$

2.4.2.2 Entire Set of Stabilizing Controllers Using Q-parametrization A controller, K, is in the entire set of stabilizing controllers, $\mathcal{K}$, for the feedback system only if Q is in $\mathcal{S}$ [10]. The controller can also be written as a ratio of coprime factorization in $\mathcal{S}$, N_c and M_c [10].

$$\mathcal{K} = \left\{ K = \frac{X + MQ}{Y - NQ} : Q \in \mathcal{S} \right\} \tag{2.36}$$

$$K = \frac{N_c}{M_c}, \qquad N_c = X + MQ, \qquad M_c = Y - NQ \tag{2.37}$$

There is a uniqueness property about the Q-parametrized compensator that states: for a given internal stabilizing controller K and a set of coprime rational functions, there can only be one $Q \in \mathcal{S}$ that satisfies equation 2.36. This uniqueness property is vise versa, for a given

$Q \in \mathcal{S}$ and a set of coprime rational functions, there can only be one internally stabilizing controller K.

$$Q = \frac{YK - X}{NK + M} : Q \in \mathcal{S} \tag{2.38}$$

The Q-parametrized compensator internally stabilizes the unity feedback system as shown in figure 9, if the transfer functions relating the input signals of the components: e and x_2 to the external signals: r and d are stable. This implies the roots of $1 + GK$ must have magnitudes less then one for stability.

$$\begin{pmatrix} e \\ x_2 \end{pmatrix} = \frac{1}{1 + GK} \begin{bmatrix} 1 & -G \\ K & 1 \end{bmatrix} \begin{pmatrix} r \\ d \end{pmatrix} \tag{2.39}$$

2.4.2.3 Transforming a Feedback Controls Problem into a Model-Matching Problem There are four closed-loop transfer functions that are expressed in equation 2.39. These closed-loop transfer functions are: the sensitivity function, S, the complementary sensitivity function, T, the product of the plant and sensitivity function, GS, and the product of the compensator and sensitivity function, KS. These closed-loop transfer functions can be expressed by the coprime rational functions using equation 2.34 and equation 2.36 for the plant and controller respectively.

$$S = M(Y - NQ) \tag{2.40}$$

$$T = N(X + MQ) \tag{2.41}$$

$$GS = N(Y - NQ) \tag{2.42}$$

$$KS = M(X + MQ) \tag{2.43}$$

By expressing these transfer functions using the coprime rational functions, the feedback control problem was turned into a feedforward control problem since those relationships are affine in Q. This makes adaptation easy since LMS can be used to update the dynamics of the Q parameter in equation 2.36. Feedforward control techniques is used to update Q using adaptive filter theory, resulting in an adaptive compensator as discussed later.

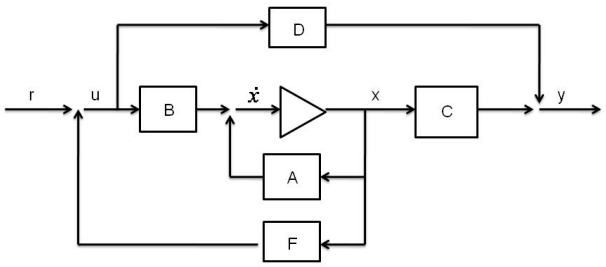

Figure 11: Schematic of the state feedback block diagram where the states are $x \in R^{n\times 1}$ and $F \in R^{1\times n}$. The triangle represents integration. M and N are the transfer functions: u/r and y/r respectively.

2.4.2.4 Controller Design Using State-Space Techniques This section discusses the theory of Q-parametrized compensation using state-space methods.

Controller parameterization can also be implemented using state-space techniques. The state-space representation for the plant, G, is

$$G \sim \begin{bmatrix} A & B \\ C & D \end{bmatrix}, \tag{2.44}$$

where A is the state matrix, B is the input matrix, C is the output matrix, and D is the feedforward matrix. The dimensions for each matrix are given in terms of the number of states, n, the number of inputs, q, and the number of outputs, p, as follows: $A \in R^{n\times n}$, $B \in R^{n\times q}$, $C \in R^{p\times n}$ and $D \in R^{p\times q}$.

The state-space representations for the coprime rational polynomials of the plant: $N, M \in \mathcal{S}$ are obtained similarly to state feedback design. If the plant is controllable, a matrix $F \in R^{1\times n}$ can be chosen to find N and M [10, 4]. The state space representations for M and N are from r to u and r to y respectively from figure 11.

$$\begin{aligned} M &\sim \begin{bmatrix} A+BF & B \\ F & 1 \end{bmatrix} \\ N &\sim \begin{bmatrix} A+BF & B \\ C+DF & D \end{bmatrix} \end{aligned} \tag{2.45}$$

The state space representations for the additional coprime rational functions: $X, Y \in \mathcal{S}$ are obtained by choosing a real matrix H, $H \in R^{n\times 1}$, that causes the state matrix, $A+HC$, to be stable [10].

$$\begin{aligned} X &\sim \begin{bmatrix} A+HC & H \\ F & 0 \end{bmatrix} \\ Y &\sim \begin{bmatrix} A+HC & -B-HD \\ F & 1 \end{bmatrix} \end{aligned} \tag{2.46}$$

2.4.3 Least Mean Squares

This section discusses how the parameters of the Q-parametrized compensator are updated using a least mean square (LMS) approach. The Q parameter in the Q-parametrized compensator is modeled as a finite impulse response (FIR) filter. LMS is used to update the weight coefficients of the Q parameter, resulting in an adaptive compensator. The theory of LMS is explained through the theory of the steepest descent method.

2.4.3.1 Steepest Descent Method LMS algorithm is based on minimizing a cost function. The mean squared error, $J(n)$, is the quadratic cost function that expresses the expected square of the error, $e(n)$, for each discrete time step, n [25]. The error $e(n)$ is the difference between the desired signal, $d(n)$, and the estimated signal, $y(n)$.

$$J(n) = \frac{1}{2}E[e^2(n)] \tag{2.47}$$

LMS is a recursive method used to adaptively adjust the FIR filter coefficients to produce an estimated signal of the desired signal using a linear combination of the input signal, $x(n)$, in such a way to minimize $J(n)$ [25]. The block diagram representation of filter optimization is shown in figure 12. The desired signal is a single value at each time step resulting in the estimated signal being the inner product between the weight coefficients, $\vec{w}(n)$, and the filter input, $\vec{x}(n)$ at each time step [25].

$$y(n) = \vec{w}(n)^T\vec{x}(n)) \tag{2.48}$$

$$e(n) = d(n) - y(n) = d(n) - \vec{w}(n)^T\vec{x}(n) \tag{2.49}$$

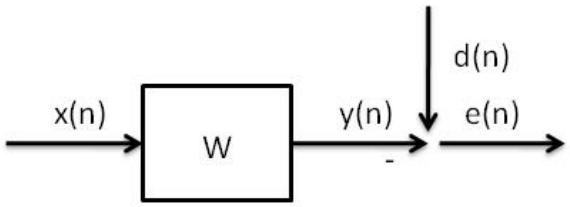

Figure 12: Block diagram representation of filter optimization. w is the filter weights, $d(n)$ is the desired signal, $y(n)$ is the estimate signal, $x(n)$ is the input signal into the tapped delay line, and $e(n)$ is the error signal.

The cost function, $J(n)$, can be rearranged by substituting the error, equation 2.49, into equation 2.47, where σ_d^2 is the expected value for the variance of the desired signal, p_{dx} is the expected value of the cross correlation between $x(n)$ and $d(n)$, and R_x is the expected value for the correlation matrix of the input, $x(n)$ [25].

$$J(n) = \frac{1}{2}\sigma_d^2 - \vec{w}(n)^T p_{dx} + \frac{1}{2}\vec{w}(n)^T R_x \vec{w}(n) \tag{2.50}$$

$$\sigma_d^2 = E[d^2(n)] \tag{2.51}$$

$$\vec{p}_{dx} = E[d(n)\vec{x}(n)] \tag{2.52}$$

$$\vec{R}_x = E[\vec{x}(n)\vec{x}^T(n)] \tag{2.53}$$

The weight coefficients, $\vec{w}(n)$, are continuously updated until their optimal values are reached. The optimal weight coefficients, $\vec{w}^\circ(n)$, results in the minimum distance between the weight coefficient space and the minimum point on $J(n)$ [25]. The conditions for the weight coefficients to achieve these optimal coefficients are [25]:

- The gradient of $J(n)$ with respect to the weight coefficients, $\partial J(n)/\partial \vec{w}$, is zero

$$\frac{\partial J(n)}{\partial \vec{w}(n)} = 0 \tag{2.54}$$

- The second derivative of $J(n)$ with respect to the weight coefficients is positive

$$\frac{\partial^2 J(n)}{\partial \vec{w}^2(n)} > 0 \tag{2.55}$$

The gradient of the cost function, $\partial J(n)/\partial \vec{w}$, is obtained by taking the derivative of $J(n)$ with respect to the weight coefficients, $\vec{w}(n)$. The optimal weight coefficients are found by solving for $\vec{w}(n)$ in equation 2.56 [25].

$$\frac{\partial J(n)}{\partial \vec{w}} = -\vec{p}_{dx} + \vec{R}_x \vec{w}(n) \tag{2.56}$$

$$\vec{w}^{\circ}(n) = \vec{R}^{-1}\vec{p}_{dx} \tag{2.57}$$

The weight coefficients are updated by adjusting the current weight coefficients in the negative direction of the cost function gradient to find the weight coefficients at the next time step, $\vec{w}(n+1)$ [25]. The weight coefficients are updated as a function of μ, a step-size parameter at each time step. The step-size parameter value is important because it must be small to ensure convergence to the optimal weight coefficients however a small value leads to long convergence times [32].

$$\vec{w}(n+1) = \vec{w}(n) - \mu \frac{\partial J(n)}{\partial \vec{w}} \tag{2.58}$$

2.4.3.2 Least Mean Square Algorithm

The weight coefficients are updated with LMS similar to the steepest descent method. The necessity of using LMS is the instantaneous estimates of $\vec{p}_{dx}$ and $\vec{R}_x$ are used instead of their expected values in the gradient of the cost function [25]. The weight coefficients at the next time step, $\vec{w}(n+1)$, are dependent upon the error signal, $e(n)$, and the input signal, $x(n)$ [25].

$$\vec{w}(n+1) = \vec{w}(n) - \mu[-d(n)\vec{x}(n) + \vec{x}(n)\vec{x}^T(n)\vec{w}(n)] = \vec{w}(n) + \mu e(n)\vec{x}(n) \tag{2.59}$$

The weight coefficients will remain constant once their optimal values have been reached. However a change in the desired signal produces a nonzero error signal, resulting in the weight coefficients being updated again until their optimal values are reached.

An alternative method of obtaining the weight coefficients is by substituting the instantaneous estimate for the gradient of the cost function, $\partial J(n)/\partial \vec{w}(n)$, into equation 2.58. The

gradient of the cost function is simplified by recalling the error is a function of the weight coefficients as shown in equation 2.49.

$$J(n) = \frac{1}{2}e(n)^2 \tag{2.60}$$

$$\vec{w}(n+1) = \vec{w}(n) - \mu\frac{J(n)}{\vec{w}(n)} = \vec{w}(n) - \mu e(n)\frac{\partial e(n)}{\partial \vec{w}(n)} \tag{2.61}$$

The adaptation of the FIR weight coefficients of the Q parameter in the Q-parametrized compensator is important because LMS is used to adjust the weight coefficients to yield an adaptive compensator.

2.4.3.3 Leaky Least Mean Square Algorithm While performing the experiments of the adaptive compensators, leaky LMS was used to stabilize the LMS algorithm. The LMS algorithm may not have converged because an eigenvalue of the correlation matrix for the input signal was 0 [25]. To prevent the undamped modes becoming unstable, these modes can be forced to 0 using a leakage factor, γ, whose magnitude is less than 1 [25]. Leaky LMS is similar to normal LMS, equation 2.61, except there is a leakage factor. Another difference between the normal LMS and leaky LMS occurs when the step-size parameter is suddenly set to zero. When the step-size parameter is suddenly set to zero, the weight coefficients remains constant for normal LMS however the weight coefficients will gradually decay to zero using leaky LMS [36].

$$\vec{w}(n+1) = \gamma\vec{w}(n) - \mu e(n)\frac{\partial e(n)}{\partial \vec{w}(n)} \tag{2.62}$$

The weight coefficients are updated using normal LMS by placing equal emphasis on all the past weight coefficients. However due to the leakage factor being less than one, the weight coefficients are updated by placing more emphasis on the recent past weight coefficients by suppressing the weight coefficients that occurred in the beginning. The weight coefficients at time step k are dependent upon the initial weight coefficients and the sum of the product of the step-size parameter and the gradient of the cost function with respect to the weight coefficients.

$$\vec{w}(n+k) = \gamma^k\vec{w}(n) - \Sigma_{i=1}^{k}\gamma^{k-i}\mu e(n+i-1)\frac{\partial e(n+i-1)}{\partial \vec{w}(n+i-1)}. \tag{2.63}$$

2.5 ROBUST CONTROL

This section discusses the theory of nominal performance and robust stability. The nominal performance for the compensated feedback system quantifies the ability of the compensator to meet certain design criteria like rejecting disturbances or tracking reference signals. Typically compensators are designed for the nominal plant, the mathematical representation of the true system. However the nominal plant does not always contain all the dynamics of the true system either because the system is too complex or there is a computational limitation. Robust stability characterizes the ability of the compensator to internally stabilize a set of plants that contains the true plant to account for the unmodeled dynamics.

2.5.1 Nominal Performance

The convergence of the feedback system to its reference signal in the presence of unknown disturbances is an important consideration in control theory. However control engineers seldomly design compensators for a single disturbance or reference signal. This results in engineers relaxing the constraints of the disturbances and reference signals by forming a set of all possible references and disturbances the system can experience [10, 27]. One method to ensure good compensator performance is to assume an upper bound on the energy for both sets using signal and system norms.

The feedback system achieves disturbance rejection or good tracking performance if the magnitude of the sensitivity function, $|S(z)|$, is minimized for low frequencies. The sensitivity function relates the closed-loop transfer functions from the error signal $e(z)$ to the reference signal $r(z)$ and from the output of the system $y(z)$ to the disturbance of the system $d(z)$ as shown in figure 13.

$$S(z) = \frac{e(z)}{r(z)} = \frac{y(z)}{d(z)} = \frac{1}{1 + K(z)G(z)} \tag{2.64}$$

The sensitivity function can be minimized using a frequency weighted filter, $W_1(z)$, a real-rational function that is stable. The frequency weight scales the energy spectrum for the

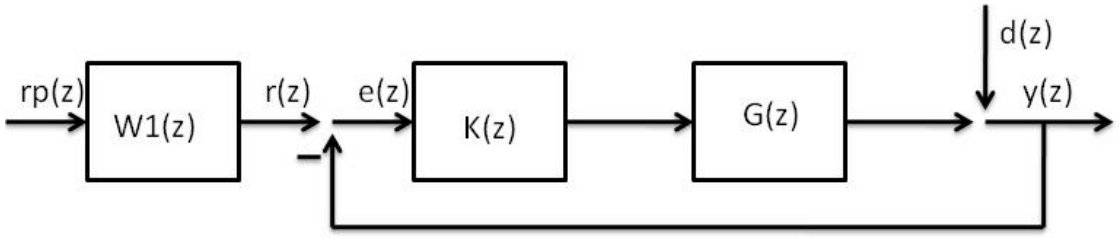

Figure 13: Schematic for nominal performance, which shows the sensitivity function is equivalent for disturbance rejection and tracking reference signals

set of prefiltered reference signals, $r_p(z)$ [10]. There is an energy constraint on the set of prefiltered reference signals that states: the energy for the prefiltered inputs is less than or equal to one [10].

$$r(z) = W_1(z)r_p(z), \qquad |r_p| \leq 1 \tag{2.65}$$

The size of the error signal, $e(z)$, is used to determine if the feedback system achieves nominal performance. The magnitude of the error signal is characterized using its 2-norm and the constraint to achieve nominal performance is the following: the 2-norm of the error signal, $||e||_2$, is less then one for all frequencies, θ.

$$||e||_2 \leq 1 \qquad \forall\theta \tag{2.66}$$

The 2-norm of the error signal is quantified using the sensitivity function and the submultiplicative property that states: the norm for the product of systems is less then or equal to the product for the norm of the individual systems.

$$||e||_2 \leq ||SW_1||_\infty ||r_p||_2 \leq ||SW_1||_\infty \leq 1, \qquad \forall\theta \tag{2.67}$$

The requirement for the feedback system to attain nominal performance is the following: the ∞-norm for the product SW_1 is less then one for all frequencies as shown in equation 2.67.

$$||SW_1||_\infty \leq 1, \qquad \forall\theta \tag{2.68}$$

2.5.2 Robust Stability

A mathematical model for the system is not a complete representation of the system because the model may not contain all the dynamics of the system. These unmodeled dynamics are crucial in terms of closed-loop stability because the simulation of the compensator on the nominal plant could yield a stable system while integrating the same compensator with the actual system can yield catastrophic effects. The unmodeled dynamics are accounted for in the analysis with the nominal plant as modeling uncertainty. Model uncertainty needs to have an upper bound to ensure internal stability of the actual system because closed-loop stability can not be guaranteed if there is no upper limit to the uncertainty [27].

There are several models to characterize the uncertainty for the unmodeled dynamics. The uncertainty model chosen is the multiplicative uncertainty model, resulting in a set of plants, $\mathcal{G}$, that contains the true plant $G_T(z)$. The true plant is a function of the nominal plant $G(z)$, the modeling uncertainty weight $W_2(z)$, and bounded uncertainty $\Delta(z)$.

$$\mathcal{G} = \{G_T(z) = [1 + \Delta(z)W_2(z)]G(z) : W_2(z), \Delta(z) \in \mathcal{S}, \|\Delta\|_\infty < 1\} \tag{2.69}$$

The modeling uncertainty weight is a fixed stable transfer function whose magnitude increases with frequency and accounts for the modeling uncertainty for all frequencies. This results in the accuracy of the model being good at low frequencies but the accuracy decreases with frequency [27]. The parameter $\Delta(z)$, accounts for the phase uncertainty in the modeling for all frequencies.

The graphical representation for the multiplicative uncertainty model is shown in figure 14, which illustrates the magnitude for the ratio of the true plant to the nominal plant, $|G_T(z)/G(z)|$. This ratio is centered in the complex plane at 1 and bounded by the magnitude of the uncertainty, $|W_2(z)|$ [10].

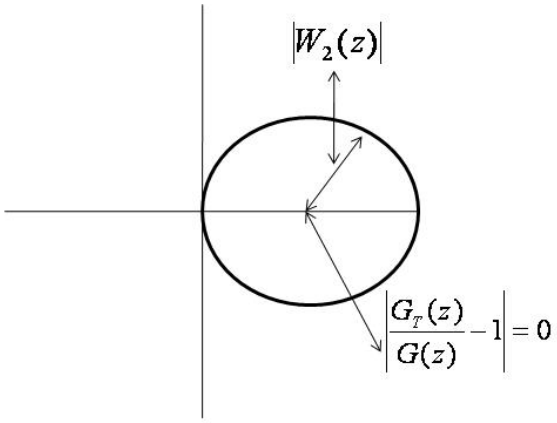

Figure 14: Schematic for the multiplicative uncertainty model in which the true plant is contained

Robust stability is achieved if the compensator causes the entire set of plants to be internally stable, resulting in the actual system being internally stable [27]. The requirement for robust stability will be derived using the small gain theorem.

2.5.2.1 Small Gain Theorem The small gain theorem is used in control theory to characterize the stability of the system using BIBO stability on the loop gain of the system.

Theorem 2 Small Gain Theorem: *The output of the system is stable by BIBO stability if* $L(z)$ *is stable and the* ∞*-norm of* $L(z)$ *is less than one for all frequencies and for all allowable* $\Delta(z)$.

$$||L||_\infty < 1, \qquad \forall\theta \tag{2.70}$$

$$||\Delta||_\infty < 1 \tag{2.71}$$

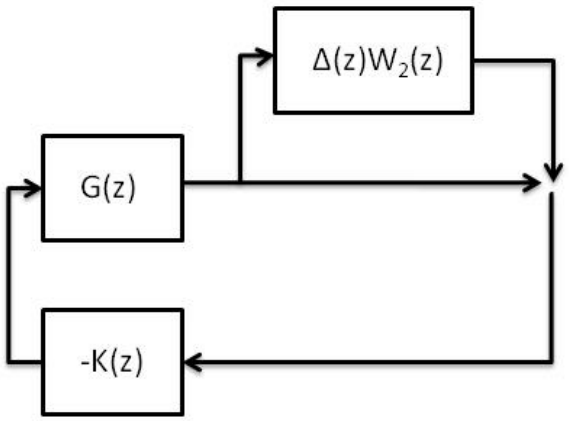

Figure 15: Feedback block diagram schematic for the true plant being modeled using multiplicative uncertainty

2.5.2.2 Robust Stability Test The requirement for the feedback system to achieve robust stability can be found using the small gain theorem and modeling the true plant with multiplicative uncertainty. The block diagram for the compensated feedback system for the true plant is shown in figure 15. Negative feedback is being emphasized by the negative sign associated with the compensator.

The simplification of figure 15 is required to apply the small gain theorem. This simplification involves breaking the paths before and after the product of $\Delta(z)W_2(z)$, resulting in two paths: a typical positive feedback loop with a feedforward gain of $-K(z)G(z)$ and the other path is the product of $\Delta(z)W_2(z)$. The typical positive feedback path is reduced to the negative of the complementary sensitivity function, $-T(z)$, as shown in figure 16.

The small gain theorem is implemented on figure 16 to obtain the requirement for robust stability that states: the ∞-norm for the loop gain of the system, $L(z) = -T(z)\Delta zW_2(z)$, is required to be less than one for all frequencies and be stable. The loop gain for the system can be reduced by applying the submultiplicative property to yield the loop gain being the product of the complementary sensitivity function and the modeling uncertainty weight, $L(z) = T(z)W_2(z)$. The final requirement for the compensated feedback system to achieve

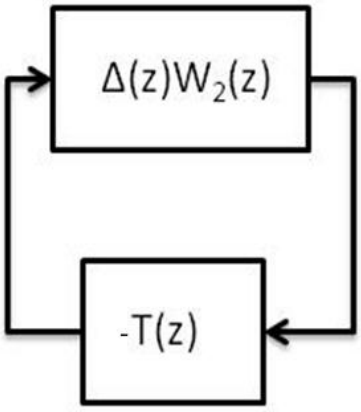

Figure 16: Reduction of the multiplicative uncertainty model for the true plant

robust stability is that the ∞-norm of the loop gain, $L(z) = T(z)W_2(z)$, be less than one for all frequencies and is stable. This implies the entire set of plants, $\mathcal{G}$, is made internally stable by the compensator, resulting in the true plant being internally stable.

$$T(z) = \frac{K(z)G(z)}{1 + K(z)G(z)} \tag{2.72}$$

$$||\Delta T W_2||_\infty \leq ||T W_2||_\infty \leq 1, \qquad \forall\theta \tag{2.73}$$

$$||T W_2||_\infty \leq 1, \qquad \forall\theta \tag{2.74}$$

3.0 ADDITIONAL REQUIREMENTS AND IMPLEMENTATION OF THE COMPENSATORS

The objective of incorporating compensation methods into the design of magnetic traps is to achieve certain requirements that the instrument can not achieve. The additional design requirements the instrument has to achieve in addition to stability is discussed first. The design of the compensators are done using frequency domain techniques, requiring the design requirements being expressed into equivalent frequency domain requirements. Nominal performance of the various compensation methods is desired, resulting in the nominal performance weight being determined. Finally, the method of implementing the adaptive Q-parametrized compensator with LMS to update the weight coefficients of the Q parameter is explained.

3.1 DESIGN GOALS FOR THE CLOSED-LOOP COMPENSATED SYSTEM

There are additional design requirements the closed-loop system has to achieve in addition to stabilizing the position of the magnetic particle. These requirements are characterized by considering the applications of the instrument. A biological specimen deforms proportional to the movement of the attached magnetic particle due to the applied magnetic force. The accurate positioning of the magnetic particle requires the compensated system to have minimum, ideally zero, steady state error for a step input.

The dynamics of biological systems occur faster due to the size of their geometric scale. The settling time and transient characteristics of the compensated system are characterized

Table 1: Design specifications that the various compensation methods must achieve

The steady state error with respect to the desired signal is zero
The settling time is 4.5 ms
Percent overshoot: 52.6

Table 2: Parameters for the functional form of the second order underdamped system

Parameter	Value
ζ	0.2
ω_n	$5.11(10^3)$ rad/s

by modeling the closed-loop system as an underdamped second order system. The magnetic particle moves through the solution at a constant velocity on the order of microns per second, however the displacement of the particle is modeled on the order of nanometers as discussed later [15]. As the magnetic particle moves through the solution at a constant velocity of 4.44 μm/s, the particle moves 1 nm in 225.23 μs. When the magnetic particle is subjected to a step input of 20 nm, the position of the magnetic particle reaches steady state in 4.5 ms. The settling time chosen for the position of the magnetic particle to converge to its reference position was 4.5 ms. The percent overshoot was chosen to be 52.6 percent for an equivalent damping ratio of 0.2. The design requirements that the magnetic trap must satisfy are summarized in table 1. The numerical values for the second order underdamped system that satisfies the design requirements are given in table 2.

3.1.1 Frequency Domain Representation of the Design Requirements

The methods for designing compensators in the frequency domain are well documented. These methods are used to analyze the performance of the various compensation techniques that are incorporated into the design of magnetic traps.

The performance of the compensation methods are analyzed in the frequency domain, resulting in the design requirements given in table 1, having to be characterized in the frequency domain. The transient characteristics are quantified in the frequency domain by the bandwidth frequency, the frequency that is 3 dB below the gain cross-over frequency, and the phase margin, the phase above $-180°$ at the gain cross-over frequency. The bandwidth for the compensated system, ω_{bw}, characterizes the desired settling time in the frequency domain while being a function of the desired damping ratio [23]. The gain cross-over frequency for the compensated system is approximated to be the bandwidth frequency that yielded the desired settling time, 1.06 kHz using equation 3.1.

$$\omega_{bw} = \frac{4}{T_s \zeta} \sqrt{(1 - 2\zeta^2) + \sqrt{4\zeta^4 - 4\zeta^2 + 2}} \tag{3.1}$$

The phase margin, PM, is a critical parameter because it quantifies the amount of damping within the system. The compensated system must have a phase margin of $20°$ by equation 3.2 to satisfy the desired percent overshoot of 52.6 percent [23].

$$Pm \sim 100 \cdot \zeta \tag{3.2}$$

3.2 NOMINAL PERFORMANCE WEIGHT

Compensator design requires a trade-off between the sensitivity function, S, and the complimentary sensitivity function, T, because the magnitude of these functions can not be less than $1/2$ concurrently. The analytic constant that must hold for all frequencies, θ, is: the sum of the sensitivity function and complimentary sensitivity function must equal one.

$$S + T = 1, \forall\theta \tag{3.3}$$

The sensitivity function of the compensated system needs to be small in low frequencies to achieve good tracking performance and disturbance rejection. This concludes the sensitivity function having to be modified in the low frequency range to minimize the effects of the Brownian disturbances using a nominal performance weight.

The various compensators are designed to achieve nominal performance, resulting in the magnitude for the product of the nominal performance weight, $W_1(z)$, and the corresponding sensitivity functions, $S(z)$, being less than one for all frequencies, $\left|W_1(e^{j\theta})S(e^{j\theta})\right| < 1 \ \forall\theta$. The nominal performance weight is characterized first in continuous-time to account for the additional design requirements being expressed in the continuous-time frequency domain. The continuous-time frequency weight accounts for the design requirements in the following way:

- $W_1(s)$ has a pole at 75 Hz. The pole is placed close to the origin to satisfy the condition for zero steady state error for a step input because a pole placed exactly at the origin causes the frequency weight to be unstable.
- $W_1(s)$ has a zero at 7.5 kHz. The zero is placed after the desired bandwidth frequency to account for the maximum of the sensitivity function due to the percent overshoot requirement.
- The gain is chosen to be 0.1399 to have the magnitude of the nominal performance weight be 0 dB at the bandwidth frequency.

$$W_1(s) = 0.1399\frac{s + 47.12(10^3)}{s + 471.2} \tag{3.4}$$

After the nominal performance weight is quantified in continuous-time, the discrete-time nominal performance weight, $W_1(z)$, is obtained using bilinear Tustin transformation with prewarp at the bandwidth frequency. Tustin transformation is used for mapping the continuous-time frequency axis to one revolution on the discrete-time frequency axis [24]. The mapping of the continuous-time frequency axis to the discrete-time frequency axis using Tustin transformations is important because aliasing is eliminated [24]. However the Tustin transformation has a nonlinear relationship between the continuous-time frequencies and the discrete-time frequencies, resulting in a continuous-time frequency and the corresponding discrete-time frequency not occurring at the same location on their respective frequency axes.

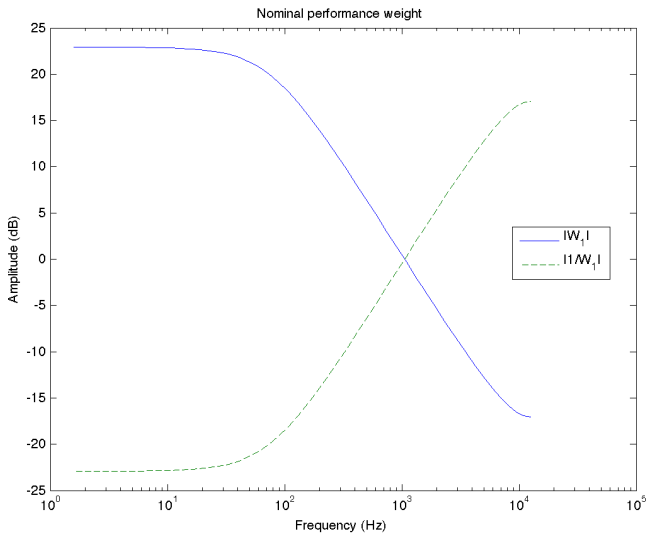

Figure 17: Frequency response function for the discrete-time nominal performance weight, $W_1(z)$, and its inverse, $1/W_1(z)$

This nonlinear relationship can be eliminated for important frequencies like the bandwidth frequency by prewarping the continuous-time frequency to the discrete time frequency [24]. This results in the frequencies that are prewarped occurring at the same location on the frequency axes.

$$W_1(z) = 0.27\frac{z - 0.0266}{z - 0.9812} \tag{3.5}$$

The magnitude plots for the discrete-time nominal performance weight, $|W_1(z)|$, and its inverse, $|1/W_1(z)|$, are shown in figure 17.

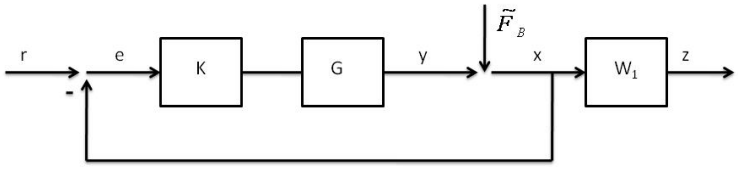

Figure 18: Block diagram schematic for the displacement of the magnetic particle where r is the desired particle position, G is the magnetic trap, y is the output of the magnetic trap, K is the Q-parametrized compensator, W_1 is the nominal performance weight, e is the error signal, and z is the frequency weighted displacement of the magnetic particle.

3.3 IMPLEMENTING THE ADAPTIVE COMPENSATOR USING LMS

This section discusses the theory necessary to adjust the weight coefficients of the Q parameter in the Q-parametrized compensator using LMS to minimize the effects of the Brownian disturbances. This is accomplished by transforming the feedback control problem into an equivalent feedforward control problem.

3.3.1 Frequency Weighted Displacement of the Magnetic Particle

The block diagram representation for the displacement of the magnetic particle, x, is shown in figure 18. The expression for the displacement of the magnetic particle is found to be a function of the sensitivity function and the complimentary sensitivity function.

$$\begin{aligned} x &= \frac{1}{1+GK}\tilde{F}_b + \frac{GK}{1+GK}r = S\tilde{F}_b + Tr \\ S &= \frac{1}{1+GK}, \qquad T = \frac{GK}{1+GK} \end{aligned} \tag{3.6}$$

The closed-loop transfer function relating the displacement of the magnetic particle to the Brownian disturbance, $x/\tilde{F}_b$ is the sensitivity function by letting the desired magnetic particle position be zero. The sensitivity function can be expressed as a function of the set of coprime rational functions that satisfies the Bezout identity to update the weight coefficients of Q

in the Q-parametrized compensator using LMS. The expression for the sensitivity function expressed by the coprime rational functions can be determined using equation 2.36 for the Q-parametrized compensator and the ratio of coprime rational functions for the plant in equation 2.34.

$$\frac{x}{\tilde{F}_b} = S = M(Y - NQ) \tag{3.7}$$

The Brownian disturbance causes the magnetic particle to constantly move in the absence of magnetic forces. The modeling of the Brownian disturbance is accomplished using white-noise as discussed later. Since white-noise has a flat power spectral density, the spectrum for the displacement of the magnetic particle is a frequency weighted version of the white-noise spectrum. The spectrum for the displacement of the magnetic particle must be minimized in the low frequency range to reduce the effects of the Brownian disturbances. This can be accomplished using a frequency weighted filter, W_1, the nominal performance weight, that reduces the spectrum for the displacement of the magnetic particle in regions where disturbance rejection is required.

The performance of the adaptive compensators is examined by analyzing the frequency weighted displacement of the magnetic particle, $z = W_1 x$. The transfer function relating the frequency weighted displacement of the magnetic particle to the Brownian disturbance, $z/\tilde{F}_b$, is the product of the nominal performance weight and the sensitivity function.

$$\frac{z}{\tilde{F}_b} = \frac{z}{x}\frac{x}{\tilde{F}_b} = W_1 S = W_1 M(Y - NQ) \tag{3.8}$$

The closed-loop transfer function, $z/\tilde{F}_b$, is affine in Q which illustrates the feedback problem is equivalent to a model-matching problem. The advantage of the feedforward problem is that it can be solved easily using adaptive filter theory. The equivalent feedforward block diagram schematic relating the frequency weighted displacement of the magnetic particle to the Brownian disturbance is shown in figure 19.

$$\begin{gathered} \frac{z}{\tilde{F}_b} = W_1 M(Y - NQ) = T_1 + T_2 Q T_3 \\ T_1 = W_1 M Y, \qquad T_2 = -W_1 N, \qquad T_3 = M \end{gathered} \tag{3.9}$$

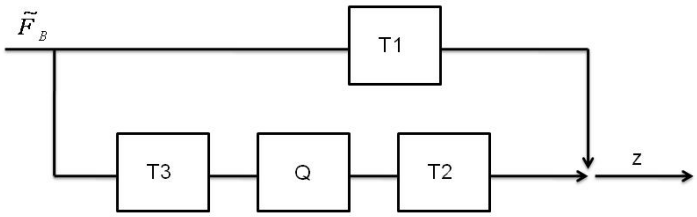

Figure 19: Equivalent model-matching block diagram schematic for the magnetic trap system, $z/\tilde{F}_b$

3.3.2 Updating the Q Parameter in the Feedfoward Problem using LMS

The frequency weighted displacement of the magnetic particle, z, is expressed by the feedforward transfer functions: T_1, T_2, and T_3, the FIR filter Q, and the Brownian disturbance, $\tilde{F}_b$. Since the frequency weighted displacement of the magnetic particle is a function of the FIR filter Q, the frequency weighted displacement is also dependent upon the FIR weight coefficients of Q. The FIR filter Q is equated to the sum of the products of the FIR weight coefficients, w_i, and the tapped delay line, $Q_i = z^{-i}$, where m is the total number of weights in the tapped delay line. The index for the tapped delay line begins at zero and finishes at $m-1$ because the initial input into the tapped delay line is used. The adaptation for the weight coefficients of Q is achieved using the instantaneous square of the frequency weighted displacement of the magnetic particle as the cost function. The weight coefficients of Q are updated in such a way to minimize the frequency weighted displacement of the magnetic particle.

$$\begin{gathered} Q = \Sigma_{i=0}^{m-1} w_i Q_i \\ z = (T_1 + T_2 Q T_3)\tilde{F}_b = (T_1 + T_2 \Sigma_i^m w_i Q_i T_3)\tilde{F}_b \\ J(n) = \frac{1}{2} z^2 \end{gathered} \tag{3.10}$$

The gradient of the cost function with respect to the weight coefficients of Q , $\partial J(n)/\partial \vec{w}(n)$, is found to be the product of the frequency weighted displacement of the magnetic particle

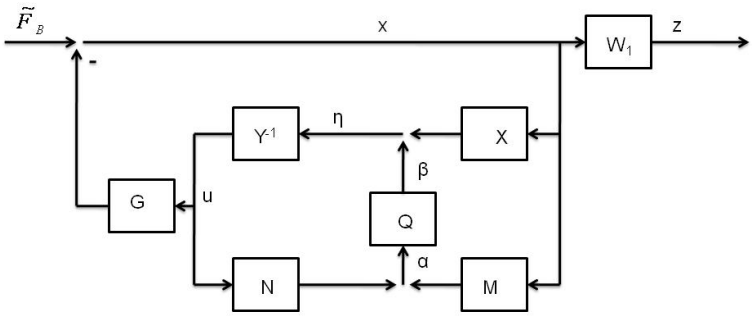

Figure 20: Equivalent feedback block diagram representation for the closed-loop transfer function $z/\tilde{F}_b$ using the coprime rational functions of the Q-parametrization compensator

and the gradient of the frequency weighted displacement of the magnetic particle with respect to the weight coefficients of Q using the chain rule.

$$\frac{\partial J(n)}{\partial \vec{w}(n)} = z\frac{\partial z}{\partial \vec{w}(n)} \tag{3.11}$$

The gradient of the frequency weighted displacement of the magnetic particle is found by taking the derivative of z with respect to the weight coefficients of Q in equation 3.10. However this gradient is dependent upon the Brownian disturbance acting upon the magnetic particle. This causes a constraint for updating the weight coefficients of Q because the Brownian disturbance is not a known signal for each discrete time step.

$$\frac{\partial z}{\partial \vec{w}(n)} = \Sigma_{i=0}^{m-1} Q_i T_2 T_3 \tilde{F}_b \tag{3.12}$$

The following illustrates how the unknown Brownian disturbance signal is characterized using known signals of the feedback block diagram as shown in figure 20, to update the weight coefficients of Q . The Q-parametrized compensator is separated into the individual elements of the coprime rational functions. This separation is critical in updating the weight coefficients of Q because the following signals are known at each time step: α the input into Q, β the output of Q, x the displacement of the magnetic particle, u the control signal, η the input into $Y^{-1}(z)$, and z the frequency weighted displacement of the magnetic particle.

Block diagram algebra can be used to demonstrate that placing the individual elements for the set of coprime rational functions is equivalent to the Q-parametrized compensator in equation 2.36. This requires each element for the set of coprime rational functions be known, including $Y^{-1}(z)$. The inverse of $Y(z)$ is found by switching the definition of the input and output variables for the state-space representation of $Y(z)$ and solving for the new state equation and new output equation. The state-space representation for $Y^{-1}(z)$ is written in matrix form where Y_A is the state matrix, Y_B is the input matrix, Y_C is the output matrix, and Y_D is the feedforward matrix of the coprime rational function $Y(z)$.

$$Y^{-1}(z) \sim \begin{bmatrix} Y_A - Y_B Y_D^{-1} Y_C & Y_B Y_D^{-1} \\ -Y_D^{-1} Y_C & Y_D^{-1} \end{bmatrix} \tag{3.13}$$

The input signal into Q, α, depends upon two known signals at each discrete time step: u the control signal and x the displacement of the magnetic particle. The output signal of $Q(z)$, β, is a frequency weighted version of its input signal, α. The input signal of $Y^{-1}(z)$, η, is the sum of two known signals: β and the frequency weighted version for the displacement of the magnetic particle, $X(z)x$. The output signal of $Y^{-1}(z)$, u, is the frequency weighted version of its input, η.

$$\alpha = Nu + Xx \tag{3.14}$$

$$\beta = Q\alpha = QNu + QMx \tag{3.15}$$

$$u = Y^{-1}(\beta + Xx) = Y^{-1}[QNu + (X + QM)x] \tag{3.16}$$

The output signal of $Y^{-1}(z)$ is manipulated to obtain the transfer function from the control signal to the displacement of the magnetic particle, u/x. The resulting transfer function is equivalent to the Q-parametrized compensator in equation 2.36, yielding the set of the coprime rational functions can be selectively placed to obtain the Q-parametrized compensator.

$$\frac{u}{x} = K = \frac{X + MQ}{Y - NQ} \tag{3.17}$$

The equivalent block diagram schematic for the compensator has been derived and the following proves the input signal of Q, α, is equivalent to a frequency weighted version of the Brownian disturbance acting on the particle. This allows the signal α to be used in

$\partial z/\partial \vec{w}(n)$, to update the weight coefficients of Q, thus minimizing the frequency weighted displacement of the magnetic particle. The signal α in equation 3.14, is written as a function of the displacement of the magnetic particle, x, by recalling the control signal is the product of the Q-parametrized compensator and the displacement of the magnetic particle, $u = Kx$. The signal α is a frequency weighted version of the Brownian disturbance by recalling the displacement of the magnetic particle is the product of the sensitivity function and the Brownian disturbance as shown in equation 3.7.

$$\begin{aligned} \alpha &= Nu + Mx = N\frac{X + MQ}{Y - NQ}x + Mx = \frac{1}{Y - NQ}x \\ \alpha &= \frac{1}{Y - NQ}x = \frac{1}{Y - NQ}M(Y - NQ)\tilde{F}_b = M\tilde{F}_b \end{aligned} \tag{3.18}$$

The resulting signal α is equivalent to the output of the Brownian disturbance being filtered by the coprime rational function M, yielding a known signal being used to update the weight coefficients of Q using LMS. The gradient of the frequency weighted displacement of the magnetic particle, $\partial z/\partial \vec{w}(n)$, equation 3.12, is now a function of a known signal for each discrete time step by equating the product of M and $\tilde{F}_b$ to α.

$$\frac{\partial z}{\partial \vec{w}(n)} = \Sigma_{i=0}^{m-1} Q_i T_2 (T_3 \tilde{F}_b) = \Sigma_{i=0}^{m-1} Q_i T_2 \alpha \tag{3.19}$$

The weight coefficients of $Q(z)$ are updated using LMS to minimize the effects of the Brownian disturbances and to minimize the frequency weighted displacement of the magnetic particle using equation 2.61. The weight coefficients at the next time step, $\vec{w}(n+1)$, is the difference of the current weight coefficients, $\vec{w}(n)$, and the product of the step-size parameter, the frequency weighted displacement of the magnetic particle and the gradient of the frequency weighted displacement of the magnetic particle, $\mu z \partial z/\partial \vec{w}(n)$.

$$w_i(n+1) = w_i(n) - \mu z \frac{\partial z}{\partial \vec{w}(n)} = \vec{w}(n) - \mu z \Sigma_{i=0}^{m-1} Q_i T_2 \alpha \tag{3.20}$$

4.0 SIMULATIONS

This chapter discusses the simulations for the various compensation methods to control the magnetic trap. The numerical values for the parameters of the magnetic trap transfer function and the effects of the Brownian disturbances acting upon the magnetic particle are quantified first. The performance of each compensator has been analyzed in the frequency domain using spectral analysis. This is particularly useful since Brownian disturbances act on the magnetic particle. Fixed gain compensation methods have been implemented with the magnetic trap to emphasize that compensation needs to satisfy the design requirements and to form a benchmark to compare the performance of the adaptive compensators. Finally, adaptive compensation has been used to control the magnetic trap.

4.1 NUMERICAL VALUES FOR THE PARAMETERS OF THE MAGNETIC PARTICLE SYSTEM

The parameters for the magnetic trap must be quantified and characterized before any compensation technique is implemented. Normally, magnetic traps exert forces on the order of piconewtons, resulting in the displacement of the magnetic particle being on the order of nanometers [13, 40]. These typical magnitudes for the magnetic force and the magnetic particle displacement are accounted for in characterizing the parameters of the magnetic trap transfer function by relating the desired displacement of the magnetic particle in nanometers to the magnetic force in piconewtons.

The magnetic particles chosen have a mean diameter of 2.88 μm. The following assumption is made about the density of the particles, ρ: the density of the particles is approximated

Table 3: Numerical values for the parameters of the magnetic trap transfer function

Parameter	Symbol	Value
Viscosity of solution	η	$984(10^{-12})$ pNs/nm^2
Density of the particle	ρ	$0.99777(10^{-24})$ kg/nm^3
Mass of the particle	m	$11.4(10^{-15})$ kg
Damping coefficient	γ	$25.6(10^{-6})$ Ns/m

as the density of the water solution after viewing the beads had little sedimentation in the microscope. The viscosity of the water solution, η, and the density of the magnetic particle, ρ, are approximated as the dynamic viscosity and the density of water at room temperature respectively [11]. The damping coefficient, $\gamma = 6\pi\eta r$, acting on the magnetic particle is a function of the product for the viscosity of the water solution and the mean radius of the magnetic particle. The numerical values for the parameters of the magnetic trap transfer function relating the displacement of the magnetic particle in nanometers to the magnetic force in piconewtons are quantified as shown in table 3.

The dynamics for the magnetic trap transfer function, the sensor, and the actuator are characterized in continuous time to account for the first principal physical laws. The overall magnetic particle system is composed of the dynamics for the magnetic trap transfer function, the sensor, and the actuator.

4.1.0.1 Magnetic Trap Dynamics The continuous-time transfer function for the magnetic trap, $G_m(s)$, equation 2.4, is characterized using the parameters in table 3. However the mass of the magnetic particle is on the order of 10^9 times smaller than the damping acting of the magnetic particle that produced a pole at 361.6 MHz. The pole at 361.6 MHz is much greater than the desired bandwidth frequency, resulting in the mass of the magnetic particle being ignored. This yields the response of the magnetic particle being dominated by the viscous effects of the water solution instead of the inertial effects by the mass. The continuous-time transfer function for the magnetic trap accounts for only the viscous ef-

Table 4: Numerical values for the function form of the magnetic trap transfer function, the transconductance amplifier, and the overall continuous-time magnetic particle system.

Parameter	Value
g_m	$38.51(10^3)$
g_A	0.5
p_A	$75.398(10^3)$
g_c	1925.51
p_c	$75.398(10^3)$

fects affecting the displacement of the magnetic particle while the numerical value for the functional form of the transfer function for the magnetic trap is given in table 4.

$$G_m(s) = \frac{1}{s(ms + \gamma)} \tag{4.1}$$

$$G_m(s) = \frac{g_m}{s} \tag{4.2}$$

4.1.0.2 Amplifier Dynamics The dynamics for the transconductance amplifier are characterized to obtain an accurate model of the instrument. The voltage to current converter is used to produce a current in the electromagnet from the input voltage into the transconductance amplifier. The transconductance amplifier, the Kepco BOP 20-5M amplifier, has a bandwidth frequency and passband gain of 12 kHz and 0.5 S respectively that is given by the manufacturer. The dynamics for the amplifier, $G_a(s)$, is characterized by modeling the amplifier as a lowpass filter with a gain of 0.5 and the cutoff frequency equated to the bandwidth frequency of the amplifier. The numerical values for the functional form of the transfer function for the transconductance amplifier are given in table 4.

$$G_a(s) = \frac{g_A}{s + p_A} \tag{4.3}$$

4.1.0.3 Magnet and Sensor Dynamics

The gain of the magnet was to be characterized by the installation of the QPD and analyzing the response of the magnetic particle for a given change in the current of the electromagnet. However while installing the QPD, one of the difference channels contained broad-band white noise. Several methods were explored in attempt to eliminate the noise but all attempts were unsuccessful. The main purpose of this thesis is to demonstrate adaptive control techniques can stabilize the position of the magnetic particle while minimizing the effects of the Brownian disturbances. The setup used to emulate the experimental conditions if the sensor worked properly will be discussed later.

In practical situations, the gain of a signal can be modified through the use of an amplifier. The gain for the magnet, κ, is arbitrarily chosen to be 10 pN/A to demonstrate the control theory satisfies the design requirements.

The dynamics for the sensor are also characterized to obtain an accurate model of the instrument. The bandwidth for the QPD is 300 kHz, given by the manufacturer, responds 25 times quicker than the dynamics of the transconductance amplifier. This results in the dynamics of the sensor being ignored because there faster than the dynamics of interest. However, the sensor would have been modeled as a low pass filter, resulting in the passband gain of the sensor having an effect on the displacement of the magnetic particle. The passband gain for the sensor, g_2, contributes to the response of the magnetic particle system, is chosen to be $10(10^{-3})$ V/nm.

4.1.0.4 Overall Magnetic Particle System Dynamics

The overall continuous-time transfer function for the magnetic particle system, $G(s)$, is the product of the transconductance amplifier dynamics, the dynamics for the magnetic trap transfer function, the gain of the magnet, κ, and the gain of the sensor, g_2. The numerical values for the functional form of the overall continuous time transfer function of the magnetic particle system, $G(s)$, are shown in table 4.

$$G(s) = \frac{g_c}{s(s + p_c)} \tag{4.4}$$

The continuous-time transfer function for the magnetic particle system is converted to discrete-time, $G(z)$, to be implemented with the linear digital control theory using zero order

hold. This requires the continuous-time magnetic particle system being sampled at a rate of at least twice the nyquist frequency to prevent aliasing. The sampling frequency chosen for the discrete-time magnetic particle system is 25 kHz.

$$G(z) = 699.4(10^{-9})\frac{z + 0.389}{(z-1)(z-0.049)} \tag{4.5}$$

4.1.1 Modeling the Brownian Disturbances

The Brownian disturbances are modeled as band-limited white noise to account for the fluctuating Brownian forces acting on the particle. The output of the band-limited white noise is modified by the gain of the sensor, g_2, to have the control system experience the actual displacement of the magnetic particle.

4.1.1.1 Analyzing the Data in the Frequency Domain Once the simulations and the experiments for the various compensation methods are performed, the data can be analyzed in the frequency domain using spectral analysis with the reference voltage being 1 V. The random characteristics due to the Brownian disturbance makes examining the performance of the various compensators difficult in the time domain. A tracking performance problem and disturbance rejection problem are equivalent, requiring the frequency response of the sensitivity function being small at low frequencies. The performance for the various compensation methods is analyzed by examining the sensitivity function, frequency weighted sensitivity function, the displacement of the magnetic particle, and the frequency weighted displacement of the magnetic particle using spectral analysis once the compensated system reached steady state.

The effects of the Brownian disturbance are analyzed by examining the spectrum for the displacement of the magnetic particle. The suppression of the Brownian disturbance using each compensation method is found by comparing the mean magnetic particle displacement in the low frequencies to the mean magnetic particle displacement at the dominant frequency.

4.2 FIXED GAIN COMPENSATION

Fixed gain compensation is incorporated into the design of the magnetic particle system to illustrate compensation methods must stabilize the position of the magnetic particle. The frequency response for the discrete-time magnetic particle system is analyzed first to determine the compensation method needed to satisfy the design requirements. The two fixed gain compensation methods incorporated into the design of the magnetic trap are: proportional gain compensation and fixed gain Q-parametrized compensation. The fixed gain Q-parametrized compensation is chosen to illustrate the compensation method satisfies the design requirements before it is used with the adaptive Q-parametrized compensation method.

4.2.1 Frequency Analysis for the Magnetic Particle System

The discrete-time magnetic particle system was examined in the frequency domain, as shown in figure 21, to analyze its performance to determine the type of compensation needed to satisfy the design requirements. The uncompensated system had a bandwidth of 3.91 mHz, which was less than the desired bandwidth of 1.06 kHz. The magnitude, M, and phase margin, PM, of the uncompensated system were found at the desired bandwidth frequency to be -108.6 dB and 76.83° respectively through linear interpolation.

The phase margin for the uncompensated system was greater than the required phase margin of 20°, yielding the transient design requirements being satisfied. This results in proportional gain compensation being required to modify the magnetic particle system to have the magnitude of its frequency response be 0 dB at the desired bandwidth frequency.

4.2.2 Proportional Gain Compensation

Proportional gain compensation was the first fixed gain compensator implemented to improve the magnitude for the frequency response of the magnetic particle system. This compensation method was chosen because a gain only affects the magnitude of the frequency response by having a constant magnitude and 0° phase for all frequencies.

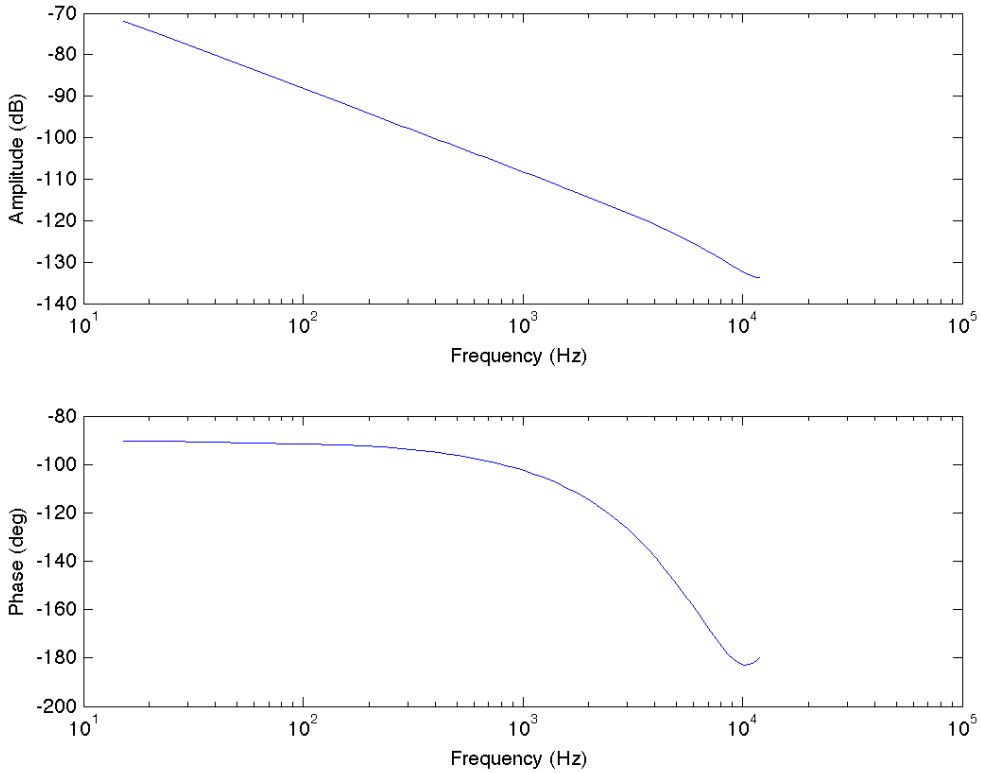

Figure 21: Frequency response for the uncompensated magnetic particle system. The magnitude plot relates the voltage output from the sensor to the voltage input of the transconductance amplifier.

The magnitude for the frequency response of the compensated system at the bandwidth frequency must be 0 dB. The gain for the proportional gain compensator, K_p, was found to be 108.6 dB by equating the magnitude for the product of the proportional gain compensator, K_p, and the magnitude for the uncompensated system at the desired bandwidth frequency, M, to one.

$$K_p M = 1 \tag{4.6}$$

$$K(z) = K_p \tag{4.7}$$

The frequency response for the loop-gain, sensitivity function and complimentary sensitivity function of the compensated system are important in determining the characteristics of the compensated system like the stability and nominal performance. The magnitude for the frequency response of the loop-gain, sensitivity function, and complimentary sensitivity function and the phase of the loop-gain for the compensated system are shown in figure 22. The closed-loop stability of the compensated system was examined by analyzing the gain margin and phase margin of its loop-gain. The gain margin and phase margin were found to be 22.26 dB and 76.83° respectively, resulting in the compensated system being closed-loop stable because both margins were positive while the closed-loop stability was verified using the Nyquist stability criterion. The nominal performance of the compensated system was determined using the nominal performance criteria as stated in equation 2.68, by analyzing the magnitude for the product of the sensitivity function and the nominal performance weight as shown in figure 23. The magnitude for the product of the sensitivity function and the nominal frequency weight, $|W_1(z)S(z)|$, was less than 0 dB for all frequencies, implying the compensated system using proportional gain compensation achieved nominal performance and also satisfied the design requirements.

Spectral analysis was performed to evaluate the performance of the proportional gain compensator once the compensated system reached steady state. The simulation for the compensated system was performed for 10 s while the spectral analysis was performed on the last 5 s of the simulation. The spectral analysis for the sensitivity function and the weighted sensitivity function is shown in figure 24 while the spectral analysis for the displacement of the magnetic particle and the frequency weighted displacement of the magnetic particle is shown

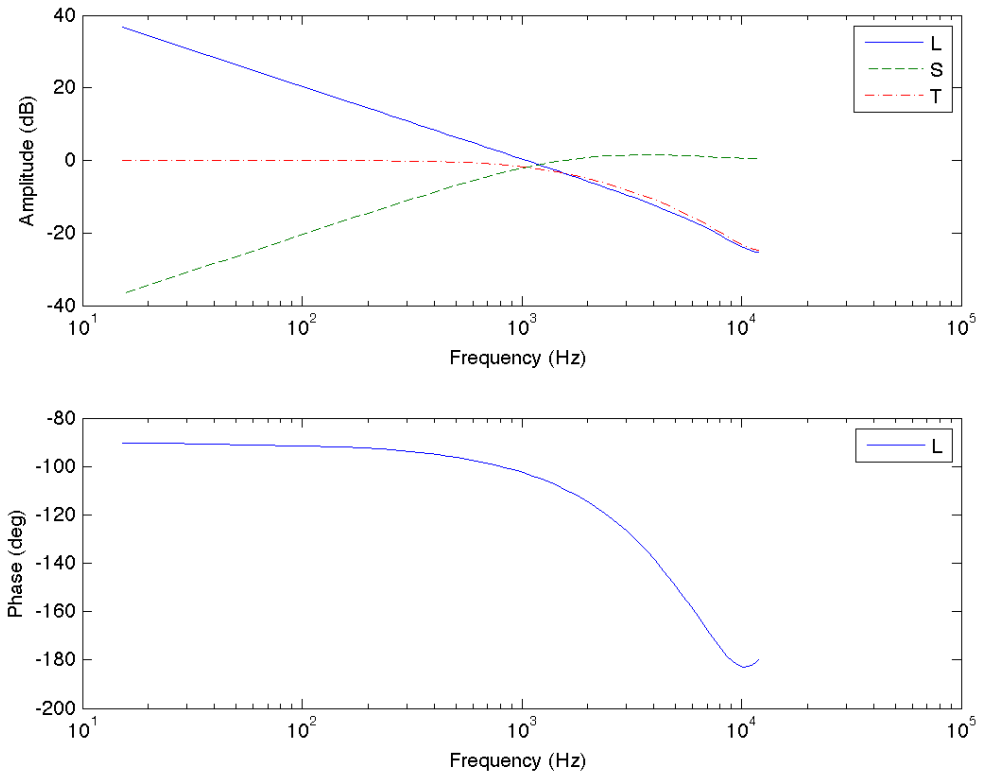

Figure 22: Frequency response for the loop-gain, sensitivity function, and complimentary sensitivity function of the compensated magnetic particle system using both proportional gain compensation and fixed gain Q-parametrized compensation for both sets of coprime rational functions.

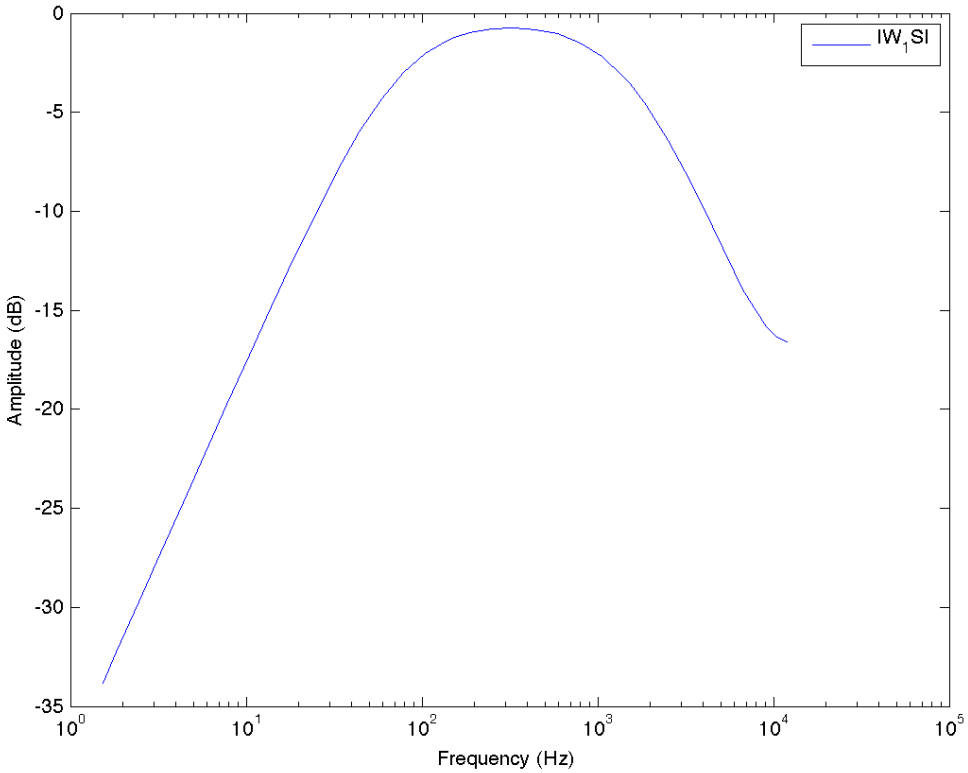

Figure 23: Shows the magnitude for the product of the sensitivity function and the nominal performance weight is less than 0 dB for all frequencies using proportional gain compensation and fixed gain Q-parametrized compensation for both sets of coprime rational functions.

in figure 25. These figures show by incorporating proportional gain compensation into the design of the magnetic particle system, the sensitivity function is small in the low frequency range thus minimizing the effects of the Brownian disturbances. The displacement of the magnetic particle is suppressed by approximately at least 23.11 dB for frequencies below 100 Hz than the mean particle displacement of -8.756 dB at the dominating frequency of 3.264 kHz.

4.2.3 Fixed Gain Q-parametrized Compensators

The second fixed gain compensation method integrated with the magnetic particle system was fixed gain Q-parametrized compensation. This compensation method was chosen to demonstrate the compensated system could satisfy the design requirements. There were two sets of coprime rational functions chosen to illustrate the uniqueness property of the Q-parametrized compensator.

The design for the discrete-time coprime rational functions required the state-space realization of the uncompensated system be controllable [4]. The controllability matrix for the uncompensated system was found to be full rank or a rank of 2, yielding the eigenvalues for the coprime rational functions can be placed in any desired location.

The dynamics for the coprime rational functions were chosen heuristically considering that the coprime rational functions had to satisfy the Bezout identity. The magnitude for the eigenvalues of the coprime rational functions were required to be less than one for stability.

The dynamics for the first set of coprime rational functions that satisfied the Bezout identity were the following:

- $N_1(z)$ and $M_1(z)$ were found using equation 2.45 and choosing the eigenvalue locations of: 0.16 and 0.17.
- $X_1(z)$ and $Y_1(z)$ were found using equation 2.46 and choosing the eigenvalue locations of: 0.14 and 0.16.

The dynamics for the second set of coprime rational functions that satisfied the Bezout identity were the following:

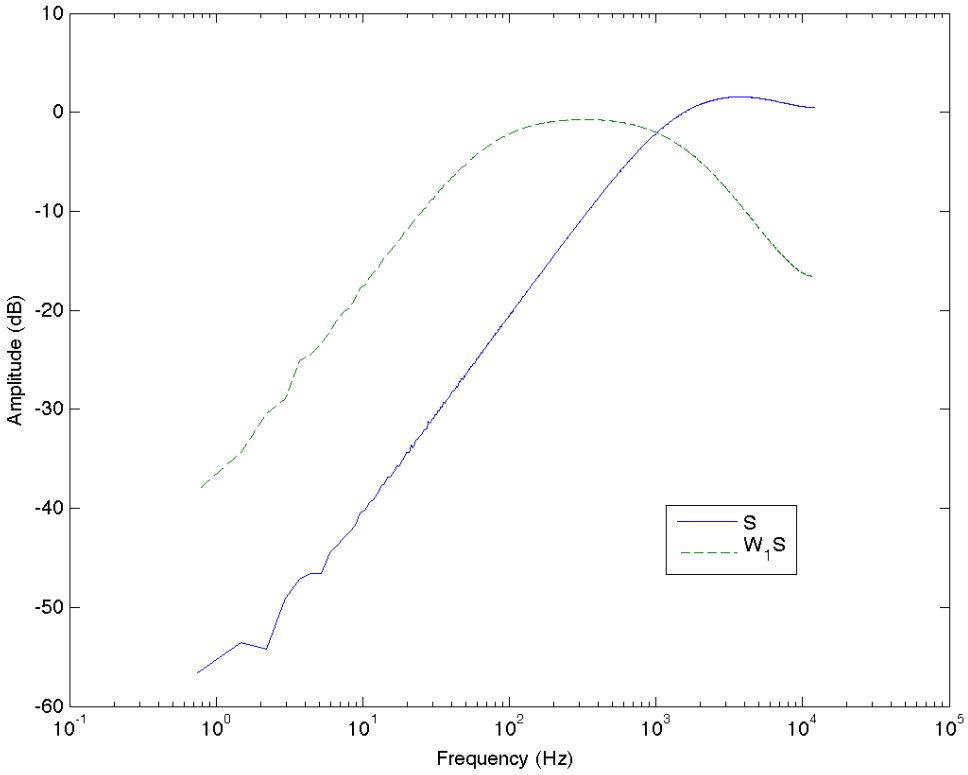

Figure 24: The spectrum for the sensitivity function and weighted sensitivity function of the compensation system using both proportional gain compensation and fixed gain Q-parametrized compensation for both sets of coprime rational functions

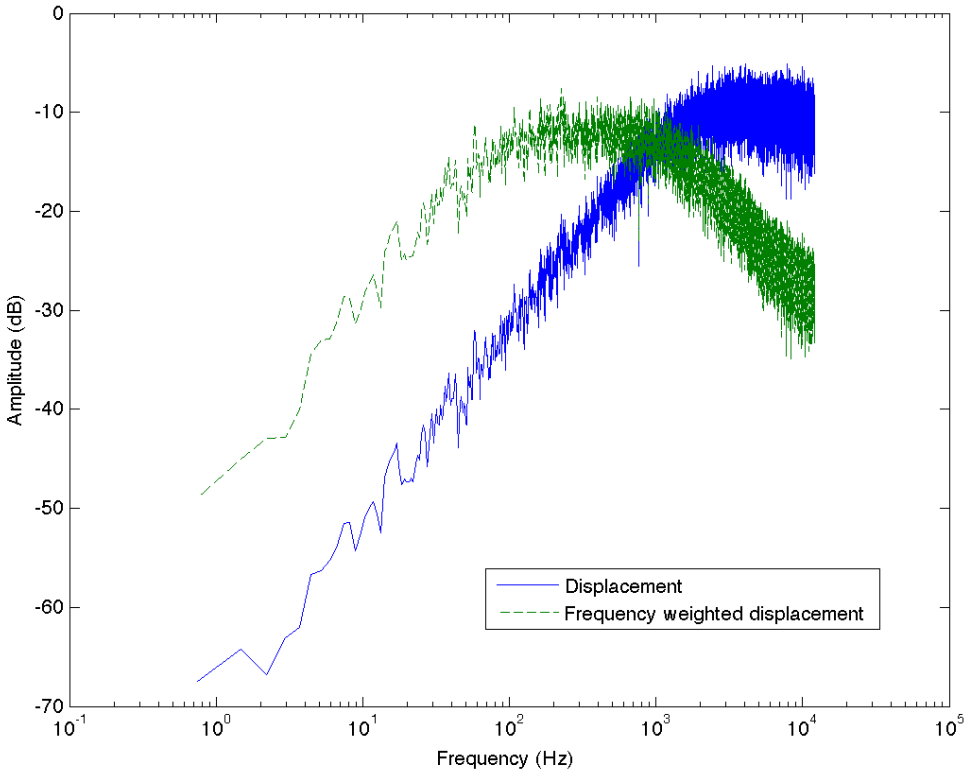

Figure 25: The spectrum for the displacement of the magnetic particle and the frequency weighted displacement of the particle using both proportional gain compensation and fixed gain Q-parametrized compensation for both sets of coprime rational functions

- $N_2(z)$ and $M_2(z)$ were found using equation 2.45 and choosing the eigenvalue locations of: 0.16 and 0.18.
- $X_2(z)$ and $Y_2(z)$ were found using equation 2.46 and choosing the eigenvalue locations of: 0.18 and 0.20.

The distinct $Q \in \mathcal{S}$ was found for each set of coprime rational functions using the proportional gain compensator as the controller in equation 2.38. The resulting Q and the respective set of coprime rational functions were used to find the fixed gain Q-parametrized compensators that should equal the proportional gain compensator of 108.6 dB. Frequency analysis was performed on the fixed-gain Q-parametrized compensators to determine if the magnitude and the phase of their frequency responses were 108.6 dB and 0° for all frequencies as shown in figure 26 and figure 27 for the first and second sets of the coprime rational functions respectively. These figures showed the magnitude of the frequency response for the fixed gain Q-parametrized compensators were essentially 108.6 dB while the phase plots were approximately 0° for all frequencies. This resulted in the fixed gain Q-parametrized compensators being equal to the proportional gain compensator as expected. The frequency response for the loop-gain, the sensitivity function, and the complimentary sensitivity function of the compensated system for both sets of coprime rational functions were equal to the frequency response functions of the compensated system using proportional gain compensation as shown in figure 22. The compensated system for both sets of coprime rational functions were found to be closed-loop stable because the gain margin and phase margin of the loop-gain were 22.26 dB and 76.83° respectively. The magnitude for the product of the compensated sensitivity function and the nominal performance weight using the fixed gain Q-parametrized compensation for both sets of coprime rational functions were equal to the magnitude for the product of the compensated sensitivity function and the nominal performance weight using proportional gain compensation as shown in figure 23. Both fixed gain Q-parametrized compensators achieved nominal performance because the magnitude for the product of the compensated sensitivity function and the nominal performance weight were less than 0 dB for all frequencies.

Spectral analysis was performed to evaluate the performance of the fixed gain Q-parametrized compensators once the compensated system reached steady state. The simulation

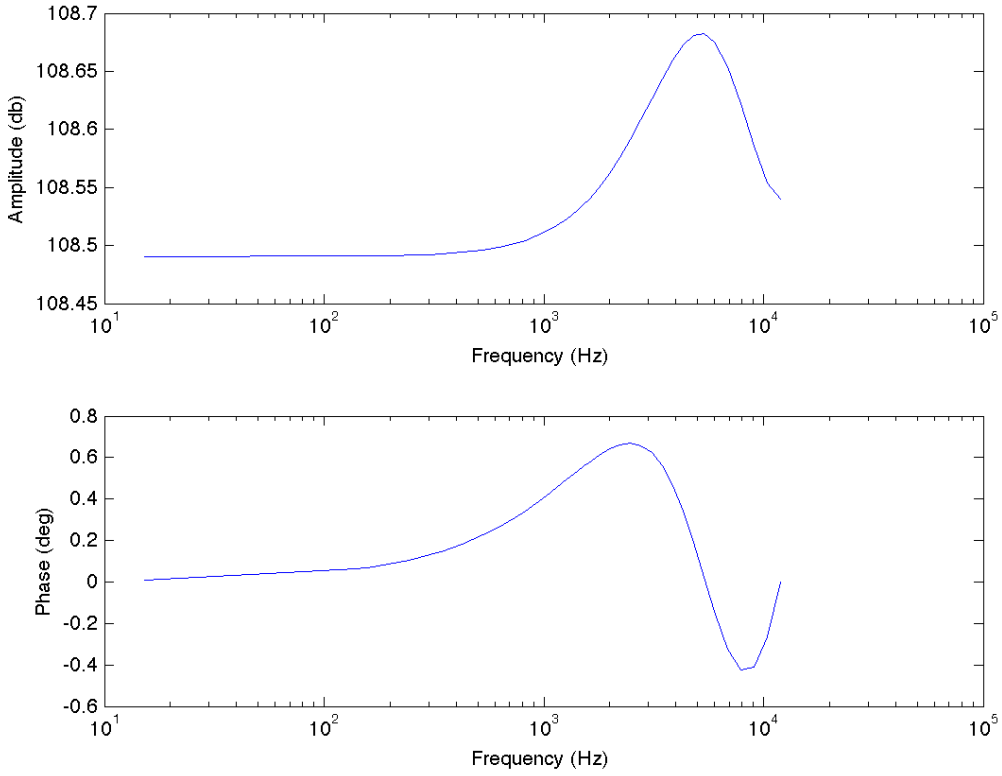

Figure 26: The frequency response for the fixed gain Q-parametrized compensator using the first set of coprime rational functions

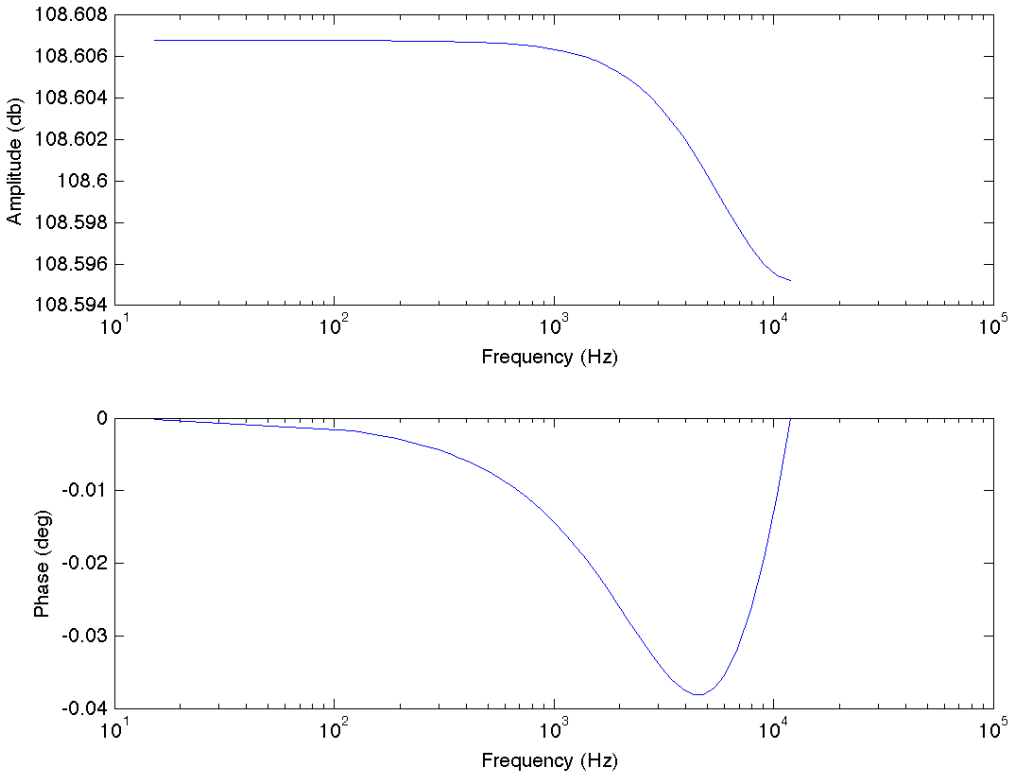

Figure 27: The frequency response for the fixed gain Q-parametrized compensator using the second set of coprime rational functions

for both fixed gain Q-parametrized compensated systems were performed for 10 s while the spectral analysis was performed on the last 5 s of the simulation. The spectral analysis for the sensitivity function and the weighted sensitivity function is shown in figure 24 while the spectral analysis for the displacement of the magnetic particle and the frequency weighted displacement of the magnetic particle is shown in figure 25. These figures show by incorporating the fixed gain Q-parametrized compensators into the design of the magnetic particle system, the sensitivity function is small in the low frequency range thus minimizing the effects of the Brownian disturbances. The displacement of the magnetic particle is suppressed by approximately at least 23.11 dB for frequencies below 100 Hz than the mean particle displacement of -8.756 dB at the dominating frequency of 3.264 kHz.

4.3 ADAPTIVE COMPENSATION

The final compensation method incorporated into the design of the magnetic particle system to satisfy the design requirements was adaptive Q-parametrized compensation. A progression from the fixed gain Q-parametrized compensation method to the adaptive Q-parametrized compensation method will be shown by using the same sets of coprime rational functions. The weight coefficients of the Q parameter in the Q-parametrized compensator were adjusted to minimize the frequency weighted displacement of the magnetic particle using LMS. The implementation of the adaptive compensation will be discussed first followed by the analysis of the adaptive compensator for both sets of the coprime rational functions.

4.3.1 Implementing Adaptive Compensators in Simulink

The implementation of the adaptive Q-parametrized compensation method was important for demonstrating that the design requirements were satisfied. The adaptive compensated system used to minimize the frequency weighted displacement of the magnetic particle is shown in figure 28, where the compensator is the compensator subsystem, LMS is the LMS subsystem, G is the magnetic particle system, W_1 is the nominal performance weight, and

the band-limited white noise is the Brownian disturbance. The displacement of the magnetic particle, the sum of the Brownian disturbance and the output of the magnetic particle system, is compared with the desired magnetic particle position then fed into the compensator subsystem and fed into the nominal performance weight to obtain the frequency weighted displacement of the magnetic particle.

The difference of the desired magnetic particle position and the displacement of the magnetic particle is fed into the compensator subsystem to adjust the dynamics of the compensator as shown in figure 29. The α signal is fed into the LMS subsystem as shown in figure 30, the graphical representation of equation 3.20, to update the weight coefficients of the Q parameter. The negative sign accounted for the feedforward transfer function T_2 being the negative product of the nominal performance weight, W_1, and the coprime rational function, N. There were $m-1$ time delays for m FIR weights because the current input into the tapped delay line was used. The weight coefficients at the current time step, $\vec{w}(n)$, were fed into the compensator subsystem to adjust the dynamics of the Q parameter, the inner product of the weight coefficients and the delayed α signal. The compensated system was analyzed to determine if the number of FIR weight coefficients affect the performance of the adaptive Q-parametrized compensator. The performance was analyzed using spectral analysis once the compensated system reached steady state for the nominal compensator, $K = X/Y$, and the adaptive compensator for different number of FIR weight coefficients. The number of FIR weights chosen for the adaptive Q-parametrized compensator for both sets of coprime rational functions were 5 and 25 FIR weights. The step-size parameter, μ, that stabilized the feedback system was $-1(10^9)$ while using the LMS subsystem in figure 30.

4.3.2 Adaptive Compensator for the First Set of Coprime Rational Functions

The first set of coprime rational functions were implemented with the adaptive Q-parametrized compensator to satisfy the design requirements. The simulation of the adaptive compensator for both FIR weight cases were performed for a time duration of 150 s to ensure the FIR weight coefficients converged to their nominal values. The FIR weight coefficients of

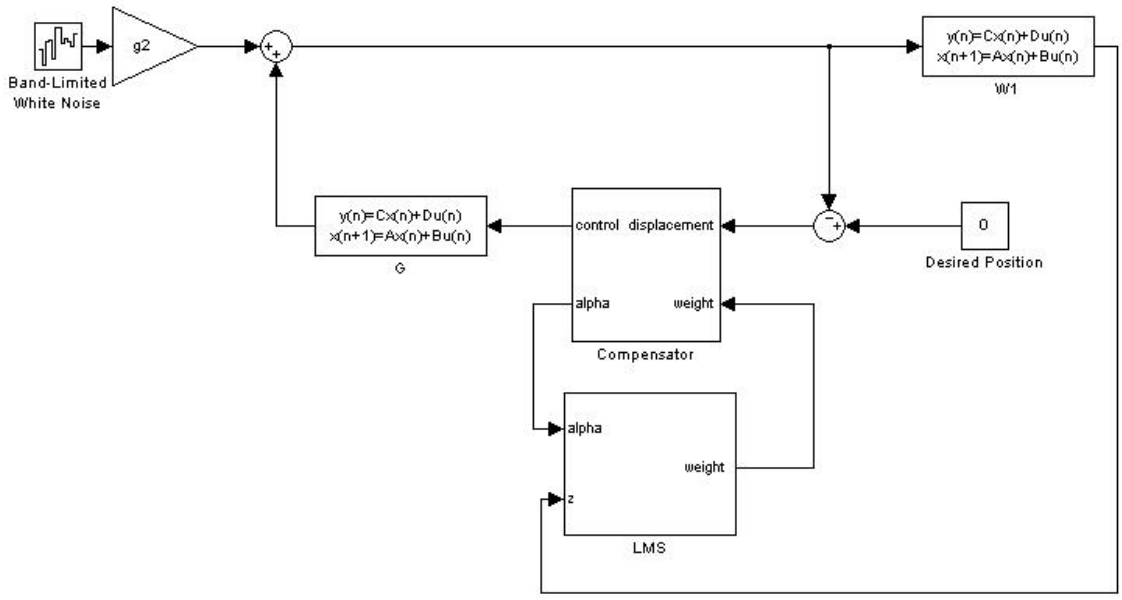

Figure 28: Adaptive compensator structure used to minimize the frequency weighted displacement of the particle.

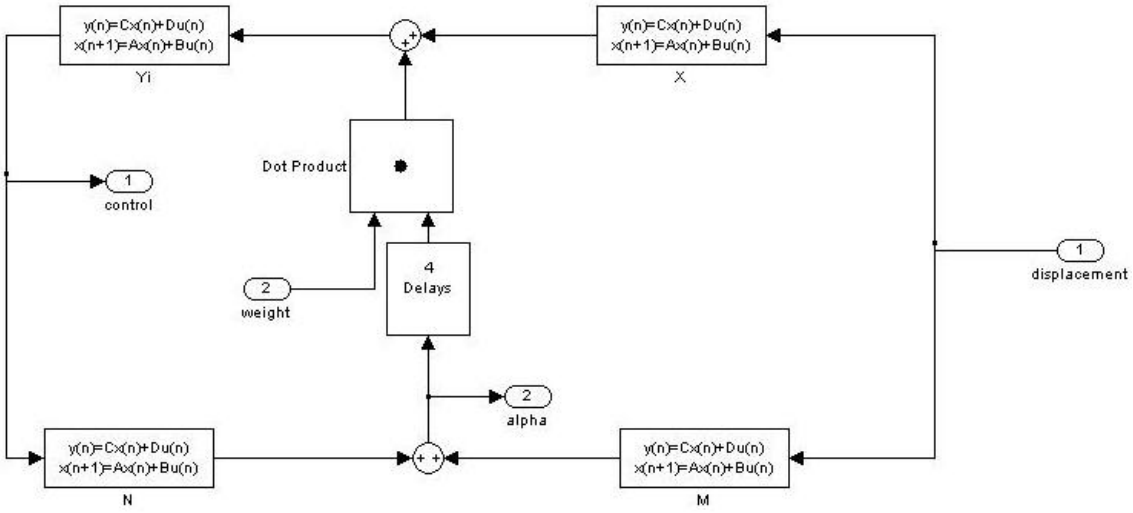

Figure 29: The controller subsystem has two inputs: the weight coefficients, *weight*, and the error in the displacement of the magnetic particle, *displacement*. There are also two outputs for the controller subsystem: the control signal, *control*, and the α signal

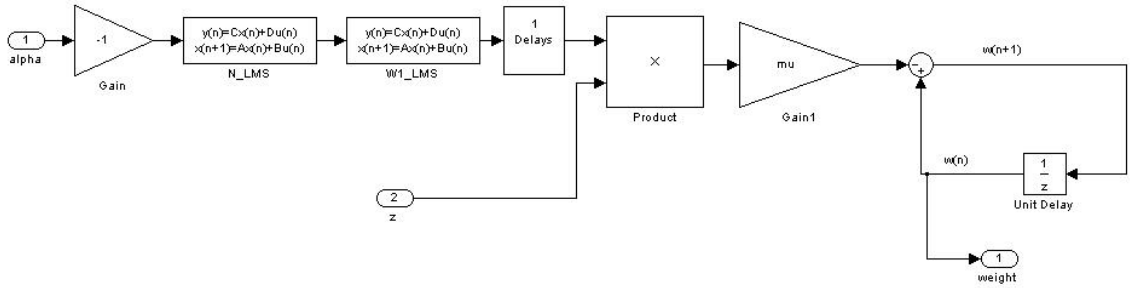

Figure 30: The LMS subsystem used to update the weight coefficients of the Q parameter. There were two inputs into the LMS structure: the input signal into the FIR filter, α, and the frequency weighted displacement of the magnetic particle, z. The weight coefficients, *weight*, were fed into the compensator structure.

the Q parameter for both FIR weight cases converged to nominal values as shown in figure 31, where the top plot is for 5 FIR weights while the bottom plot is for 25 FIR weights. Due to the complexity of the compensated system, figure 31 shows the weight coefficients that were downsampled by $2(10^3)$ that implies the adaptive compensated system was sampled at 12.5 Hz. Downsampling the adaptive compensated system is valid to show the characteristics of how the FIR weight coefficients converge to their nominal values because downsampling does not affect the performance of the system in the time domain.

The adaptive compensator was analyzed once the compensated system reached steady-state. The compensated system reached steady state when the FIR weight coefficients converged to their nominal values. The analysis was performed on the adaptive compensated system over the last 5 s of the simulation. Once the weight coefficients of Q converged, the loop-gain, the sensitivity function, and the complimentary sensitivity function for the steady state compensated system were found for both FIR weight cases. The magnitude for the frequency response of the loop-gain, the sensitivity function, and the complimentary sensitivity function and the phase of the loop-gain for the compensated system are shown in figure 32 and figure 33 respectively for the 5 and 25 FIR weights. The bandwidth frequency and the phase margin for the adaptive compensated system with 5 FIR weight coefficients were determined to be 3.88 kHz and 61.1° respectively through linear interpolation. The adaptive compensator with 5 FIR weight coefficients had a faster bandwidth frequency and a smaller phase margin than the fixed gain compensators. Since the bandwidth frequency and the phase margin for the adaptive compensator with 5 FIR weights were greater then the desired bandwidth frequency and the phase margin, the design requirements were satisfied. The bandwidth frequency and the phase margin for the adaptive compensated system with 25 FIR weight coefficients were determined to be 3.84 kHz and 61.83° respectively through linear interpolation. The adaptive compensator with 25 FIR weight coefficients had a faster bandwidth frequency and a smaller phase margin than the fixed gain compensators. Since the bandwidth frequency and the phase margin for the adaptive compensator with 25 FIR weights were greater then the desired bandwidth frequency and the phase margin, the design requirements were satisfied.

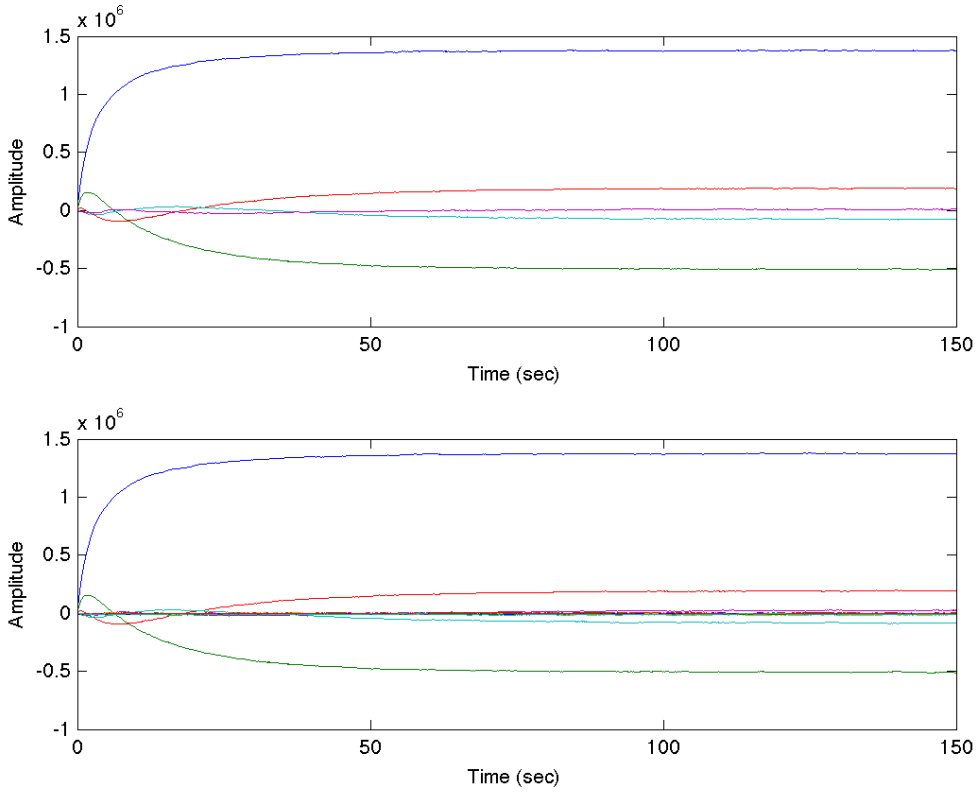

Figure 31: Shows the weights coefficients for adaptive Q-parametrized compensator reaches steady-state. The top plot is the weight coefficients using 5 FIR weights while the bottom plot is the weight coefficients using 25 FIR weights.

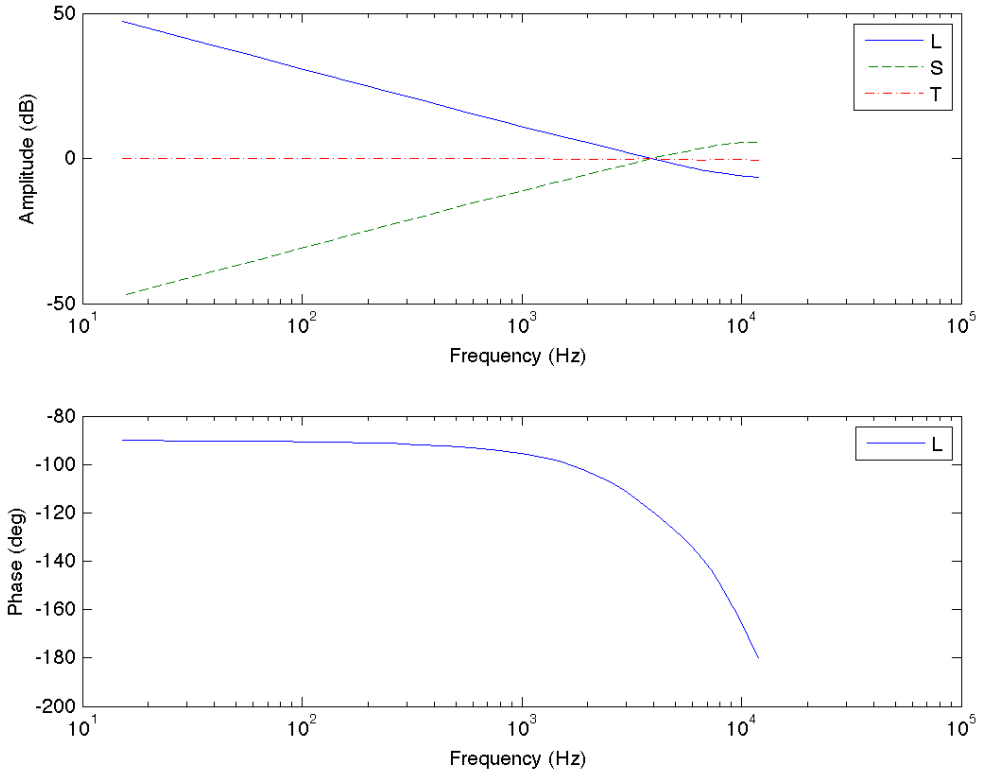

Figure 32: The magnitude for the loop-gain, sensitivity function, and complimentary sensitivity function and the phase of the loop-gain for the adaptive Q-parametrized compensated system with 5 FIR weights using the first set of coprime rational functions.

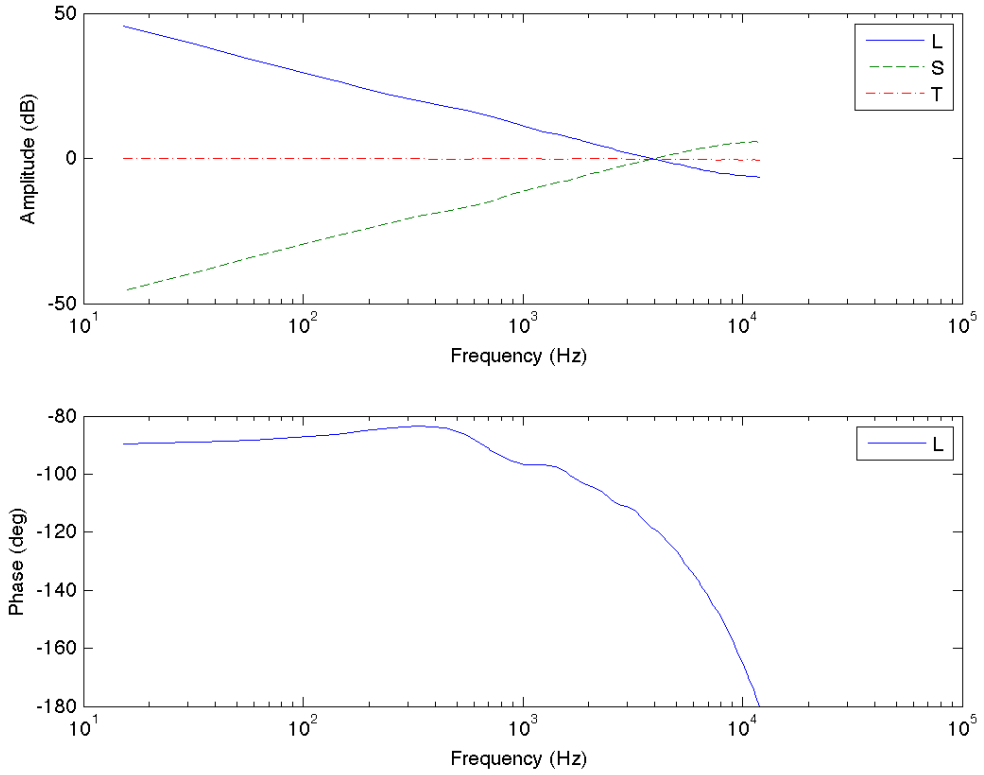

Figure 33: The magnitude for the loop-gain, sensitivity function, and complimentary sensitivity function and the phase of the loop-gain for the adaptive Q-parametrized compensated system with 25 FIR weights using the first set of coprime rational functions.

The magnitude for the closed-loop transfer function relating the frequency weighted displacement of the magnetic particle to the Brownian disturbance was equivalent to the nominal performance criteria: the magnitude for the product of the nominal performance weight and the sensitivity function. The nominal performance criteria for each FIR weight case was examined by analyzing the magnitude of $W_1(z)S(z)$ as shown in figure 34. The adaptive Q-parametrized compensator for both FIR weight cases achieved nominal performance because $|W_1(z)S(z)|$ was less than 0 dB for all frequencies. This shows the design requirements were satisfied by the adaptive Q-parametrized compensator for both FIR weight cases using the first set of coprime rational functions.

The closed-loop stability for the compensated system was examined by analyzing the compensated loop-gain using the Nyquist stability criterion for both FIR weight cases. The pole locations for the compensated loop-gains were obtained using the nominal values for the weight coefficients of the Q parameter. The magnitude for the pole locations of the compensated loop-gain for both FIR weight cases were found to be within the unit disk. Since the magnitude of the poles for the compensated loop-gains were within the unit disk, the compensated system for both FIR weight cases would be closed-loop stable if the Nyquist plots of the compensated loop-gains did not encompass -1 in the counterclockwise direction. The Nyquist plots for the compensated system for both FIR weight cases are shown in figure 35, where the top plot is the Nyquist plot using 5 FIR weights while the bottom plot is the Nyquist plot using 25 FIR weights. This shows the Nyquist plots of the compensated loop-gains did not encompass -1 in the counterclockwise direction, resulting in the adaptive Q-parametrized compensated system being closed-loop stable for both FIR weight cases using the first set of coprime rational functions.

Spectral analysis was performed on the adaptive Q-parametrized compensator to determine if the number of FIR weight coefficients effect the performance of the nominal compensator. The spectrum for the sensitivity function, frequency weighted sensitivity function, displacement of the magnetic particle, and frequency weighted displacement of the magnetic particle for the nominal compensator, 5 FIR weights, and 25 FIR weights are shown in figure 36, figure 37, figure 38, and figure 39 respectively. Figure 36 shows the sensitivity function of the nominal compensator and the adaptive compensators with the FIR weights

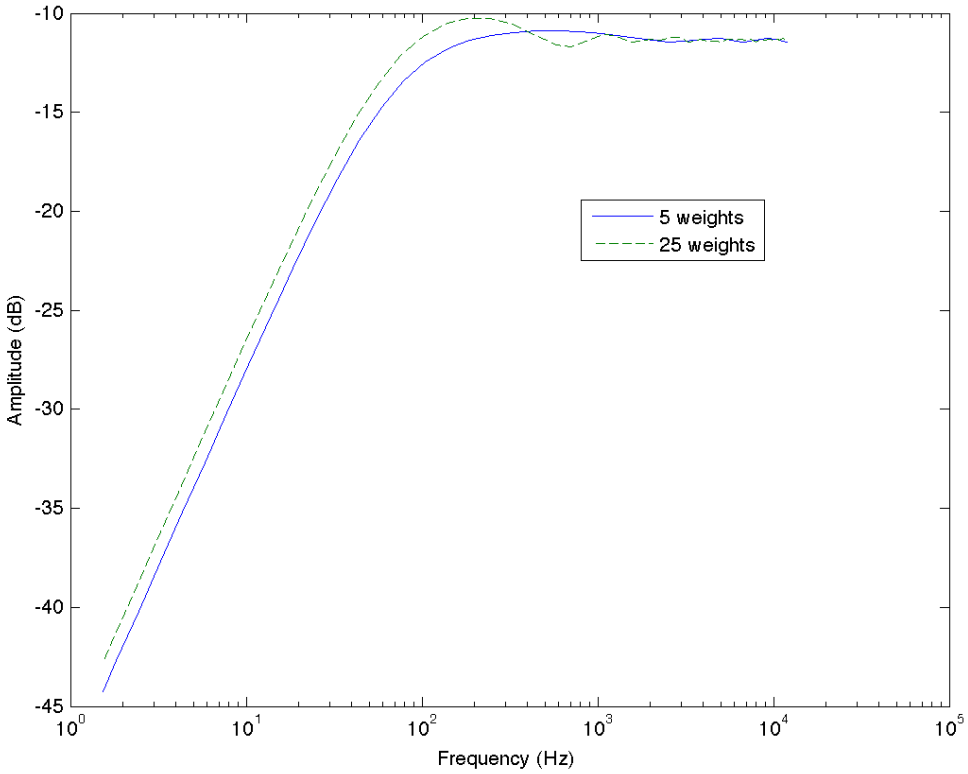

Figure 34: Magnitude of the closed-loop transfer function, $z/\tilde{F}_b$, for both FIR weight cases using the first set of coprime rational functions. This was equivalent to the nominal performance criteria, $|W_1(z)S(z)|$. The adaptive compensator for both FIR weight cases achieved nominal performance because $|W_1(z)S(z)|$ was less than 0 dB for all frequencies.

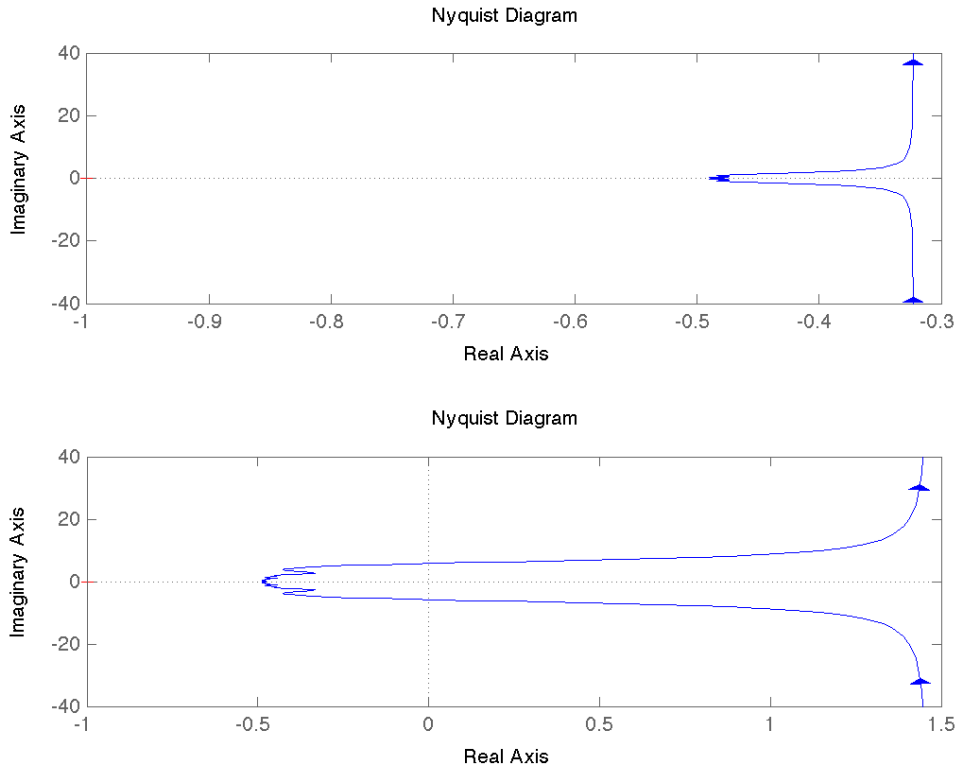

Figure 35: Nyquist plot for the compensated loop-gains using the first set of coprime rational functions. The top plot is the loop-gain for 5 weights and the bottom plot is for 25 weights

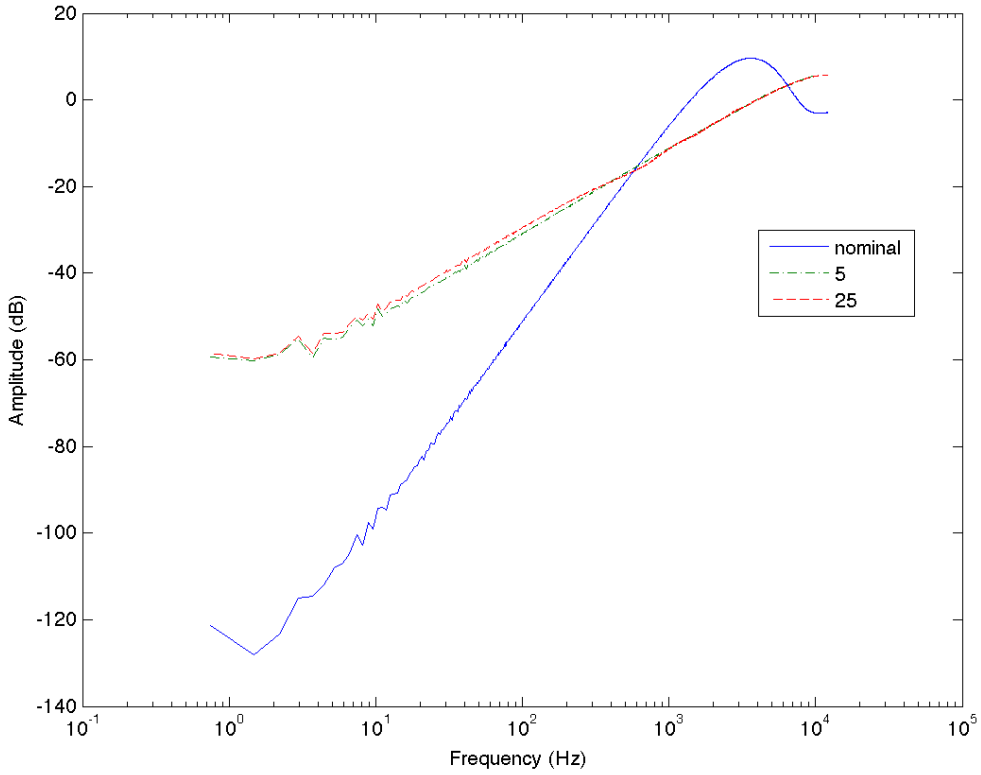

Figure 36: The spectral analysis on the sensitivity function using the adaptive Q-parametrized compensator with the first set of coprime rational functions for the nominal compensator, 5 FIR weights, and 25 FIR weights.

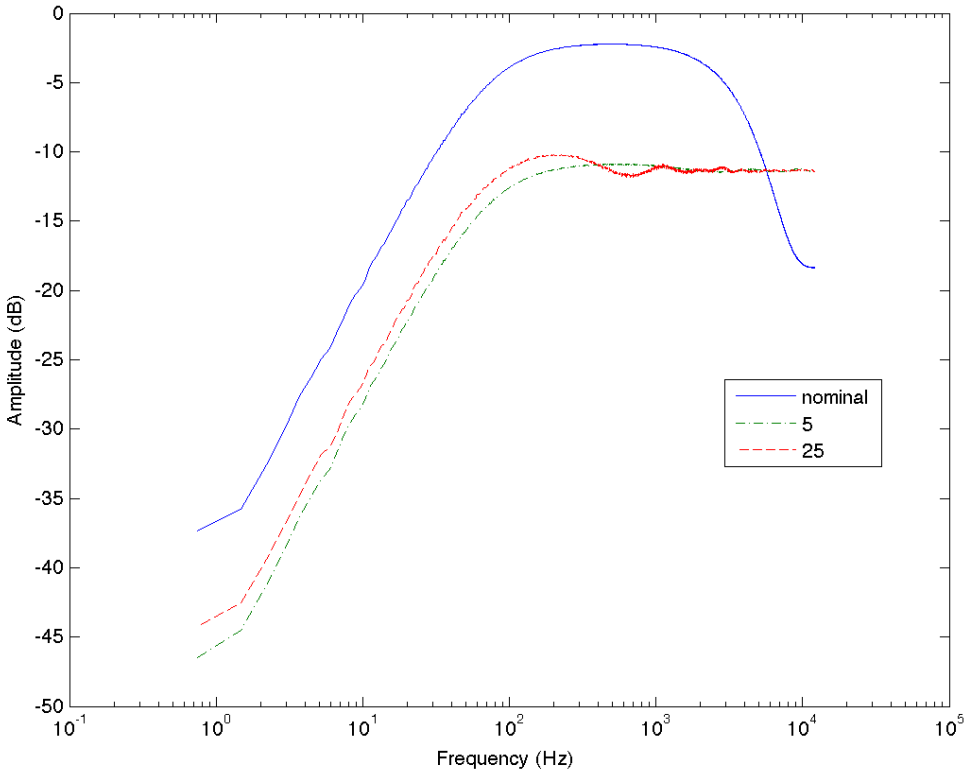

Figure 37: The spectral analysis on the frequency weighted sensitivity function using the adaptive Q-parametrized compensator with the first set of coprime rational functions for the nominal compensator, 5 FIR weights, and 25 FIR weights.

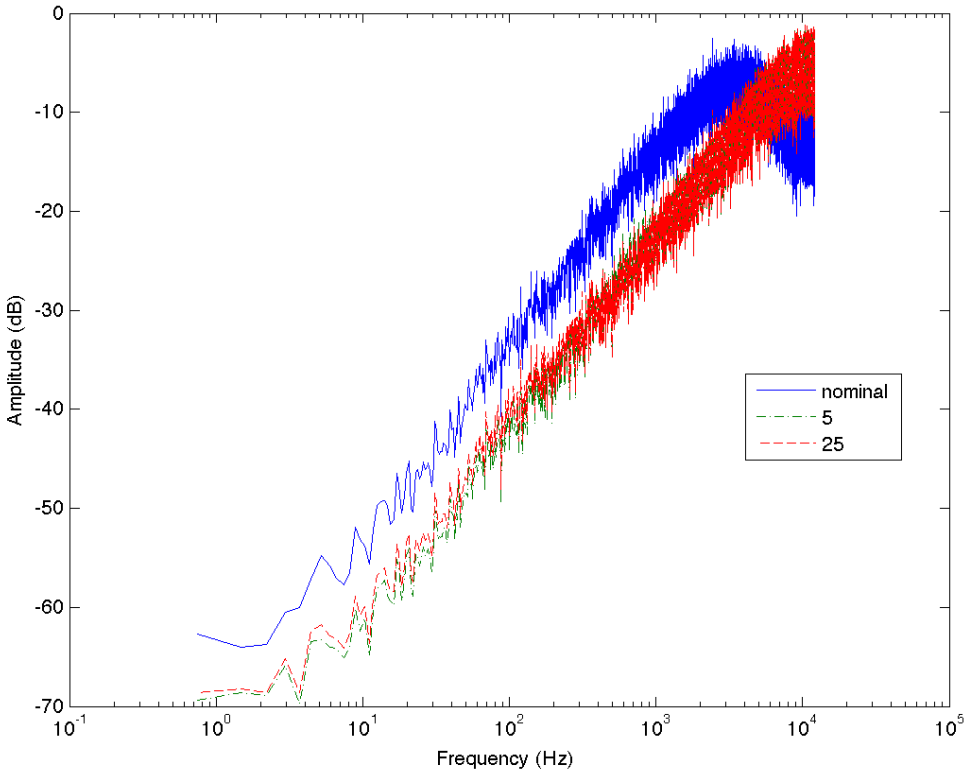

Figure 38: The spectral analysis on the displacement of the magnetic particle using the adaptive Q-parametrized compensator with the first set of coprime rational functions for the nominal compensator, 5 FIR weights, and 25 FIR weights.

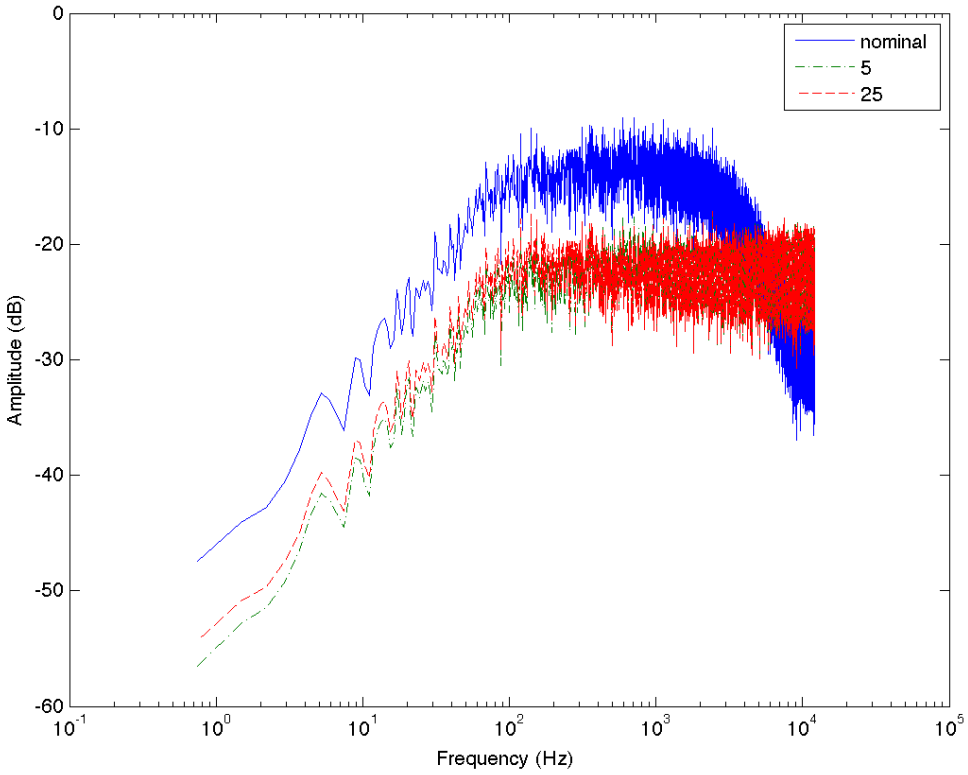

Figure 39: The spectral analysis on the frequency weighted displacement of the magnetic particle using the adaptive Q-parametrized compensator with the first set of coprime rational functions for the nominal compensator, 5 FIR weights, and 25 FIR weights.

were small in the low frequency range pertaining to the disturbance rejection, however the sensitivity function for the nominal compensator is smaller in the low frequency range than the adaptive compensators with the FIR weights. Figure 38 shows the nominal compensator is able to suppress the movement of the magnetic particle due to the Brownian disturbance by approximately at least 26.49 dB for frequencies less than or equal to 100 Hz than the mean particle displacement of -6.988 dB at the dominating frequency of 3.37 kHz. This results in the effects of the Brownian disturbance being minimized in the low frequency range or the range of frequencies that pertains to disturbance rejection. The number of the FIR weight coefficients does have an effect of the performance of the adaptive Q-parametrized compensator. The displacement of the magnetic particle is suppressed greater in the low frequency range as the number of the FIR weight coefficients decrease. The spectrum for the frequency weighted displacement of the magnetic particle shows by using the FIR weight coefficients the frequency weighted displacement of the magnetic particle is minimized for all frequencies while the nominal compensator may not be minimized for all frequencies. In addition as the number of the FIR weight coefficients decrease, the frequency weighted displacement of the magnetic particle was minimized more.

4.3.3 Adaptive Compensator for the Second Set of Coprime Rational Functions

The second set of coprime rational functions were implemented with the adaptive Q-parametrized compensator to satisfy the design requirements. The simulation of the adaptive compensator for both FIR weight cases were performed for a time duration of 150 s to ensure the FIR weight coefficients converged to their nominal values. The FIR weight coefficients of the Q parameter for both FIR weight cases converged to nominal values as shown in figure 40, where the top plot is for the 5 FIR weights while the bottom plot is for the 25 FIR weights. Due to the complexity of the compensated system, figure 40 shows the weight coefficients that were downsampled by $2(10^3)$ that implies the adaptive compensated system was sampled at 12.5 Hz. Downsampling the adaptive compensated system is valid to show the characteristics of how the FIR weight coefficients converged to their nominal values because downsampling does not affect the performance of the system in the time domain.

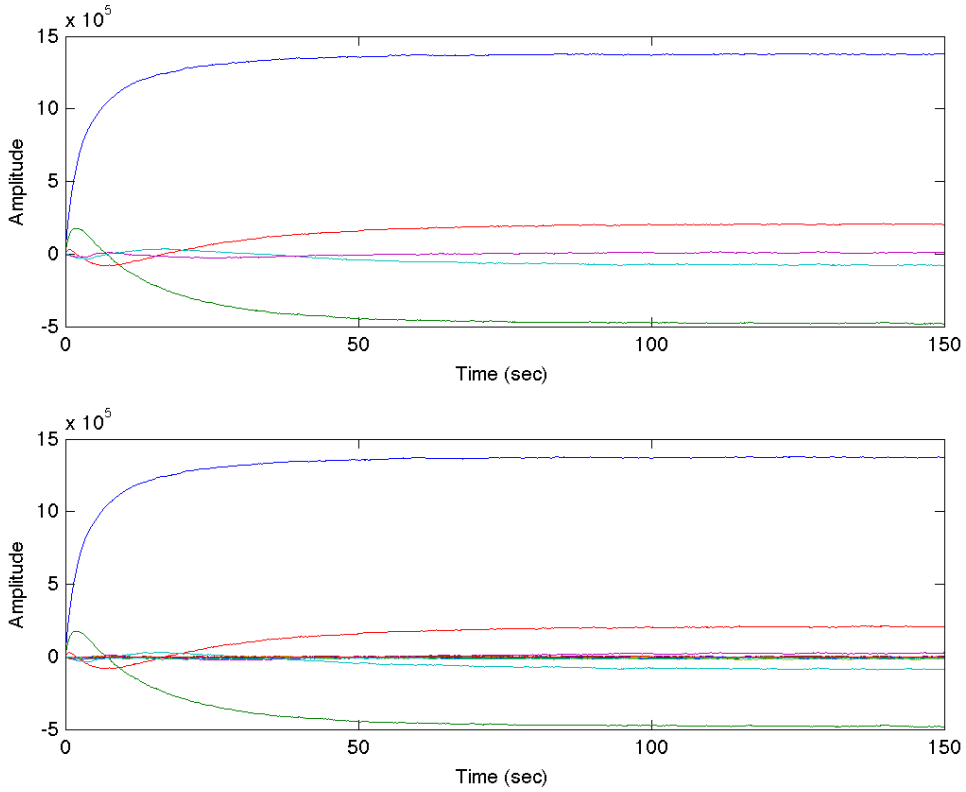

Figure 40: Shows the weights coefficients for adaptive Q-parametrized compensator reaches steady-state. The top plot is the weight coefficients using 5 FIR weights while the bottom plot is the weight coefficients using 25 FIR weights.

The adaptive compensator was analyzed once the compensated system reached steady-state. The compensated system reached steady state when the FIR weight coefficients converged to their nominal values. The analysis was performed on the adaptive compensated system over the last 5 s of the simulation. Once the weight coefficients of the Q parameter converged, the loop-gain, the sensitivity function, and the complimentary sensitivity function for the steady state compensated system were found for both FIR weight cases. The magnitude of the frequency response for the loop-gain, the sensitivity function, and the complimentary sensitivity function and the phase of the loop-gain for the compensated system are shown in figure 41 and figure 42 respectively for the 5 and 25 FIR weights. The bandwidth frequency and the phase margin for the adaptive compensated system with 5 FIR weight coefficients were determined to be 3.87 kHz and 61.09° respectively through linear interpolation. The adaptive compensator with 5 FIR weight coefficients had a faster bandwidth frequency and a smaller phase margin than the fixed gain compensators. Since the bandwidth frequency and the phase margin for the adaptive compensator with 5 FIR weights were greater than the desired bandwidth frequency and the phase margin, the design requirements were satisfied. The bandwidth frequency and the phase margin for the adaptive compensated system with 25 FIR weight coefficients were determined to be 3.82 kHz and 63.35° respectively through linear interpolation. The adaptive compensator with 25 FIR weight coefficients had a faster bandwidth frequency and a smaller phase margin than the fixed gain compensators. Since the bandwidth frequency and the phase margin for the adaptive compensator with 25 FIR weights were greater than the desired bandwidth frequency and the phase margin, the design requirements were satisfied.

The magnitude for the closed-loop transfer function relating the frequency weighted displacement of the magnetic particle to the Brownian disturbance was equivalent to the nominal performance criteria: the magnitude for the product of the nominal performance weight and the sensitivity function. The nominal performance criteria for each FIR weight case was examined by analyzing the magnitude of $W_1(z)S(z)$ as shown in figure 43. The adaptive Q-parametrized compensator for both FIR weight cases achieved nominal performance because $|W_1(z)S(z)|$ was less than 0 dB for all frequencies. This shows the design requirements were

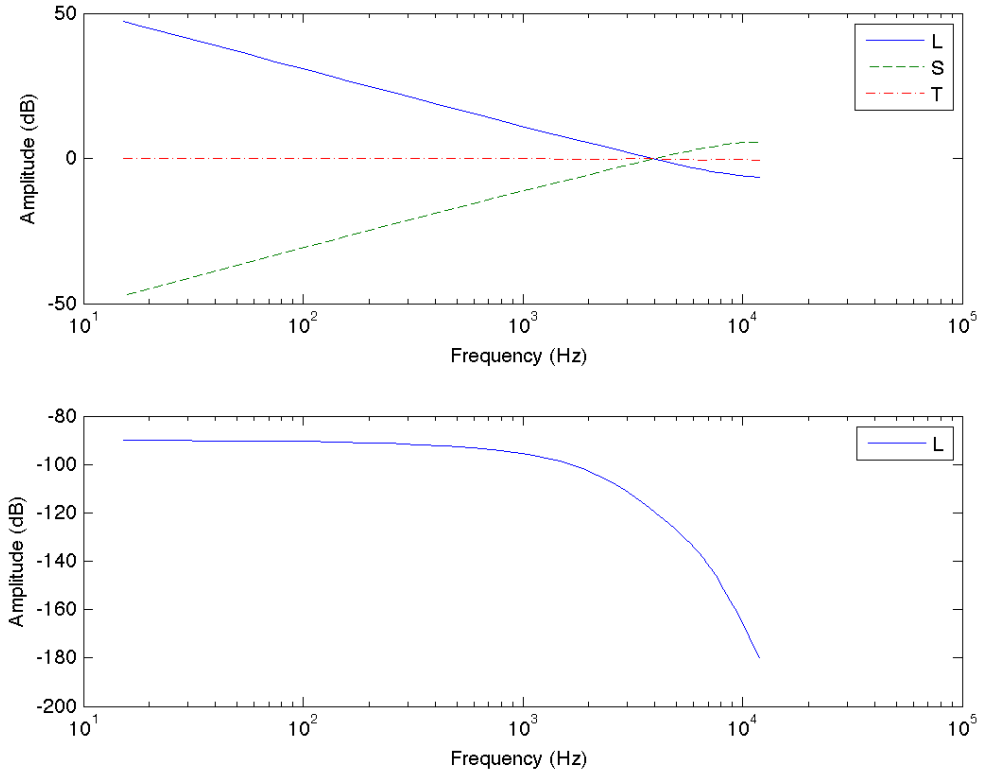

Figure 41: The magnitude for the loop-gain, sensitivity function, and complimentary sensitivity function and the phase of the loop-gain of the adaptive Q-parametrized compensated system for 5 FIR weights using the second set of coprime rational functions.

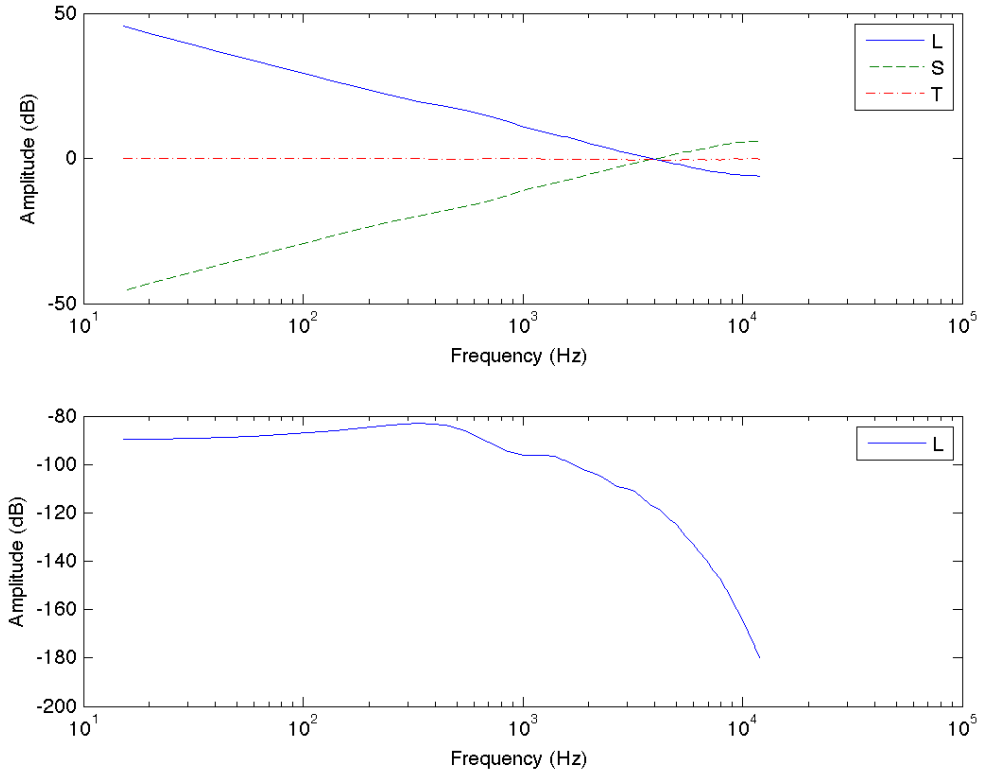

Figure 42: The magnitude for the loop-gain, sensitivity function, and complimentary sensitivity function and the phase of the loop-gain of the adaptive Q-parametrized compensated system for 25 FIR weights using the second set of coprime rational functions.

satisfied by the adaptive Q-parametrized compensator for both FIR weight cases using the second set of coprime rational functions.

The closed-loop stability for the compensated system was examined by analyzing the compensated loop-gain using the Nyquist stability criterion for both FIR weight cases. The pole locations for the compensated loop-gains were obtained using the nominal values for the weight coefficients of the Q parameter. The magnitude of the pole locations for the compensated loop-gain for both FIR weight cases were found to be within the unit disk. Since the magnitude of the poles for the compensated loop-gains were within the unit disk, the compensated system for both FIR weight cases would be closed-loop stable if the Nyquist plots of the compensated loop-gains did not encompass -1 in the counterclockwise direction. The Nyquist plots for the compensated system for both FIR weight cases are shown in figure 44, where the top plot is the Nyquist plot using 5 FIR weights while the bottom plot is the Nyquist plot using 25 FIR weights. This shows the Nyquist plots of the compensated loop-gains did not encompass -1 in the counterclockwise direction, resulting in the adaptive Q-parametrized compensated system being closed-loop stable for both FIR weight cases using the second set of coprime rational functions.

Spectral analysis was performed on the adaptive Q-parametrized compensator to determine if the number of FIR weight coefficients effects the performance of the nominal compensator. The spectrum for the sensitivity function, frequency weighted sensitivity function, displacement of the magnetic particle, and frequency weighted displacement of the magnetic particle for the nominal compensator, 5 FIR weights, and 25 FIR weights are shown in figure 45, figure 46, figure 47, and figure 48 respectively. Figure 45 shows the sensitivity function of the nominal compensator and the adaptive compensators with the FIR weights were small in the low frequency range that pertains to disturbance rejection however the sensitivity function for the nominal compensator is smaller in the low frequency range than the adaptive compensators with the FIR weights. Figure 47 shows the nominal compensator is able to suppress the movement of the magnetic particle by approximately at least 25.25 dB for frequencies less than or equal to 100 Hz than the mean particle displacement of -7.845 dB at the dominating frequency of 3.16 kHz. This results in the effects of the Brownian disturbance being minimized in the low frequency range or the range of frequencies that

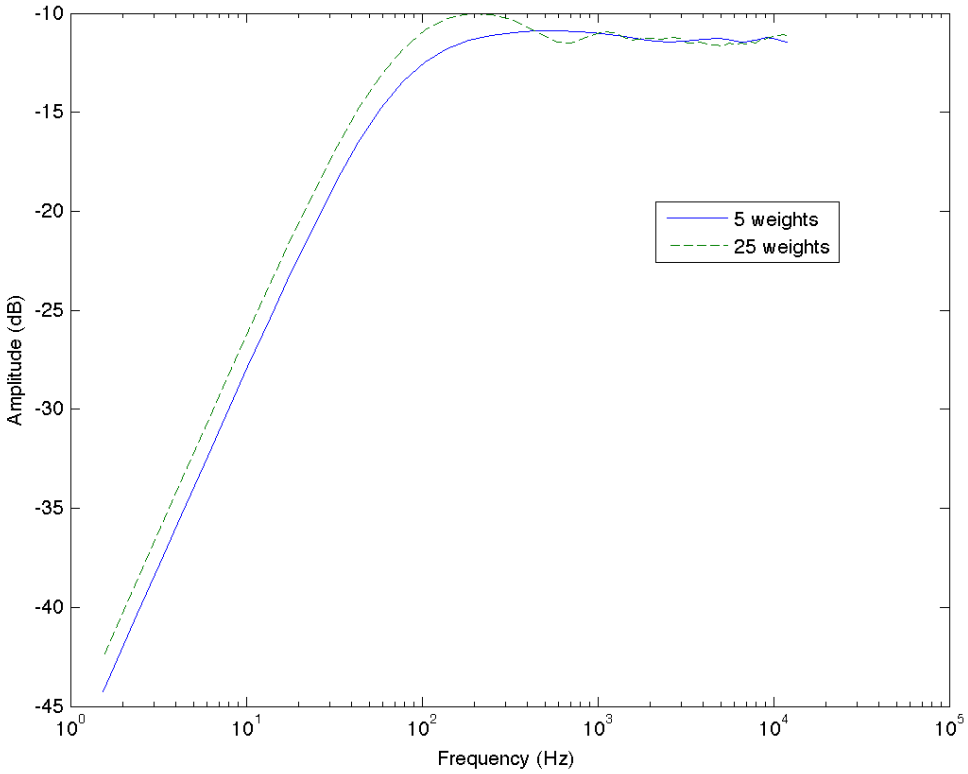

Figure 43: Magnitude of the closed-loop transfer function, $z/\tilde{F}_b$, for both FIR weight cases using the second set of coprime rational functions. This was equivalent to the nominal performance criteria, $|W_1(z)S(z)|$. The adaptive compensator for both FIR weight cases achieved nominal performance because $|W_1(z)S(z)|$ was less than 0 dB for all frequencies.

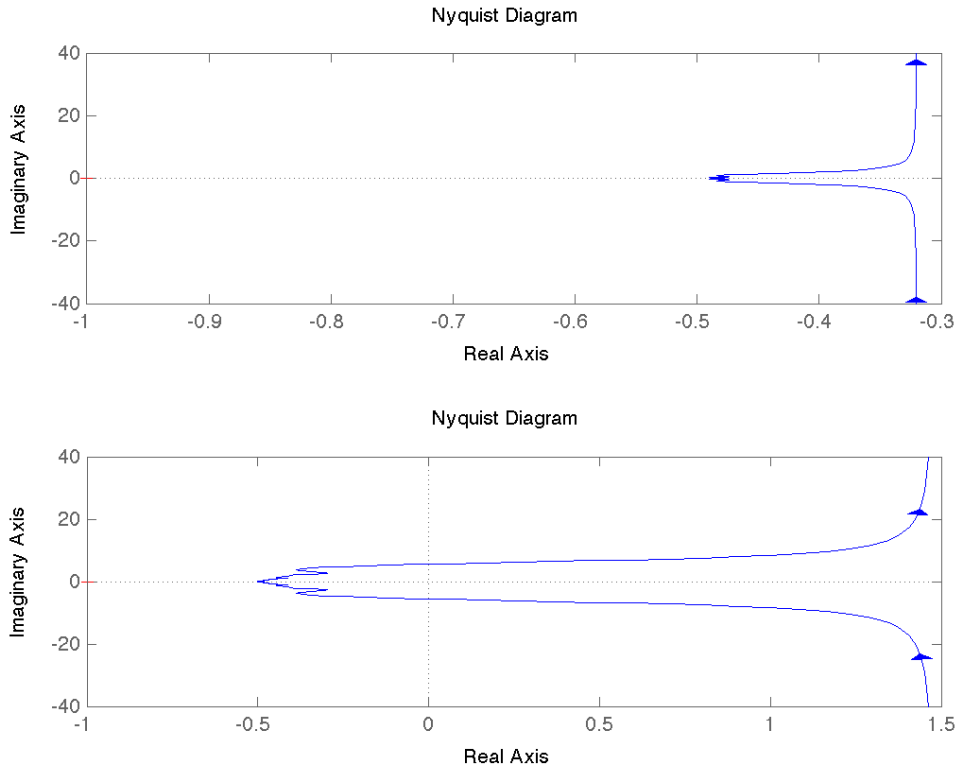

Figure 44: Nyquist plot for the compensated loop-gains using the second set of coprime rational functions. The top plot is the loop-gain for 5 weights and the bottom plot is for 25 weights

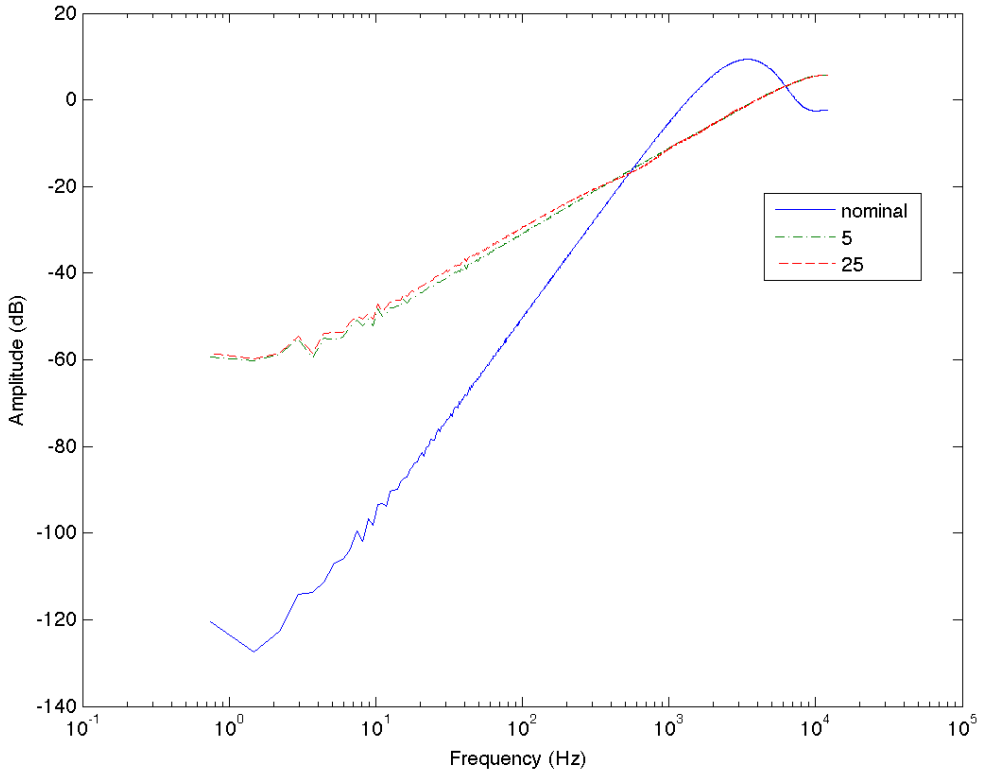

Figure 45: The spectral analysis on the sensitivity function using the adaptive Q-parametrized compensator with the second set of coprime rational functions for the nominal compensator, 5 FIR weights, and 25 FIR weights.

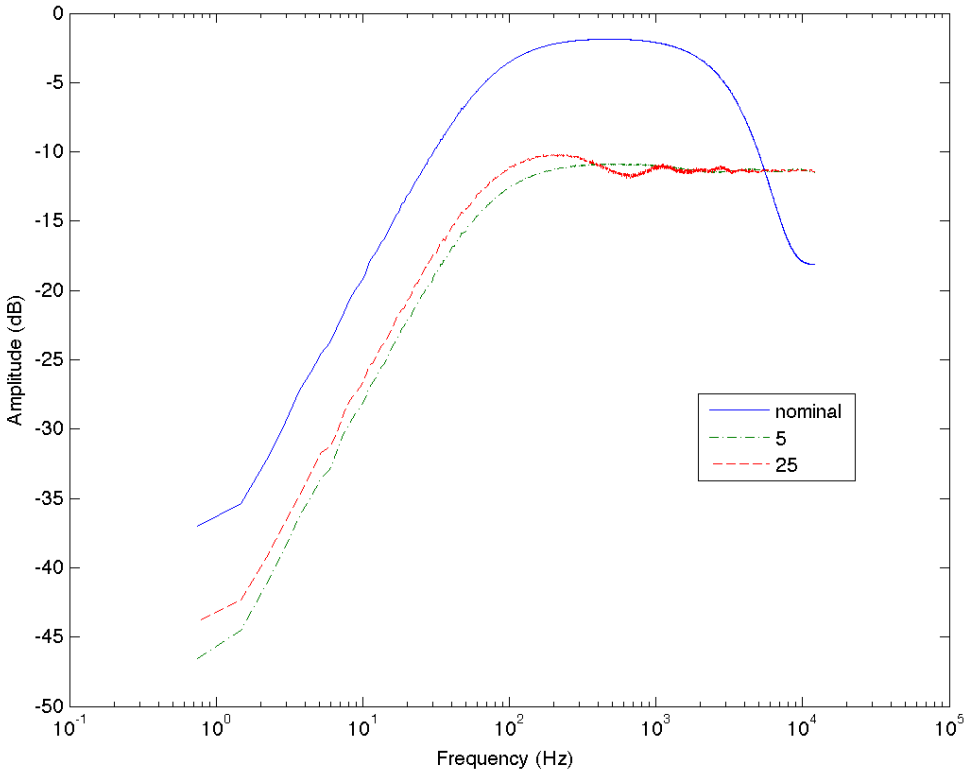

Figure 46: The spectral analysis on the frequency weighted sensitivity function using the adaptive Q-parametrized compensator with the second set of coprime rational functions for the nominal compensator, 5 FIR weights, and 25 FIR weights.

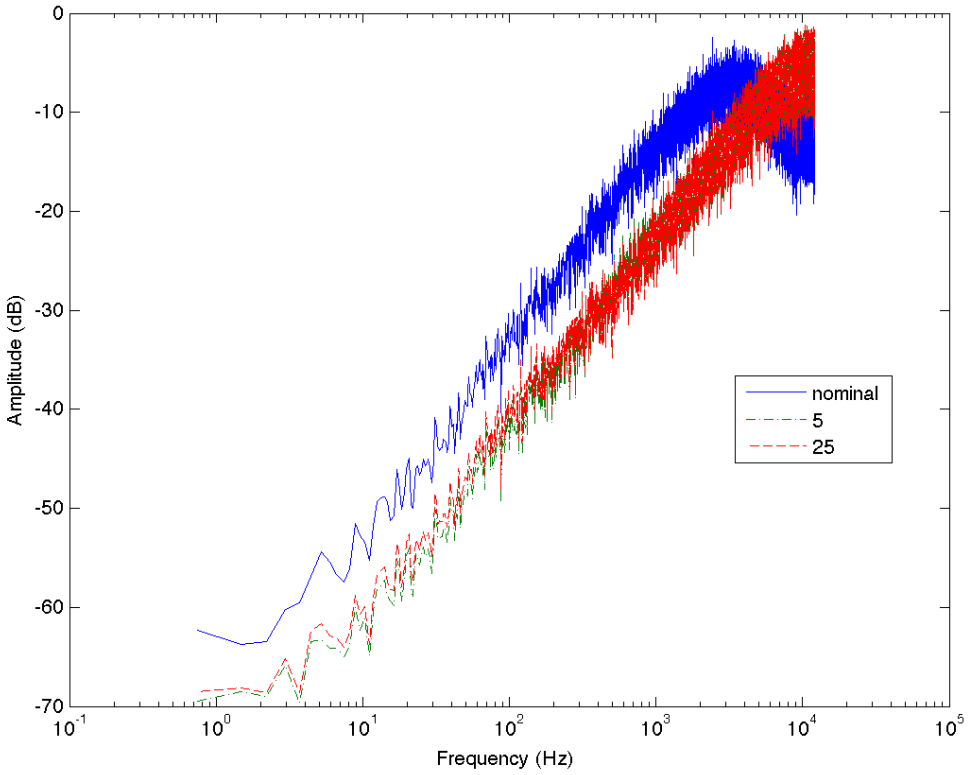

Figure 47: The spectral analysis on the displacement of the magnetic particle using the adaptive Q-parametrized compensator with the second set of coprime rational functions for the nominal compensator, 5 FIR weights, and 25 FIR weights.

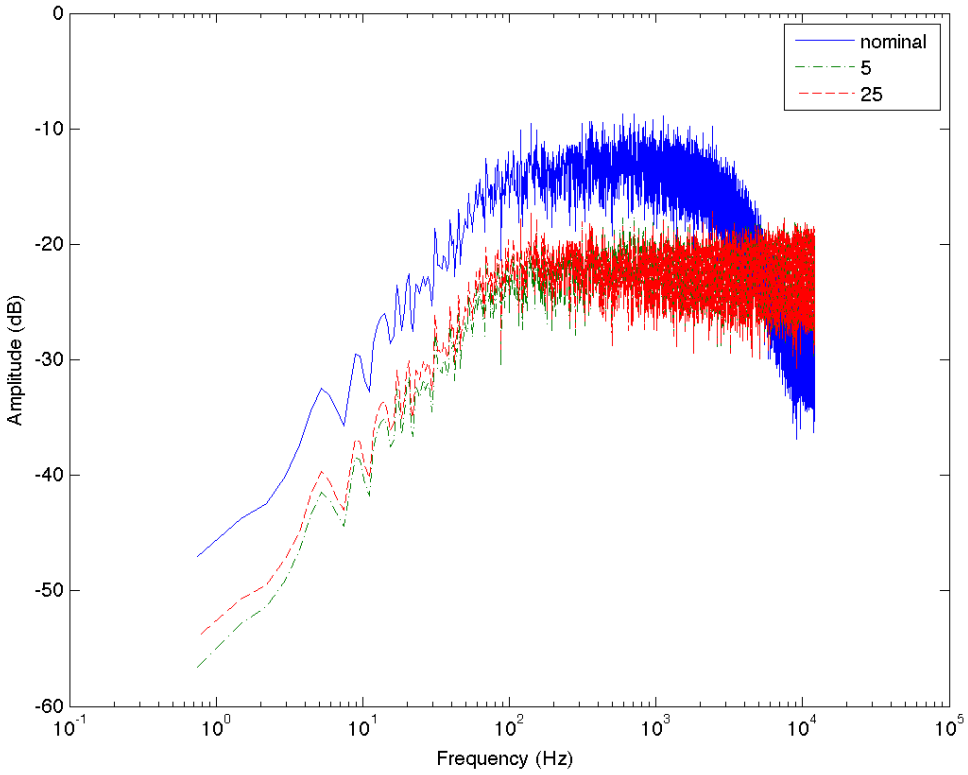

Figure 48: The spectral analysis on the frequency weighted displacement of the magnetic particle using the adaptive Q-parametrized compensator with the second set of coprime rational functions for the nominal compensator, 5 FIR weights, and 25 FIR weights.

pertains to disturbance rejection. The number of the FIR weight coefficients does have an effect on the performance of the adaptive Q-parametrized compensator. The displacement of the magnetic particle was suppressed greater in the low frequency range as the number of FIR weight coefficients decrease. The spectrum for the frequency weighted displacement of the magnetic particle shows by using the FIR weight coefficients the frequency weighted displacement of the magnetic particle is minimized for all frequencies while the nominal compensator may not be minimized for all frequencies. In addition as the number of FIR weight coefficients decreases, the frequency weighted displacement of the magnetic particle was minimized more.

5.0 EXPERIMENTAL RESULTS

This chapter discusses the experimental results for the various compensation methods that were incorporated into the design of the magnetic particle system to minimize the effects of the Brownian disturbances. The experimental method used to emulate the actual experimental conditions since the sensor was not working properly is discussed first. Finally the experimental results for the various compensation methods are given.

5.1 EXPERIMENTAL METHODS AND CONDITIONS

The demonstration of the performance for the various compensation methods was important to illustrate the capabilities of the compensators. The method used to demonstrate the experimental conditions without using a sensor was performed in the following way: two controller boards with analog to digital, A/D, and digital and analog, D/A, compatibilities, dSpace DS1104 RD controller boards, were connected together. One dSpace board contained the discrete-time magnetic particle system and the Brownian disturbance while the other board contained the feedback compensation structure. The control signal from the dSpace board containing the compensator was sent through a D/A port and fed into the dSpace board containing the magnetic particle system using an A/D port. The control signal was sent through the magnetic particle system and superimposed with the Brownian disturbance to obtain the displacement of the magnetic particle. The displacement of the magnetic particle was sent through a D/A port and fed into the dSpace board containing the compensator structure using an A/D port that was then compared to the desired position of the mag-

netic particle to create an error signal. The desired position of the magnetic particle was set to 0 nm to have the movement of the magnetic particle be caused by only the Brownian disturbance.

The D/A and A/D ports of the dSpace boards had 16 and 12 bits of resolution respectively while the dynamic range of the dSpace boards were ± 10 V. To ensure the control signal and the displacement of the magnetic particle were within the dynamic range of the dSpace boards, each signal if needed was modified by a gain that had units of volts per volts, to place the signal within the dynamic range of the dSpace boards to prevent saturation. After the signals were multiplied by its respective gain before being sent through the D/A ports, the signals were also multiplied by the reciprocal of the gain on the other dSpace board to have the control system experience the actual signals.

5.1.1 The Discrete-Time Magnetic Particle System for the Experiments

The experiments for the various compensation methods were initially performed having the sampling frequency for both dSpace boards being equal to 25 kHz. The internal clocks on the dSpace boards should of had been in sync by having the same sampling frequency, resulting in the dSpace boards commuting information correctly. As the control signal from the compensator dSpace board is fed into the magnetic particle system dSpace board, the resulting displacement of the magnetic particle should of had been fed into the compensator dSpace board as the control signal at the next time step is fed into the magnetic particle system dSpace board. However while performing the experiments, the control signal and the displacement of the magnetic particle were experiencing unexpected physical phenomena or beat frequency characteristics when the experiments were running for long time durations. One explanation for the beat frequency phenomena is the internal clocks of the dSpace boards were out of sync, causing one dSpace board being a multiple of a time step off of the other dSpace board. The method used to eliminate the beat frequency phenomena in the control signal and the displacement of the magnetic particle was changing the sampling frequency of

Table 5: The gain used to modify the control signal to use the dynamic range of the dSpace boards using fixed gain compensation

Gain variable	c1 (V/V)
Value	$6.66(10^{-6})$

the dSpace board containing the magnetic particle system and the Brownian disturbance by an irrational number to 35.35 kHz. The discrete-time magnetic particle system was changed as a result of the sampling frequency being changed.

$$G(z) = 423(10^{-9})\frac{(z+0.5025)}{(z-1)(z-0.1185)} \tag{5.1}$$

5.2 RESULTS FOR THE FIXED GAIN COMPENSATORS

This section discusses the experimental results for the fixed gain compensators to minimize the effects of the Brownian disturbances. The first fixed gain compensator incorporated into the design of the magnetic particle system was the proportional gain compensator. Finally the results for the two fixed gain Q-parametrized compensators are given.

Fixed gain compensation methods were first incorporated into the design of the magnetic particle system using the dSpace boards. The control signal and the displacement of the particle were examined to determine if these signals needed to be modified to be within the dynamic range of the dSpace boards. The simulation of the fixed gain compensation methods were performed for 10 s to determine if these signals had to be modified. The displacement of the magnetic particle was within the dynamic range of the dSpace, resulting in the control signal being modified by a gain $c1$ as shown in table 5. The block diagram schematic of the fixed gain compensator structure on the compensator dSpace board is shown in figure 49, where W_1 is the nominal performance weight, K is the fixed gain compensator. The control signal was scaled down to be within the dynamic range of the dSpace boards and

was multiplied by a gain of 0.1 to counteract the dSpace board automatically multiplying the signal by a gain of 10 during the D/A process. The displacement of the magnetic particle was amplified by a gain of 10 to counteract the dSpace board automatically multiplying the signal by 0.1 during the A/D conversion.

The control signal from the compensator dSpace board was fed to the magnetic particle system on the other dSpace board as shown in figure 50, where the gain $1/c_1$ modifies the control signal to have the magnetic particle system experience the actual control signal, the band-limited white noise is the Brownian disturbance while the gain g_2 converts the displacement of the particle, due to the Brownian disturbance, into voltage.

5.2.1 Proportional Gain Compensation

The experiment for the proportional gain compensator was performed using ControlDesk, an experimental software environment that is able to change the numerical values of the parameters during the experiment and saves data. The performance of the proportional gain compensator was evaluated by analyzing the displacement of the magnetic particle and the frequency weighted displacement of the magnetic particle using spectral analysis for a time duration of 2 s. The spectral analysis for the displacement of the magnetic particle and the frequency weighted displacement of the magnetic particle are shown in figure 51 and figure 52 respectively. The evaluation of the proportional gain compensator will be given after the fixed gain Q-parametrized compensators.

5.2.2 Fixed Gain Q-Parametrized Compensation

The final fixed gain compensation method applied to the magnetic particle system was the two fixed gain Q-parametrized compensators to demonstrate the compensator structure minimized the effects of the Brownian disturbances before the weight coefficients of Q were adjusted with LMS to minimize the frequency weighted displacement of the magnetic particle.

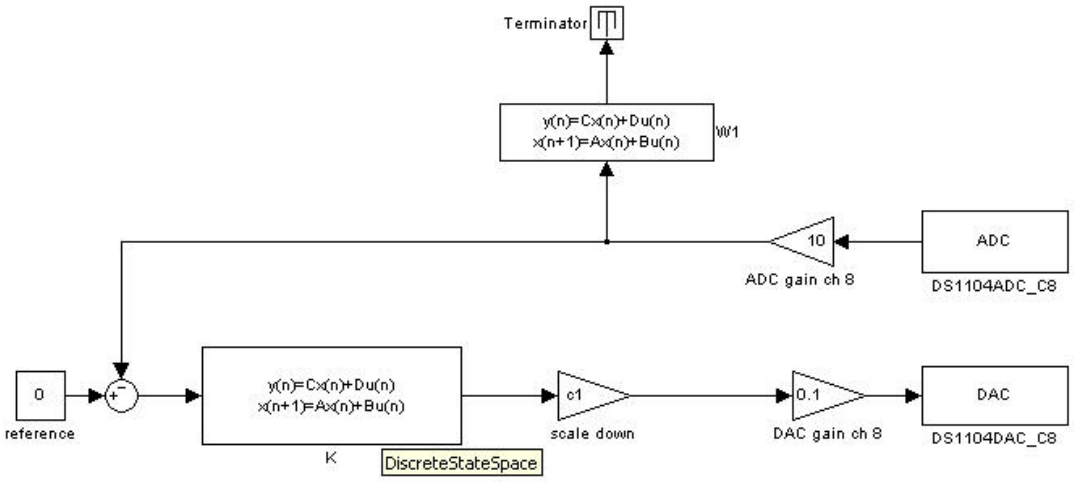

Figure 49: The fixed gain compensator structure on the controller dSpace board to minimize the Brownian disturbances and to stabilize the position of the magnetic particle using fixed gain compensation methods. The compensator, K, is either the proportional gain compensator or the fixed gain Q-parametrized compensator depending on the compensation method being used.

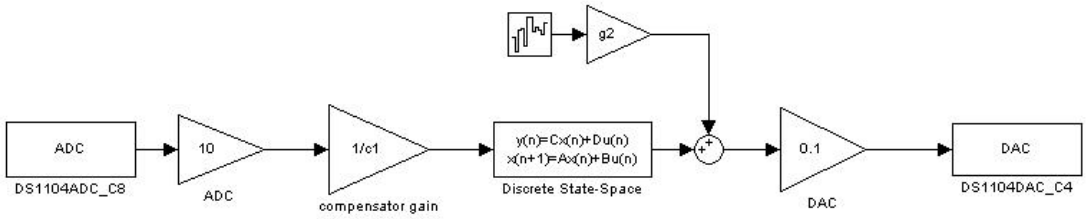

Figure 50: The block diagram schematic of the magnetic particle system on the other dSpace board. This schematic is the same for the various compensation methods except the gain of $1/c_1$ changes depending on the compensation method being used.

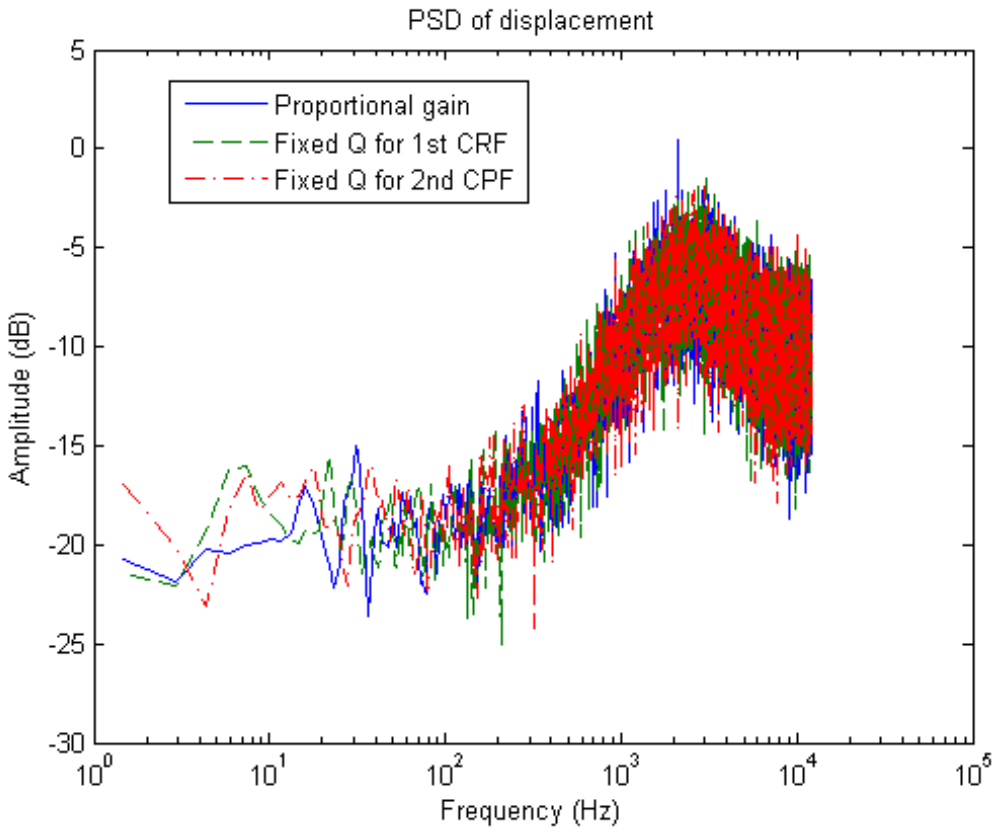

Figure 51: Experimental displacement of the magnetic particle using spectral analysis for the proportional gain compensation and the fixed gain Q-parametrized compensation for both sets of coprime rational functions.

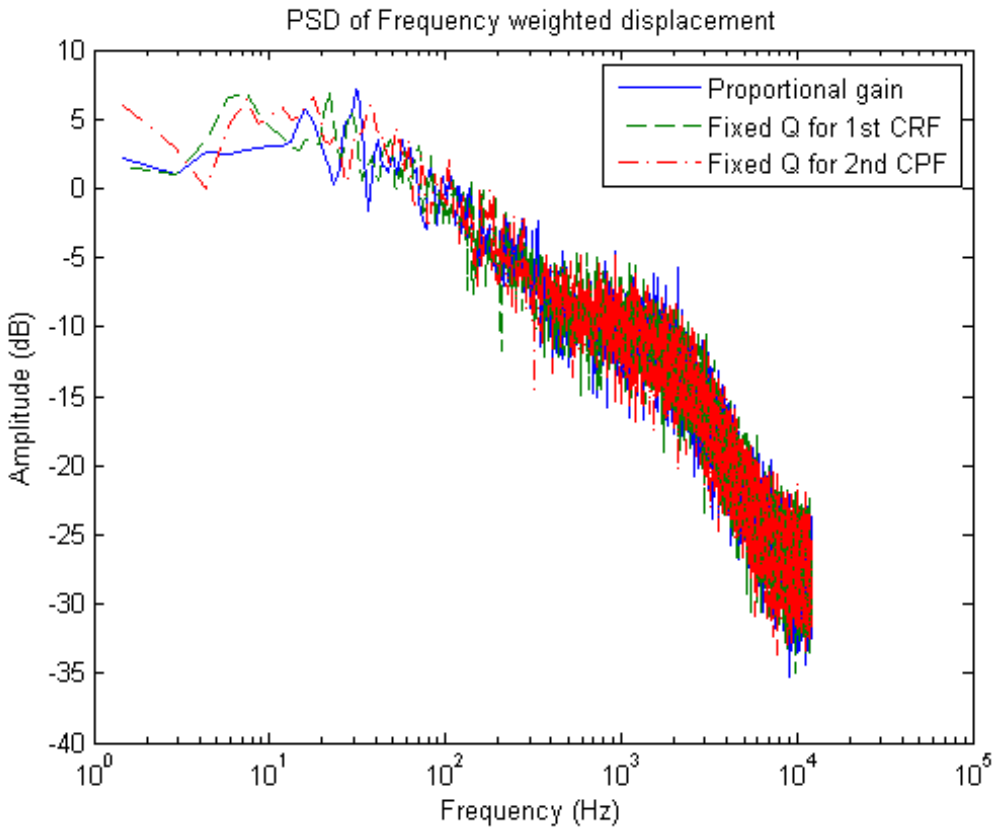

Figure 52: Experimental frequency weighted displacement of the magnetic particle using spectral analysis for the proportional gain compensation and the fixed gain Q-parametrized compensation for both sets of coprime rational functions.

5.2.2.1 Data for the First Set of Coprime Rational functions

The experiment for the first set of coprime rational functions with the fixed gain Q-parametrized compensator was performed using ControlDesk. Spectral analysis was used to evaluate the performance of the compensator by analyzing the displacement of the magnetic particle and the frequency weighted displacement of the magnetic particle for a time duration of 2 s. The experimental displacement of the magnetic particle and the frequency weighted displacement of the magnetic particle using the fixed gain Q-parametrized compensation with the first set of the coprime rational functions are shown in figure 51 and figure 52 respectively.

5.2.2.2 Data for Second Set of Coprime Rational Functions

The experiment for the fixed gain Q-parametrized compensator using the second set of coprime rational functions was performed using ControlDesk. Spectral analysis was used to evaluate the performance of the compensator by analyzing the displacement of the magnetic particle and the frequency weighted displacement of the magnetic particle for a time duration of 2 s. The experimental displacement of the magnetic particle and the frequency weighted displacement of the magnetic particle using the fixed gain Q-parametrized compensation with the second set of the coprime rational functions are shown in figure 51 and figure 52 respectively.

5.2.3 Analysis of the Performance for the Fixed Gain Compensators

The spectral analysis of the proportional gain compensator and the fixed gain Q-parametrized compensators with both sets of coprime rational functions showed the displacement of the magnetic particle, as shown in figure 51, was approximately equal for frequencies greater than or equal to 100 Hz. The displacement of the magnetic particle was different using the different compensation methods for frequencies less than 100 Hz. The Brownian disturbances were suppressed by an average of 13.206 dB, 13.086 dB, and 12.56 dB for the proportional gain compensator and the fixed gain Q-parametrized compensator using the first and second sets of coprime rational functions respectively for frequencies less than 100 Hz from the mean particle displacement of -6.184 dB at the dominating frequency of 2.615 kHz.

The frequency weighted displacement of the magnetic particle for the proportional gain compensation and the fixed gain Q-parametrized compensation using the first and second sets of coprime rational functions were equal for frequencies higher than approximately 86 Hz. The fixed gain compensation methods may not of had minimized the frequency weighted displacement of the magnetic particle. The adaptive Q-parameterized compensators were used to minimize the effects of the Brownian disturbances acting on the magnetic particle by minimizing the frequency weighted displacement of the magnetic particle for all frequencies.

5.3 ADAPTIVE COMPENSATION

The final compensation method incorporated into the design of the magnetic particle system was the adaptive Q-parametrized compensation to minimize the effects of the Brownian disturbances. This was accomplished by adjusting the weight coefficients of the Q parameter in the Q-parametrized compensator with LMS to minimize the frequency weighted displacement of the magnetic particle. Similarly to the simulation of the adaptive compensators, different number of weight coefficients were used to determine if the number of FIR weights effects the performance of the adaptive compensator with respect to the nominal compensator, $K = X/Y$. The number of FIR weights used for the experiments were 2, 5, and 10 FIR weights. The leakage factor, γ, and the step-size parameter, μ, chosen to stabilize the LMS structure were 0.9999995 and $500(10^3)$ respectively.

The control signal and the displacement of the magnetic particle were examined to determine if these signals needed to be modified to be within the dynamic range of the dSpace boards. The simulation of the adaptive compensators were performed for 600 s to ensure the weight coefficients converged to their nominal values. The last 5 s of the simulation was analyzed, yielding the control signal had to be modified by a gain of c_1, given in table 6, to be within the dynamic range of the dSpace boards.

The block diagram schematic for the feedback adaptive compensator on the compensator dSpace board is shown in figure 53, where controller is the compensator subsystem, LMS is the LMS subsystem, W_1 is the nominal performance weight, and the gain c_1 scales down

Table 6: The gain used to modify the control signal to use the dynamic range of the dSpace boards using the adaptive Q-parametrized compensation methods

Gain variable	c1 (V/V)
Value	$2(10^{-6})$

the control signal to be within the dynamic range of the dSpace boards. The schematic for the magnetic particle system and the Brownian disturbance was the same schematic used for the fixed gain compensators as shown in figure 50.

5.3.1 First Set of Coprime Rational Functions

The experiment was performed using the first set of coprime rational functions for the three FIR weight cases and the nominal compensator with ControlDesk. The convergence of the weight coefficients to their nominal values were important in analyzing the steady-state compensated system with spectral analysis. The time duration for the FIR weight cases varied to ensure the weight coefficients converged to nominal values as shown in figure 54, where the top plot is for the 2 FIR weights, the middle plot is for 5 FIR weights, and the bottom plot is for 10 FIR weights. The weight coefficients for the three FIR weight cases, as shown in figure 54, were downsampled by 2000 or sampled at 12.5 Hz to show the weights converged to nominal values due to the complexity of the feedback compensated system. Downsampling the compensated system to show the FIR weights converged to their nominal values was valid because the information of the compensated system is not affected in the time domain by the sampling frequency. Once the weight coefficients converged to their nominal values, the performance of the adaptive Q-parametrized compensators for the three FIR weight cases and the nominal compensator were examined using spectral analysis. Spectral analysis was used to analyze the steady state displacement of the magnetic particle and the frequency weighted displacement of the magnetic particle as shown in figure 55 and figure 56 respectively for a time duration of 2 s.

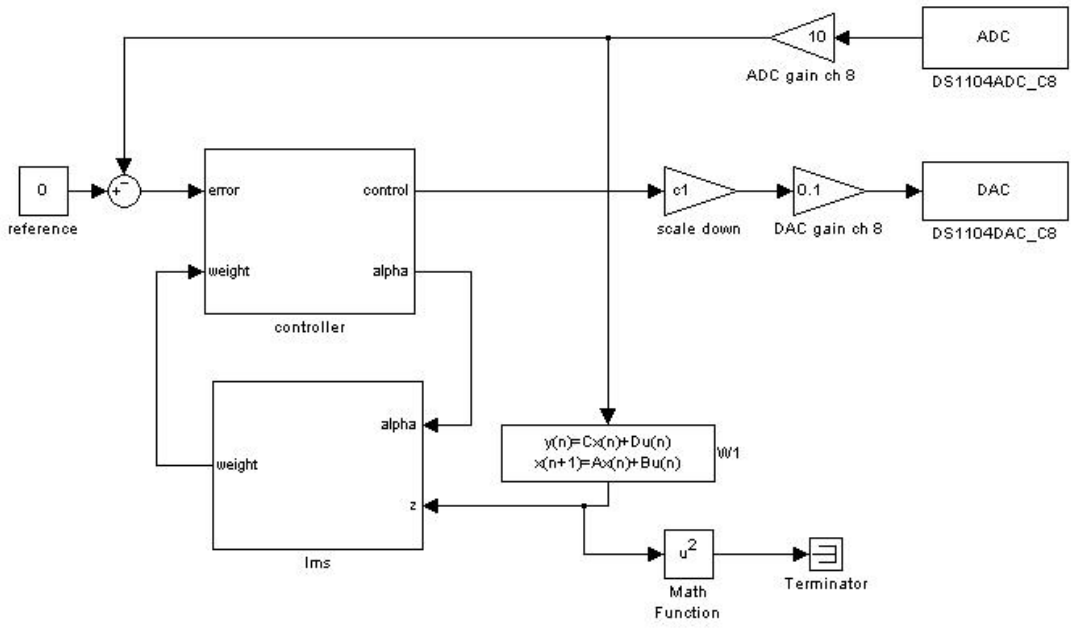

Figure 53: The adaptive compensator structure on the controller dSpace board to minimize the Brownian disturbances and to stabilize the position of the magnetic particle using adaptive compensation.

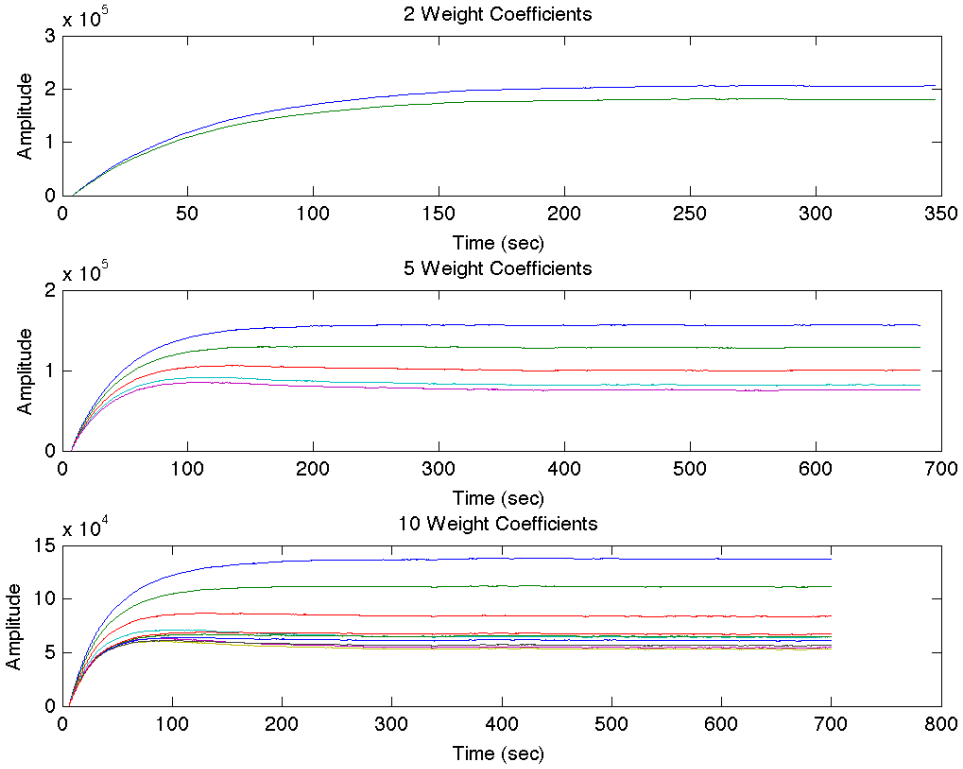

Figure 54: Experimental FIR weights for the adaptive Q-parametrized compensator using the first set of coprime rational functions with 2, 5, and 10 FIR weight coefficients.

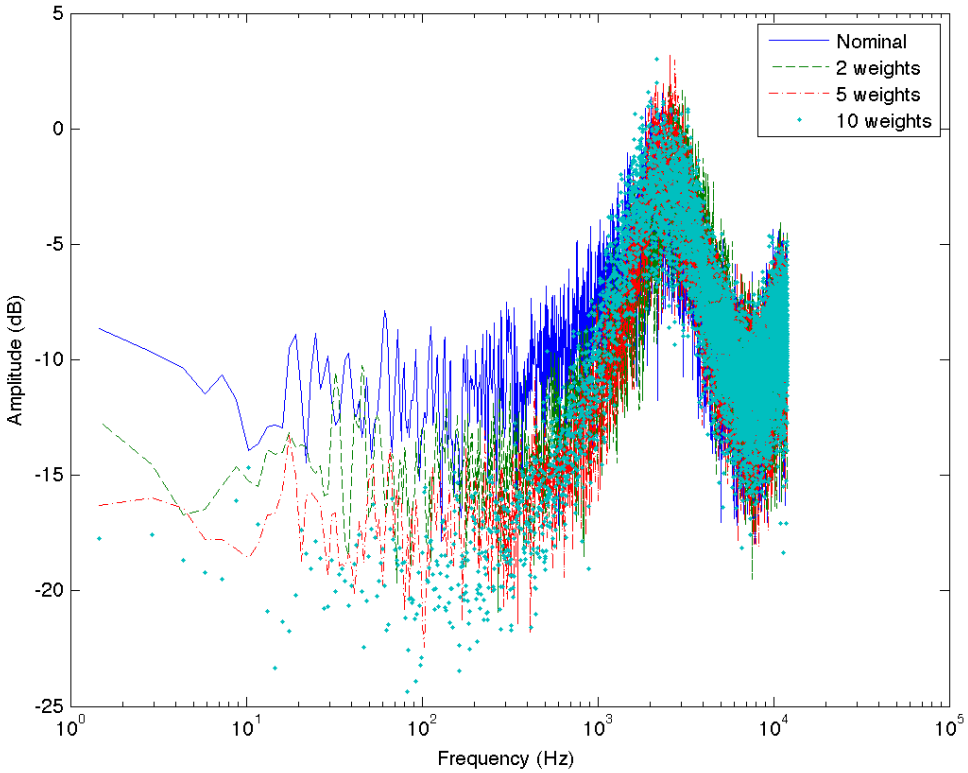

Figure 55: Experimental displacement of the magnetic particle using spectral analysis for the adaptive Q-parametrized compensator using the first set of coprime rational functions with the nominal compensator and the three FIR weight cases.

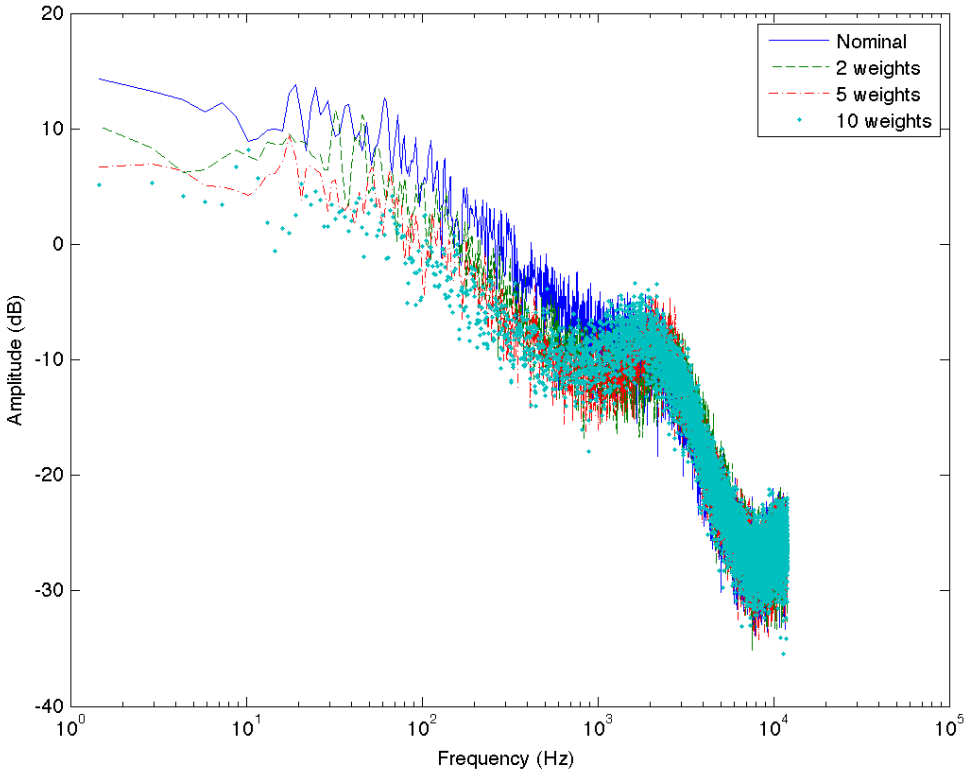

Figure 56: Experimental frequency weighted displacement of the magnetic particle using spectral analysis for the adaptive Q-parametrized compensator using the first set of coprime rational functions with the nominal compensator and the three FIR weight cases.

The spectral analysis for the displacement of the magnetic particle yields as the number of FIR weight coefficients increased, the Brownian disturbances were suppressed more than with the nominal compensator in the low frequency range as shown in figure 55. The effects of the Brownian disturbances being decreased as the number of the FIR weights increased was expected because the number of the FIR weights is equivalent to the number of independent variables used to minimize the frequency weighted displacement of the magnetic particle. As the number of the FIR weights increase, the frequency weighted displacement of the magnetic particle should decrease in the low frequency range as expected as shown in figure 56.

The Brownian disturbance was suppressed by an average of 8.55 dB, 11.78 dB, 14.00 dB, and 15.45 dB for the nominal compensator and the adaptive Q-parametrized compensator using 2, 5, and 10 FIR weights respectively for frequencies less than 400 Hz than the mean particle displacement of -2.99 dB at the dominating frequency of 2.28 kHz.

5.3.2 Second Set of Coprime Rational Functions

The experiment was performed using the second set of coprime rational functions for the three FIR weight cases and the nominal compensator with ControlDesk. The convergence of the weight coefficients to their nominal values were important in analyzing the steady-state compensated system using spectral analysis. The time duration for the FIR weight cases varied to ensure the weight coefficients converged to nominal values as shown in figure 57, where the top plot is for the 2 FIR weights, the middle plot is for 5 FIR weights, and the bottom plot is for 10 FIR weights. The weight coefficients for the three FIR weight cases, as shown in figure 57, were downsampled by 2000 or sampled at 12.5 Hz to show the weights converged to nominal values due to the complexity of the feedback compensated system. Downsampling the compensated system to show the FIR weights converged to their nominal values was valid because the information of the compensated system is not affected in the time domain by the sampling frequency. Once the weight coefficients converged to their nominal values, the performance of the adaptive Q-parametrized compensators for the three FIR weight cases and the nominal compensator were examined using spectral analysis.

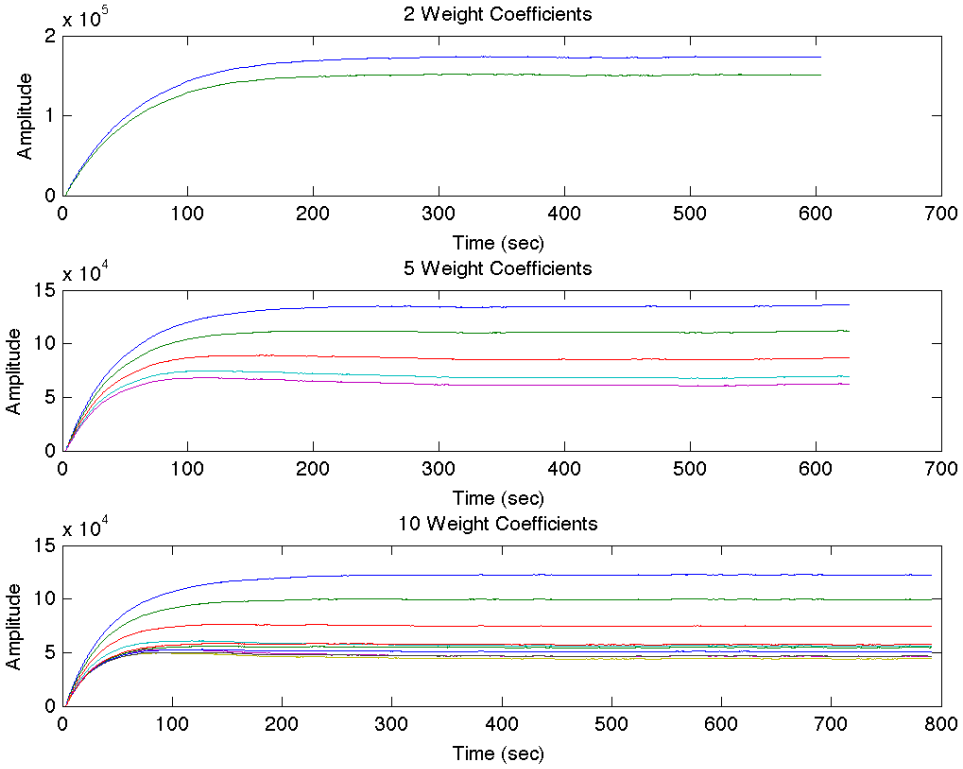

Figure 57: Experimental FIR weights for the adaptive Q-parametrized compensator using the second set of coprime rational functions with 2, 5, and 10 FIR weight coefficients.

Spectral analysis was used to analyze the steady state displacement of the magnetic particle and the frequency weighted displacement of the magnetic particle as shown in figure 58 and figure 59 respectively for a time duration of 2 s.

The spectral analysis for the displacement of the magnetic particle yields as the number of FIR weight coefficients increased, the Brownian disturbances were suppressed more than with the nominal compensator in the low frequency range as shown in figure 58. The effects of the Brownian disturbances being decreased as the number of the FIR weights increased was expected because the number of the FIR weights is equivalent to the number of independent variables used to minimize the frequency weighted displacement of the magnetic particle. As the number of the FIR weights increase, the frequency weighted displacement of the magnetic particle should decrease in the low frequency range as expected as shown in figure 59.

The Brownian disturbance was suppressed by an average of 9.81 dB, 12.46 dB, 14.48 dB, and 14.48 dB for the nominal compensator and the adaptive Q-parametrized compensator using 2, 5, and 10 FIR weights respectively for frequencies less than 400 Hz than the mean particle displacement of -2.871 dB at the dominating frequency of 2.41 kHz.

The nominal compensator and the adaptive Q-parametrized compensator using 2 and 5 FIR weight cases suppressed the Brownian disturbances slightly more with the second set of coprime rational functions than with the first set of coprime rational functions. The Brownian disturbances were suppressed more with the first set of coprime rational functions for the adaptive Q-parametrized compensator using 10 FIR weights than with the first set of coprime rational functions.

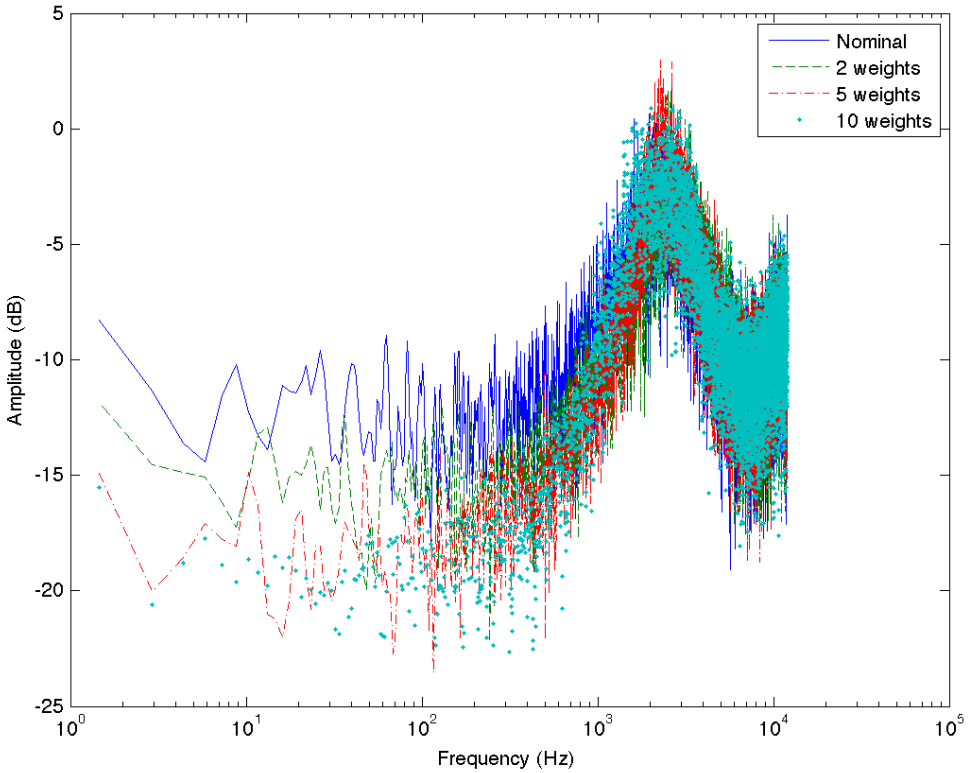

Figure 58: Experimental displacement of the magnetic particle using spectral analysis for the adaptive Q-parametrized compensator using the second set of coprime rational functions with the nominal compensator and the three FIR weight cases.

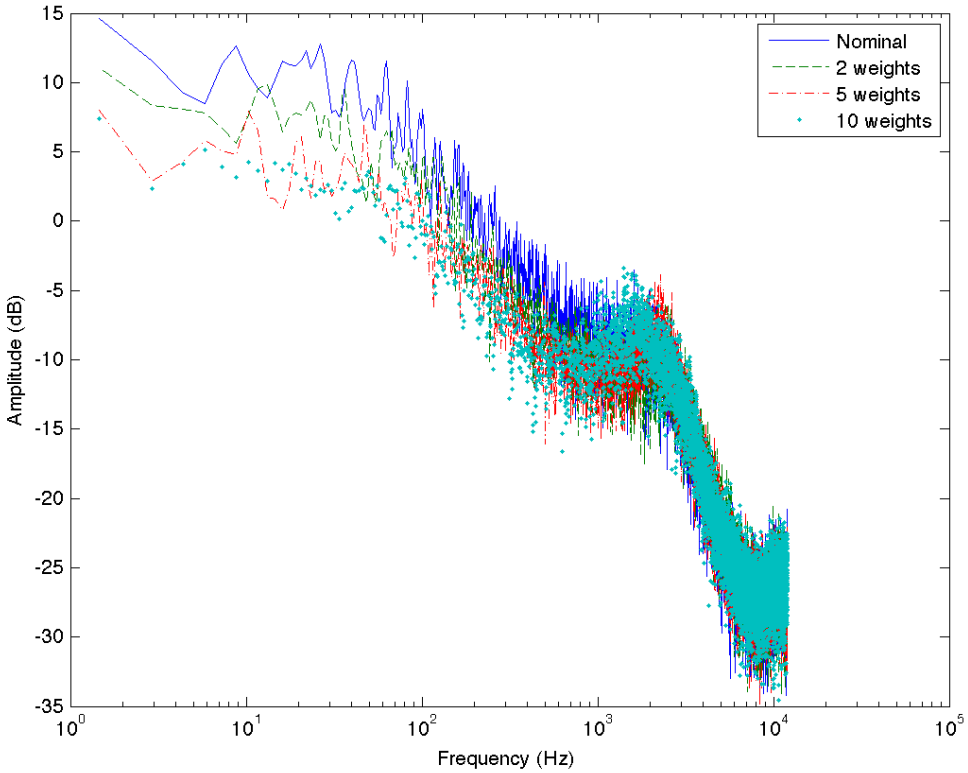

Figure 59: Experimental frequency weighted displacement of the magnetic particle using spectral analysis for the adaptive Q-parametrized compensator using the second set of co-prime rational functions with the nominal compensator and the three FIR weight cases.

6.0 SUMMARY

This chapter gives a summary of the work presented in this thesis, highlights the major aspects, and list the recommendations that would further enhance the work.

6.1 DISCUSSION

Compensation methods had to be incorporated into the design of the magnetic trap to stabilize the position of the magnetic particle and to minimize the effects of the Brownian disturbances. The performance of the various compensation methods were analyzed in the frequency domain using spectral analysis. This required the sensitivity function of the compensated system be small in low frequencies to reject disturbances. The sensitivity function was reduced in low frequencies using a nominal performance weight that reduced the effects of the Brownian disturbances. The analysis of the open-loop magnetic particle system resulted in two compensator structures being chosen to achieve the design requirements: proportional gain compensation and Q-parametrized compensation, that characterized the entire set of stabilizing compensators. The Q-parametrized compensator structure was used for a fixed gain compensator and the adaptive compensator. The closed-loop transfer functions for the feedback block diagram schematic of the magnetic trap were affine in Q, allowing the adaptive feedback control problem to be converted into a model-matching problem where LMS was used to adjust the parameters of Q, that was modeled as an FIR filter. The adaptive Q-parametrized compensator reduced the effects of the Brownian disturbance by updating the weight coefficients of Q with LMS to minimize the frequency weighted displacement of the magnetic particle.

The compensation methods were simulated to show the design requirements were satisfied, the Brownian disturbances were reduced, and nominal performance was achieved before the experiments were performed. The fixed gain Q-parametrized compensators were equated to the proportional gain compensator using two sets of coprime rational functions by the uniqueness property of the Q-parametrized compensator to show the compensated system satisfied the design requirements before LMS was used to updated the parameters of Q. This resulted in the fixed gain compensators having the same performance. The fixed gain compensators stabilized the position of the magnetic particle, achieved nominal performance, and reduced the effects of the Brownian disturbance by 23.11 dB for frequencies below 100 Hz than at higher frequencies. The two adaptive Q-parametrized compensators were simulated while considering how different number of FIR weight coefficients affected the performance of the compensated system by choosing 5 and 25 FIR weight coefficients. The adaptive compensator for both FIR weight cases were able to stabilize the position of the magnetic particle, achieve nominal performance, increase the compensated bandwidth frequency by approximately a factor of 3.8, and reduce the effects of the Brownian disturbance. This results in the position of the magnetic particle reaching its desired position faster using adaptive control methods than using fixed gain control methods . The performance of the adaptive Q-parametrized compensator for both FIR weight cases were better than the nominal compensator, however the performance for both FIR weight cases were approximately equal. This was unexpected because as the number of FIR weights increased, there were more independent variables to minimize the frequency weighted displacement of the magnetic particle. The simulation for the various compensation methods proved the position of the magnetic particle was stabilized, the compensated system achieved nominal performance, and the effects of the Brownian disturbance were reduced.

The experiments for the various compensation methods were performed by connecting two dSpace boards together because the sensor setup was not working properly. The various compensation structures were on one dSpace board that fed the control signal to the other dSpace board, containing the magnetic particle system and the Brownian disturbance, to produce the displacement of the magnetic particle that was fed back into the compensator dSpace board. While performing the experiments, the control signal and the displacement

of the magnetic particle contained beat frequency phenomena as the result of one dSpace board being a multiple of a time step off from the other dSpace board. This was unexpected because the internal clocks of the dSpace boards should have been in sync since the sampling periods were the same on both boards. The method used to eliminate the beat frequency called for the sampling frequency of the dSpace board containing the magnetic trap to be changed by an irrational number. The spectral analysis for the fixed gain compensators showed that the displacement of the magnetic particle was reduced in the low frequencies as shown in figure 60. This resulted in the fixed gain compensators reducing the effects of the Brownian disturbances.

The experiments for the adaptive Q-parametrized compensators were performed while considering how different number of FIR weight coefficients affected the performance of the nominal compensator by choosing 2, 5, and 10 FIR weight coefficients. While performing these experiments, leaky LMS had to be used to stabilize the LMS algorithm. The spectrum for the displacement of the magnetic particle was suppressed more in the low frequency range as the number of FIR weight coefficients increased using both the first and second sets of coprime rational functions as shown in figure 60. This resulted in the effects of the Brownian disturbances being suppressed more as the number of FIR weight coefficients increased because there were more independent variables to minimize the frequency weighted displacement of the magnetic particle.

The work presented in this thesis assumed there was only one experimental condition because the sensor was not working properly. This resulted in the viscous force acting on the magnetic particle being modeled using Stokes drag without the Oseen boundary condition and the magnetic properties of the magnetic particle did not change because the gain of the magnet was arbitrarily chosen to demonstrate the control theory satisfied the design requirements. When the exact experimental conditions for the magnetic trap are known, the experimental results indicated that fixed gain compensation will stabilize the position of the magnetic particle and reduce the effects of the Brownian disturbance, thus produces good compensator performance. However, determining these experimental conditions, requires an enormous amount of time resulting in biophysicists spending minimal time working on their experiments. The use of an adaptive Q-parametrized compensator structure that uses LMS

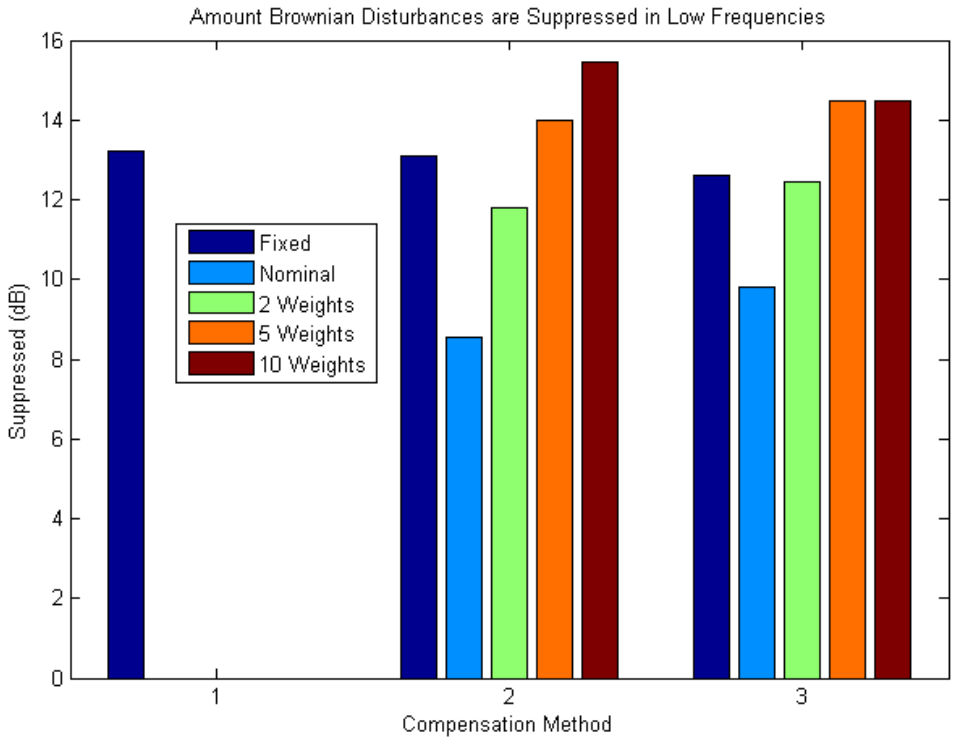

Figure 60: Graph showing the amount the Brownian disturbances are suppressed for each compensation method. Compensation method 1, 2, and 3 are the proportional gain compensation, the Q-parametrized compensation structure using the first set of coprime rational functions, and the Q-parametrized compensation structure using the second set of coprime rational functions.

to update the FIR weight coefficients of the Q parameter to minimize the frequency weighted displacement of the magnetic particle alleviates biophysicists of the time spent designing compensators to meet their experimental conditions. For any experimental condition and a number of FIR weights, there exists optimal weight coefficients that minimizes the frequency weighted displacement of the magnetic particle. The adaptive Q-parametrized compensator structure alleviates users of the trouble of designing fixed gain compensators by finding the optimal weight coefficients that minimizes the frequency weighted displacement of the magnetic particle for the current experimental conditions.

6.2 CONCLUSION

Magnetic traps are a vital instrument for allowing biophysicists to study the behavior of biological systems and processes. They manipulate magnetic objects by applying a magnetic force under the influence of magnetic fields. However the manipulation of the magnetic particle is cumbersome due to the dynamics of the instrument changing per experiment.

Adaptive control can be incorporated into the design of magnetic traps to alleviate users of designing compensators to control the position of the magnetic particle. Adaptive control automatically adjusts the parameters of the compensator to ensure the instrument satisfies specific requirements. An adaptive Q-parametrized compensator structure with LMS allows users to concentrate more effort on their experiments by finding the optimal weight coefficients that minimizes a frequency weighted displacement of the magnetic particle for the current experimental conditions.

6.3 FUTURE WORK

This research showed that incorporating an adaptive Q-parametrized compensator structure into the design of magnetic traps the position of the magnetic particle was stabilized and the effects of the Brownian disturbances were reduced. The following recommendations will

enhance this research by implementing the various compensation methods on the actual magnetic particle system and analyzing the performance of different adaptive compensators.

- The experimental results were produced by connecting two dSpace boards together because the sensor was not working properly. The broad-band white noise in the QPD difference signal can be eliminated by properly aligning an optical system to move the angular spectrum of the scattered light reflected from the particle, at the back focal plane of the microscope objective, to measure the displacement of the particle. This will result in a magnetic particle system that is able to manipulate and measure the position of the magnetic particle in real time.
- Once the sensor is working properly, robust stability theory should be incorporated into the design of the compensators. The model of the magnetic particle system was used to demonstrate the various compensation methods satisfied the design requirements. However the model of the magnetic particle system could vary from the actual system which could yield poor compensator performance. Robust stability would avoid the complications of not having the exact mathematical description of the system by characterizing a compensator that stabilizes the position of the magnetic particle for a set of plants that contains the actual magnetic particle system.
- The weight coefficients of Q were updated to obtain the optimal set of basis in the Q space that minimized the frequency weighted displacement of the particle. The set of basis chosen for Q had increase powers of z^{-1}. This set of basis produced good compensator performance, however different sets of basis should be analyzed to determine the best compensator performance for a given set of coprime rational functions.
- Finally, there were two sets of coprime rational functions chosen for the adaptive Q-parametrized compensator to satisfy the design requirements. These two sets of coprime rational functions produced good compensator performance, however other sets should be considered for a given Q to determine the set of coprime rational functions that yields the best compensator performance.

BIBLIOGRAPHY

[1] Francois Amblard, Bernald Yurke, Andrew Pargellis, and Stanislas Leibler. A magnetic manipulator for studying local rheology and micromechanical properties of biological systems. *Review of Scientific Instruments*, 67:818–827, 1996.

[2] Andreas R. Bausch, Winfried Moller, and Erich Sackmann. Measurement of local viscoelasticity and forces in living cells by magnetic tweezers. *Biophysical Journal*, 76:573–579, 1999.

[3] Andreas R. Bausch, Florian Ziemann, Alexei A. Boulbitch, Ken Jacobson, and Erich Sackmann. Local measurements of viscoelastic parameters of adherent cell surfaces by magnetic bead microrheometry. *Biophysical Journal*, 75:2038–2049, 1998.

[4] William L. Brogan. *Modern Control Theory*. Prentice-Hall Inc., 1991.

[5] Carlos Bustamante, Jed C. Macosko, and Gijs J.L. Wuite. Grabbing the cat by the tail: Manipulating molecules one by one. *Nature*, 1:130–136, 2000.

[6] Chi-Han Chiou, Yu-Yen Huang, Meng-Han Chiang, Huei-Huang Lee, and Gwo-Bin Lee. New magnetic tweezers for investigation of the mechanical properties of single dna molecules. *Nanotechnology*, 17:1217–1224, 2006.

[7] Geoffrey M. Cooper. *The Cell A Molecular Approach*. ASM Press, third edition, 2004.

[8] Anthony H.B. de Vries, Bea E. Krenn, Roel van Driel, and Johannes S. Kanger. Mirco magnetic tweezers for nanomanipulation inside live cells. *Biophysical Journal*, 88:2137–2144, 2005.

[9] C.A. Desoer, Ruey-Wen Liu, J. Murray, and R. Saeks. Feedback system design: The fractional representation approach to analysis and synthesis. *IEEE Transcations of Automatic Control*, 25:399–412, 1980.

[10] John C. Doyle, Bruce A. Francis, and Allen R. Tannenbaum. *Feedback Control Theory*. Dover Publications, 2008.

[11] Robert W. Fox, Alan T. McDonald, and Philip J. Pritchard. *Introduction to FLUID MECHANICS*. John Wiley & Sons, Inc, sixth edition, 2001.

[12] M.E.J. Friese, H. Rubinsztein-Dunlop, N.R. Heckenburg, and E.W. Dearden. Determination of the force constant of a single-beam gradient trap by measurement of backscattered light. *Applied Optics*, 35:7112–7116, 1996.

[13] Charlie Goose and Vincent Croquette. Magnetic tweezers: Micromanipulation and force measurement at the molecular level. *Biophysical Journal*, 82:3314–3329, 2002.

[14] David J Griffiths. *Introduction to Electrodynamics*. Prentice-Hall Inc., 1999.

[15] Charbel Haber. Magnetic tweezers for DNA micromanipulation. *Review of Scientific Instruments*, 71:4561–4570, 2000.

[16] John Happel and Howard Brenner. *Low Reynolds Number Hydrodynamics with Special Applications to Particulate Media*. Prentice-Hall Inc., 1965.

[17] Basarab G. Hosu and Karoly Jakab. Magnetic tweezers for intracellular applications. *Review of Scientific Instruments*, 74:4158–4163, 2003.

[18] IEEE. *Adaptive Feedback Control*, volume 75, 1987.

[19] Thomas Kailath. A view of three decades of linear filtering theory. *IEEE Transcations of Information Theory*, 2:146–181, 1974.

[20] R.E. Kalman. A new approach to linear filtering and prediction problems. *Transactions of the ASME - Journal of Basic Engineering*, 82:35–45, 1960.

[21] Daniel R. McAdams. Measuring inter-particle forces at an interface with optical tweezers and a long working-distance objective lens. Master's thesis, University of Pittsburgh, 2008.

[22] K.C. Neuman, T. Liionnet, and J.F. Allemand. Single-molecule micromanipulation techniques. *Annual Review of Materials Research*, 37:33–67, 2007.

[23] Norman S. Nise. *Control Systems Engineering*. John Wiley and Sons, 2004.

[24] A.V. Oppenheim, R.W. Shafer, and J.R. Buck. *Discrete-Time Signal Processing*. Prentice Hall, second edition, 1998.

[25] Alexander D. Poularikas and Zayed M. Ramadan. *Adaptive Filtering Primer with Matlab*. Taylor & Francis Group, 2006.

[26] Matthew N.O. Sadiku. *Elements of Electromagnetics*. Saunders College Publishing, 1994.

[27] Richaro S. Sanchez-Pena and Mario Sznaier. *Robust Systems Theory and Applications*. John Wiley and Sons, 1998.

[28] Shankar Sastry and Marc Bodson. *Adaptive Control Stability, Convergence, and Robustness*. Prentice-Hall Inc., 1989.

[29] Benjamin Shapiro, Roland Probst, Hugh E. Potts, Declan A. Diver, and Andreas S. Lubbe. Control to concentrate drug-coated magnetic particles to deep tissue tumors for targeted cancer chemotherapy. IEEE Conference on Decision and Control, 2007.

[30] Sergey S. Shevkoplyas, Adam C Siegel, Robert M. Westervelt, Mara G. Prentiss, and George M. Whitesides. The force acting on a supermagnetic bead due to an applied magnetic field. *Lab on a Chip*, 7:1294–1302, 2007.

[31] T.R. Strick, J.F. Allemand, D. Bensimon, A. Bensimon, and V. Croquette. The elasticity of a single supercoiled DNA molecule. *Science*, 271:1835–1837, 1996.

[32] John R. Treichler, C. Richard Johnson, Jr., and Michael G. Larimore. *Theory and Design of Adaptive Filters*. John Wiley & Sons, Inc, 1987.

[33] M. Vidyasagar, H. Schneider, and B.A. Francis. Algebraic and topological aspects of feedback stabilization. *IEEE Transcations of Automatic Control*, 27:880–894, 1982.

[34] Giovanni Volpe, Gregory Kozyreff, and Dmitri Petrov. Backscattering position detection for photonic force microscopy. *Journal of Applided Physics*, 102, 2007.

[35] Thomas Weyh, Nicole Seidl, Bernhard Gleich, Christoph Alexiou, Martin Koch, and Bernhard Wolf. Control of drug-carrying magnetobeads by magnetic gradient-fields. IEEE Conference on Nanotechnology, 2004.

[36] B. Widrow and S.D. Stearns. *Adaptive Signal Processing*. Prentice Hall, INC., 1985.

[37] D.C. Youla, H.A. Jabr, and Jr J.J. Bongiorno. Modern wiener-hopf design of optimal controllers - part ii: The multvariable case. *IEEE Transcations of Automatic Control*, 21:319–338, 1976.

[38] Hugh D. Young and Roger A. Freedman. *UNIVERSITY PHYSICS*, volume II. Pearson Education, Inc., Second custom edition for University of Pittsburgh edition, 2004.

[39] F. Ziemann, J. Radler, and E. Sackmann. Local measurements of viscoelastic moduli of entangled actin networks using an oscillating magnetic bead micro-rheometer. *Biophysical Journal*, 66:2210–2216, 1994.

[40] Jordanka Zlatanova and Sanford H. Leuba. Magnetic tweezers: a sensitive tool to study DNA and chromatin at the single-molecule level. *Biochemistry and Cell Biology*, 81:151–159, 2003.